ISSN 0280-5316
ISRN LUTFD2/TFRT--5841--SE

Dual motor control for backlash reduction

Johannes Schiffer

Department of Automatic Control
Lund University
June 2009

Lund University
Department of Automatic Control
Box 118
SE-221 00 Lund Sweden

Document name
MASTER THESIS

Date of issue
June 2009

Document Number
ISRN LUTFD2/TFRT--5841--SE

Author(s)
Johannes Schiffer

Supervisor
Assoc.Prof. A. Robertsson Automatic Control, Lund
Dipl. –Ing. S. Schuler Systems Theory and Automatic Control, Univ. of Stuttgart
Prof. A. Rantzer Automatic Control, Lund (Examiner)
Prof. F. Allgöwer Systems Theory and Automatic Control, Univ. of Stuttgart (Examiner)

Sponsoring organization

Title and subtitle
Dual motor control for backlash reduction (Dubbelmotorreglering för glappreducering)

Abstract
Within the EU FP-6 project SMErobot^{TM} a new type of high-performance robots has been developed by ABB Robotics, the Robotics Lab at Lund University and Güdel AG, Switzerland. The new design is based on a parallel configuration of the robot´s joints (parallel robots). The main novelty of that concept is its completely new parallel kinematic structure, which allows to exploit all the advantages in terms of performance and cost of parallel kinematics, e.g. having only axial forces in the arm links. Consequently, this new type of robot can be used in many applications, such as laser, water and plasma jet cutting, gluing, assembly and machining. However, the actuator and drive-line of the robot are based on the “Rack-and-pinion principle”. This leads to some difficulties concerning the positioning accuracy and the stiffness, as flexibility and backlash will occur in both the ordinary gearbox and in the mechanical connection to the rail. To fulfill the requirements on the robot, these effects need to be eliminated. The approach of the present work is to reduce these effects by using two motors for each cart instead of the conventional use of only one. Furthermore also position measurements along the rails are used in addition to the motor angle positions. For this configuration, a nonlinear model is derived and the effects of the additional motor on the system performance and stability are analyzed. Furthermore, several nonlinear, smooth switching control laws for the operation of the system are presented. The theoretical results are furthermore verified with an experimental setup representing a simplified implementation of the dual motor driven robot.

Keywords

Classification system and/or index terms (if any)

Supplementary bibliographical information

ISSN and key title
0280-5316

ISBN

Language
English

Number of pages
143

Recipient’s notes

Security classification

http://www.control.lth.se/publications/

Diploma Thesis IST-55

Dual motor control for backlash reduction

Johannes Schiffer

Supervisor:

Assoc. Prof. A. Robertsson,

Dept. of Automatic Control, Lund University

Prof. A. Rantzer,

Dept. of Automatic Control, Lund University

Dipl.-Ing. S. Schuler,

Inst. for Systems Theory and Automatic Control, University of Stuttgart

University of Stuttgart

Institute for Systems Theory and Automatic Control

Prof. Dr.–Ing. F. Allgöwer

June, 10th 2009

Kurzfassung

Im Rahmen des EU FP-6 Projektes SMErobot^{TM} wurde von ABB Robotics, dem Robotics Lab der Universität Lund und der Güdel AG, Schweiz ein neuartiger Robotertyp entwikkelt. Das Konzept basiert auf einer parallelen Anordnung der Gelenke des Roboters. Diese vollständig neue parallelkinematische Struktur ermöglicht es, alle Vorteile paralleler Kinematiken in Bezug auf Leistung und Kosten, wie z.B. lediglich axiale Kräfte in den Armgliedern und gleichzeitig großem verfügbarem Arbeitsraumvolumen, auszuschöpfen. Somit ist der Roboter für viele verschiedene Anwendungsbereiche, wie z.B. Laser-, Wasserstrahl- und Plasmaschneiden, Kleben, sowie Montage- oder Bearbeitungsvorgänge, hochinteressant.

Die Antriebsanlage basiert jedoch auf dem Prinzip des "Zahnstangenantriebs". Dies führt zu Schwierigkeiten bei der Positionsgenauigkeit und der Steifigkeit des Systems, da sowohl im Getriebe als auch in der mechanischen Verbindung zur Schiene mechanisches Spiel und insbesonder Zahnradspiel vorhanden ist. Diese Effekte müssen unterdrückt werden, um die hohen Ansprüche an den Roboter erfüllen zu können.

Der Ansatz der vorliegenden Arbeit beabsichtigt hierzu zwei Motoren pro Cart, statt wie herkömmlich nur einen Motor, einzusetzen. Desweiteren sollen Messungen der translatorischen Position des Carts auf der Schiene zusätzlich zu den Motorpositionen zur Verfügung stehen. Für diesen Aufbau wird ein nichtlineares Modell hergeleitet und die Auswirkungen des zusätzlichen Motors auf die Systemleistung und -stabilität werden untersucht. Ferner werden verschiedene nichtlineare, glatt schaltende Regelungskonzepte für den Betrieb des Systems eingeführt. Die theoretischen Ergebnisse werden an einem Versuchsaufbau, der eine vereinfachte Implementierung des zweimotorigen Roboters darstellt, getestet.

Acknowledgments

The work resulting in this thesis was carried out at the Department of Automatic Control, LTH, Lund University, Sweden within an Erasmus exchange program between Lund University and the University of Stuttgart.

I would like to thank the following people who all contributed in some form to the success of this endevour:

My supervisors Anders Robertsson and Anders Rantzer at the Department of Automatic Control, as well as Frank Allgöwer and Simone Schuler at the Institute for Systems Theory and Automatic Control for supporting my work and making my stay in Lund possible. Furthermore, I am very grateful to Leif Andersson for his help and advices regarding all type of computer and software related aspects.

All other people at the department for their help, discussions, suggestions and for making my time there pleasant.

My Erasmus-coordinators Jürgen Mayer in Stuttgart and Anna Skarman in Lund, as well as Ursula Meiser at the Office of International Affairs of the University of Stuttgart.

My family for their love and support. Especially, I would like to thank my parents, for giving me so much freedom of choice in my life and supporting me during all that time.

All my friends.

Contents

List of Figures

List of Tables

Chapter 1

Introduction

1.1 Parallel kinematic robots

Within the EU FP6-project SMErobot^{TM} [1] a new type of a high-performance robot has been developed by ABB Robotics, the Robotics Lab at Lund University and Güdel AG, Switzerland.

The new design is based on the parallel configuration of the robot´s joints (parallel robots), see Fig. 1.1. The main novelty of that concept is its completely new parallel kinematic structure, which allows to exploit all the advantages in terms of performance and cost of parallel kinematics, e.g. having only axial forces in the arm links.

The robot has a large open workspace, is modular and easy to scale. Additionally it has the benefit of very low inertias of the moving robot parts. These characteristics, combined with the high stiffness of joints and arms, allow to build high-performance robots in terms of speed, mechanical bandwidth, accuracy and stiffness. The high mechanical bandwidth of the robot makes it much more suitable for stiff contact force control tasks than ordinary serial manipulators.

Further features are low actuator power and energy consumption, due to the low inertia and the non-redundancy of the robot, which makes it easy to assemble and disassemble without the need of complicated mechanical adjustment procedures. However, there need to be efficient calibration methods to guarantee the absolute accuracy of the manipulator

Figure 1.1: New parallel kinematic robot concept developed within the SMErobot^{TM}-project. The carts (red) are controlled in a coordinated way along three rails to move the tool/end-plate along a desired trajectory.

after the assembly. The design of the robot allows the wrist to be moved by three high performance linear actuators via six links. These three base joints can then be enhanced with a serial or parallel wrist to extend the robot´s range of motion to six DOFs.

Consequently, this new type of robot can be used in many applications, such as laser, water and plasma jet cutting, gluing, assembly and machining. Therefore, it is interesting for many industrial small and medium enterprises (SME).

1.2 Problem formulation

The actuator and drive-line of the robot is based on the “Rack-and-pinion principle”, see Fig. 1.2. This leads to some difficulties concerning the positioning accuracy and the stiffness, as flexibility and backlash will occur in both the ordinary gearbox and in the mechanical connection to the rail. To fulfill the demands on the robot, these effects need to be eliminated.

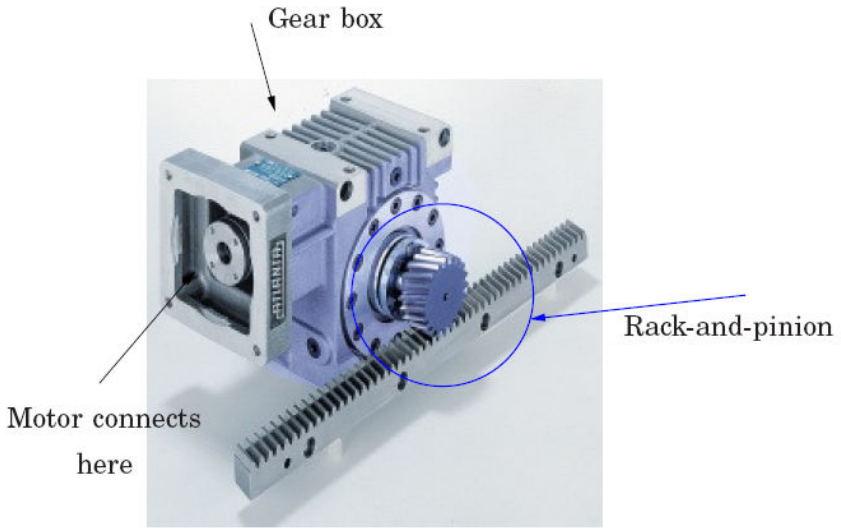

Figure 1.2: Rack-and-pinion for converting rotational into translational motion

There has already been done a lot of research on backlash-effects in mechanical systems, but in most cases the achieved performance is not good enough for the present case. A good overview of available publications about this topic can be found in [2] and [3]. A more extensive work is [4].

The approach of the present work is to use two motors for each cart instead of the conventional use of only one motor. Furthermore also position measurements along the rails are used in addition to the motor angle positions. In this way, it may be possible to use both motors for improved acceleration, but more important to let them work in opposite directions for improved positioning and stiffness. One motor can act as spring and brake to reduce the backlash, as can be seen in Fig. 1.3.

This idea has been developed within the SMErobot^{TM} project and is currently tested by Güdel AG in Switzerland. Some previous work can be found in [5]. Besides, there are only a few papers, which report on similar implementations for antennas [8], tracking platforms [9] and servo-systems [11].

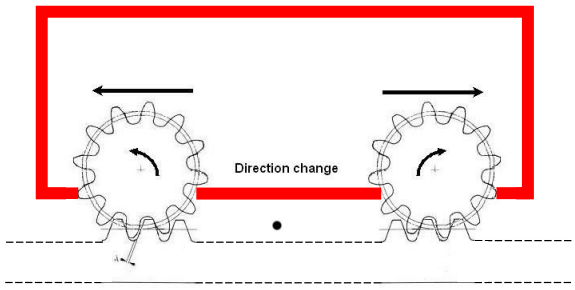

Figure 1.3: Backlash in gearbox and rails by using two motors, which work in opposite directions for improved positioning and stiffness. One motor can act as spring and brake to reduce the backlash.

1.3 Outline of the thesis

At first, the described problem is simplified in Chapter 2 by substituting one motor by a constant torque acting directly on the load. This leads to a nonlinear two-mass system exhibiting backlash. A linear controller for the cart position is designed and the resulting closed-loop system is analyzed regarding its equilibrium points and their stability characteristics under the influence of the constant torque input. Further, several operating strategies for the constant torque based on a switching variable are introduced and tested in simulations.

In Chapter 3, the theoretical results obtained before are studied on an experimental setup representing a two-mass system.

Subsequently, the model of Chapter 2 is extended to a three-mass system in Chapter 4. This system is analyzed regarding local and global stability assuming a constant input on one of the motors. Different nonlinear control and switching strategies for the operation of the system are presented and tested in Matlab/Simulink as well as in the modeling and simulation tool Dymola. As consequence of an additional switching between the driving roles of both motors, a nonlinear MIMO controller is presented. The aim is to define a hybrid control law based on switching variable, which has to be determined. Additionally a coordinated control of the motors for optimal performance is derived.

Chapter 2

Dual motor control of a nonlinear two-mass system

In a first step, the complexity of the problem is reduced by considering a system which consists of only two masses, one representing a load and one representing a motor.

This kind of system has been well-studied in literature since the 1940s, due to the fact that in most cases the considered plants which exhibit backlash-effects may be modeled as such a two-mass system. As in the present case, commonly, the first mass represents the motor, while the second mass represents the load. Both masses are typically considered to be connected by a mass or inertia free shaft. Some older and more recent research on this standard plant can be found in [4], [13].

Additionally it is assumed, that the system has a second motor which acts directly on the load. This second motor may generally be used to simulate load-disturbance effects. But in the present case, it will be used to simulate the second motor of the desired dual-motor-drive aiming to close the backlash gap with a torque acting in opposite direction of the driving torque.

The chapter is structured as follows: First a nonlinear model of a two-mass system with its respective parameters is derived in Section 2.1. In Section 2.2 a linear cascaded controller for the position of the load is designed. The controller consists of a PID-controller for the absolute translational position x_{pos} in the outer-loop and a PI-controller for the

motor velocity ω_l. Subsequently, an analysis of the system´s equilibrium points and their stability characteristics is provided in Section 2.3, assuming a constant torque acting on the load side. For the analysis, a dead-zone is used to represent the backlash. In Section 2.5 the system performance is then evaluated in simulations and related to the results of the previous analysis. In order to improve the system performance different strategies for the operation of the second motor are presented and tested in simulations.

2.1 Modeling of a nonlinear two-mass system

A model describing the simplified process can be formulated as follows

$$\begin{aligned} J_m\dot{\omega}_m &= -c_m\omega_m - T_s + T_{m1} \\ J_l\dot{\omega}_l &= -c_l\omega_l + T_s + T_{m2} \\ x_{pos} &= r_l\Theta_l \\ \omega_d &= \omega_m - \omega_l \end{aligned} \tag{2.1}$$

with

$$\dot{\Theta}_m = \omega_m,\ \dot{\Theta}_l = \omega_l,\ \dot{\Theta}_d = \omega_d,$$

$$T_s = \begin{cases} k_s(\Theta_d - \Theta_b) + c_s\omega_d, & \text{contact} \\ 0, & \text{backlash} \end{cases} \tag{2.2}$$

and

$$\dot{\Theta}_b = \begin{cases} \max(0, \Delta\dot{\Theta}_d + \frac{k_s}{c_s}(\Theta_d - \Theta_b)), & \Theta_b = (-\alpha) \\ \dot{\Theta}_d + \frac{k_s}{c_s}(\Theta_d - \Theta_b), & |\Theta_b| < \alpha \\ \min(0, \Delta\dot{\Theta}_d + \frac{k_s}{c_s}(\Theta_d - \Theta_b)), & \Theta_b = \alpha. \end{cases} \tag{2.3}$$

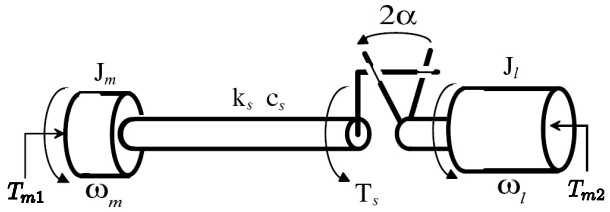

Figure 2.1: Schematic representation of a nonlinear two-mass system with backlash

J_m [kgm^2] represents the motor moment of inertia, c_m [Nm/(rad/s)] the viscous motor friction and J_l and c_l the equivalent parameters on the load side. T_{m1} [Nm] is the driving motor torque, whereas T_{m2} [Nm] is an additional controllable torque acting on the load. A schematic representation of a two-mass system exhibiting backlash is shown in Fig. 2.1.

The shaft is considered to be an inertia free spring with internal damping. The parameters k_s [Nm/rad] and c_s [Nm/(rad/sec)] represent the shaft elasticity and its inner damping respectively. T_s [Nm] is the shaft torque between motor and load. The shaft torque T_s is a function of the relative position angle Θ_d [rad] and the relative velocity ω_d [rad/sec], as well as the backlash angle Θ_b [rad], which is denoted with 2α. The gear ratio is assumed to be 1.

To establish a connection to the intrinsically considered process, namely the dual motor control of a parallel kinematic robot, it is additionally assumed, that the two-mass system moves in translational direction with $x_{pos} = r_l\Theta_l$ [m] describing its translational position. The absolute position of the load is denominated as x_{pos} [m], while the radius of the load is r_l [m].

The used state-space representation of the backlash angle was developed by Nordin *et.al* [4]. In [4] respectively [7] different models for an elastic free shaft with backlash are analyzed with the result that the commonly used modified dead-zone model does not always reflect the real physical behavior of the system e.g., it can lead to obtain a pull force for the shaft torque at the side of the backlash, where physically only a push force is possible.

In [7] a further modification of the modified dead-zone model is introduced and analyzed, but no improvement can be achieved. In the same paper another model for the backlash is presented and named *exact model*, which is the one used in the present modeling. It is shown that the behavior of that model is then closer to the real physical process. However, following the analysis in [7] both models are an exact description of the backlash if the shaft is modeled as a pure spring without damping, that is $c_s = 0$.

For the presented simulations the following set of parameters is used

$$\begin{aligned} J_m &= 0.4 && [kgm^2] \\ c_m &= 0.1 && [Nm/(rad/s)] \\ J_l &= 5.6 && [kgm^2] \\ c_l &= 1 && [Nm/(rad(s)] \\ k_s &= 3300 && [Nm/rad] \\ c_s &= 1 && [Nm/(rad/s)] \\ r_l &= 0.01 && [m] \\ \alpha &= 5 && [deg]. \end{aligned}$$

This set has been mostly taken out of [2] and will be used as example for a nominal case study in this chapter.

According to equation (2.2) the operation modes of the system are distinguished between the two cases: system in contact and system in backlash.

When the system is in contact, torque transmission between the motor and the load is possible, whereas there is no torque transmission in the backlash case. The conditions for the backlash case, can be summarized as follows

$$\text{backlash} = \begin{cases} \Theta_b = (-\alpha) \wedge \omega_b > 0 \\ |\Theta_b| < \alpha \\ \Theta_b = \alpha \wedge \omega_b < 0. \end{cases} \tag{2.4}$$

For all other cases the system is in contact mode, that is

$$\text{contact} = \begin{cases} \Theta_b = \alpha \wedge \omega_b \geq 0 \\ \Theta_b = (-\alpha) \wedge \omega_b \leq 0. \end{cases} \tag{2.5}$$

Note that the impact when the backlash gap closes is assumed to be inelastic, [7].

2.1.1 Matlab/Simulink model

The implemented model is shown in Fig. 2.2. The model has two inputs, which are the torques of the driving motors and several outputs including the angle positions of motor and load and its respective velocities. Additionally the shaft torque and the absolute position are available.

Nevertheless, only the absolute position of the load (x_{pos}), the motor and load angle positions (Θ_m, Θ_l) and the motor velocity ω_m are considered to be measurable, as this represents the given situation on the real robot.

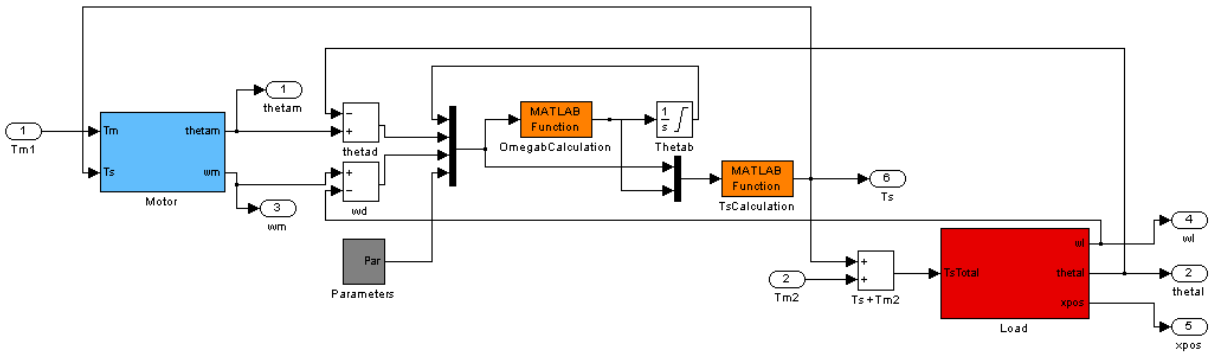

Figure 2.2: Nonlinear two-mass system of Eq. 2.1 in Simulink.

2.2 Linear position control of a nonlinear two-mass system

In this section a linear controller for the absolute position x_{pos} of the considered system is designed. The design is carried out formulating some rather weak requirements on the step response of the system, which does not reflect the commonly used input references in robotics. However, it might be valid in the present case, as the control-design task is regarded as a minor point compared to the analysis of the system performance under backlash effects.

2.2.1 Controller design

For the design of the linear controller, the nonlinear two-mass system described in Section 2.1 is reduced to a linear system, that is the backlash is neglected. Thus, the model reduces to

$$\begin{aligned} J_m\dot{\omega}_m &= -c_m\omega_m - T_s + T_{m1} \\ J_l\dot{\omega}_l &= -c_l\omega_l + T_s + T_{m2} \\ x_{pos} &= r_l\Theta_l \\ \omega_d &= \omega_m - \omega_l \end{aligned} \tag{2.6}$$

with

$$\dot{\Theta}_m = \omega_m,\ \dot{\Theta}_l = \omega_l,\ \dot{\Theta}_d = \omega_d$$

and

$$T_s = k_s\Theta_d + c_s\omega_d \tag{2.7}$$

where the variables and parameters have the same physical meaning as in Section 2.1. A schematic view of the system is given in Fig. 2.3. This linear model is equal to the case

'System in contact' of the nonlinear model. The measured outputs of the system are the absolute position of the cart x_{pos}, the motor position angle Θ_m and the motor velocity ω_m. A state space realization of the system can be formulated as:

$$\dot{x} = Ax + Bu + HT_{m2} \tag{2.8}$$
$$y = Cx,$$

where

$$x = \begin{bmatrix} \Theta_l & \Theta_m & \omega_l & \omega_m \end{bmatrix}^T, \tag{2.9}$$

$$u = T_{m1}, \tag{2.10}$$

$$A = \begin{bmatrix} 0 & 0 & 1 & 0 \\ 0 & 0 & 0 & 1 \\ -\frac{k_s}{J_l} & \frac{k_s}{J_l} & -\frac{c_s+c_l}{J_l} & -\frac{c_s}{J_l} \\ 0 & 0 & 0 & -\frac{c_m}{J_m} \end{bmatrix}, \tag{2.11}$$

$$B = \begin{bmatrix} 0 \\ 0 \\ 0 \\ \frac{1}{J_m} \end{bmatrix}, \tag{2.12}$$

$$H = \begin{bmatrix} 0 \\ 0 \\ \frac{1}{J_l} \\ 0 \end{bmatrix}, \tag{2.13}$$

$$C = \begin{bmatrix} rl & 0 & 0 & 0 \\ 0 & 1 & 0 & 0 \\ 0 & 0 & 1 & 0 \end{bmatrix}. \tag{2.14}$$

With this representation it can be easily shown that the system has three poles in the LHP and one pole on the origin. Furthermore, the system is fully controllable as well as observable.

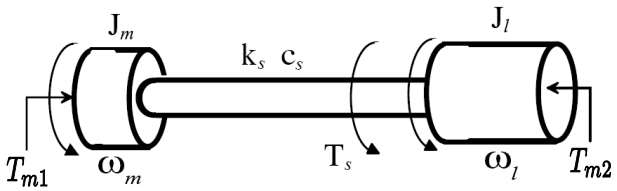

Figure 2.3: Schematic representation of a linear two-mass system.

The desired controller should fulfill the following requirements:

- No overshoot
- Fast response (rise time <5 [s]).

In order to achieve these aims, a cascade structure is implemented. The inner loop controller is a PI-controller and its control variable is the motor velocity ω_m, whereas the outer loop controller is a PID-controller with the absolute position x_{pos} as control variable.

The implemented controller structure is shown in Fig. 2.4. The corresponding control laws in the Laplace domain are

$$\begin{aligned} U_h(s) =& K_{P,out}((\beta_{out} Y_{ref}(s) - Y_{meas}(s)) + \frac{1}{T_{i,out} s} E(s) \\ &+ \frac{T_{d,out} s}{1 + \frac{T_{d,out} s}{N}} (\gamma_{out} Y_{ref}(s) - Y_{meas}(s))), \end{aligned} \tag{2.15}$$

where

$$K_{P,out} = 200 \tag{2.16}$$

$$\beta_{out} = 0 \tag{2.17}$$

$$T_{i,out} = 1.5 \tag{2.18}$$

$$T_{d,out} = 0.05 \tag{2.19}$$

$$\gamma_{out} = 0 \tag{2.20}$$

$$N = 20 \tag{2.21}$$

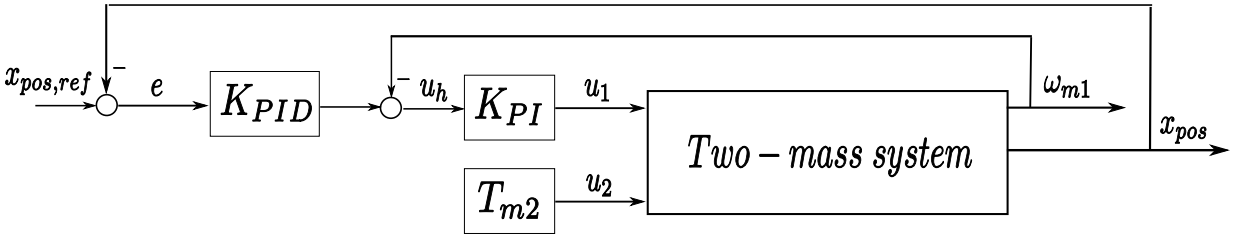

Figure 2.4: Control structure of the linear two-mass system. The controller includes modifications on the setpoint weighting and the limitation of the derivative gain.

and

$$U_1(s) = K_{P,in}((\beta_{in} Y_{ref}(s) - Y_{meas}(s)) + \frac{1}{T_{i,in} s} E(s)), \tag{2.22}$$

where

$$K_{P,in} = 50 \tag{2.23}$$

$$\beta_{in} = 0 \tag{2.24}$$

$$T_{i,in} = 0.3. \tag{2.25}$$

It holds that $E(s) = Y_{ref}(s) - Y_{meas}(s)$. The inner loop controller as well as the outer loop controller are formulated including a setpoint weighting in the P-part, expressed with the parameter $\beta \in [0, 1]$. Setting $\beta < 1$ helps to avoid an overshoot in the step response, this holds especially for $\beta = 0$ as implemented in both cases. Furthermore, the D-part of $K_{PID,x_{pos}}$ is modified in a similar manner, including also a weighting parameter $\gamma_{out} \in [0, 1]$ for the setpoint weighting, which is set to $\gamma_{out} = 0$ and a limitation of the derivative gain. The latter is formulated as a low-pass filter, which prevents of applying the derivation to high frequency measurement-noise. The parameter N represents the maximum derivative gain and is set to $N = 20$ (see [12]).

This design leads to the step response shown in Fig. 2.5. The step height is set to 0.1 [m]. The design requirements are fulfilled and the controller gives a stable closed-loop performance. Furthermore the closed-loop system is fully controllable.

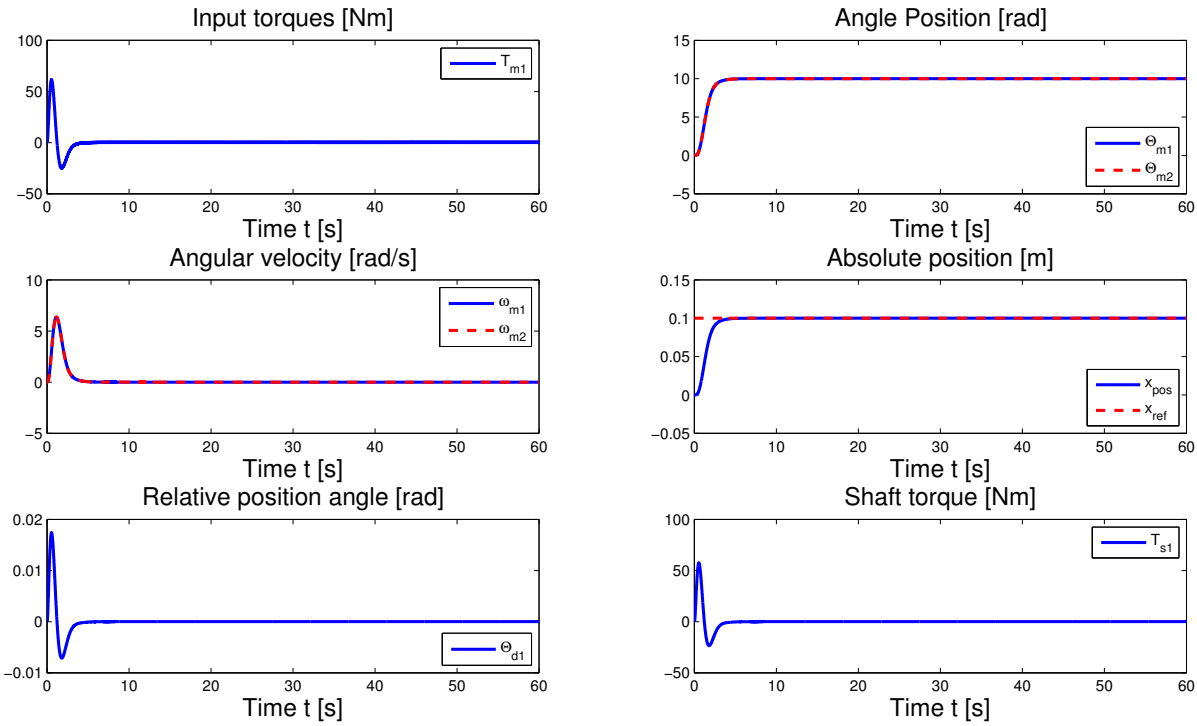

Figure 2.5: Step response of the linear two-mass system using the designed controller in Section 2.2.

2.2.2 State-space representation of the control structure

A state-space representation for the outer-loop PID controller is

$$\dot{x} = \begin{bmatrix} -\frac{N}{T_{d,out}} & 0 \\ 0 & 0 \end{bmatrix} x + \begin{bmatrix} \gamma_{out}\frac{N^2}{T_{d,out}} & -\frac{N^2}{T_{d,out}} \\ \frac{1}{T_{i,out}} & -\frac{1}{T_{i,out}} \end{bmatrix} \begin{bmatrix} x_{pos,ref} \\ x_{pos,meas} \end{bmatrix} \tag{2.26}$$

$$u_h = \begin{bmatrix} -K_{p,out} & K_{p,out} \end{bmatrix} x + \begin{bmatrix} K_{p,out}(N\gamma_{out} + \beta_{out}) \\ -K_{p,out}(N+1) \end{bmatrix}^T \begin{bmatrix} x_{pos,ref} \\ x_{pos,meas} \end{bmatrix}.$$

The states are defined as

$$x_1 = PID_D \tag{2.27}$$

$$x_2 = PID_I.$$

The inner-loop PI controller can be represented in the state-space in the following way

$$\begin{aligned} \dot{x}_3 &= 0\ x_3 + \begin{bmatrix} \frac{1}{T_{i,in}} & -\frac{1}{T_{i,in}} \end{bmatrix} \begin{bmatrix} \omega_m \\ u_h \end{bmatrix} \\ u_1 &= K_{p,in} x_3 + \begin{bmatrix} K_{p,in}\beta_{in} & -K_{p,in} \end{bmatrix} \begin{bmatrix} \omega_m \\ u_h \end{bmatrix}. \end{aligned} \tag{2.28}$$

The state x is defined as

$$x_3 = PI_I. \tag{2.29}$$

The overall control structure can be formulated in state-space representation as follows

$$\begin{aligned} \begin{bmatrix} \dot{x}_1 \\ \dot{x}_2 \\ \dot{x}_3 \end{bmatrix} &= \begin{bmatrix} -\frac{N}{T_{d,out}} & 0 & 0 \\ 0 & 0 & 0 \\ -\frac{K_{p,out}}{T_{i,in}} & \frac{K_{p,out}}{T_{i,in}} & \end{bmatrix} x \\ &+ \begin{bmatrix} \gamma_{out}\frac{N^2}{T_{d,out}} & -\frac{N^2}{T_{d,out}} & 0 \\ \frac{1}{T_{i,out}} & -\frac{1}{T_{i,out}} & 0 \\ \frac{K_{p,out}(N\gamma_{out}+\beta_{out})}{T_{i,out}} & \frac{-K_{p,out}(N+1)}{T_{i,in}} & -\frac{1}{T_{i,in}} \end{bmatrix} \begin{bmatrix} x_{pos,ref} \\ x_{pos,meas} \\ \omega_m \end{bmatrix} \end{aligned} \tag{2.30}$$

$$\begin{aligned} u_1 &= \begin{bmatrix} -K_{p,in}K_{p,out}\beta_{in} & K_{p,in}K_{p,out}\beta_{in} & K_{p,in} \end{bmatrix} x \\ &+ \begin{bmatrix} K_{p,in}K_{p,out}\beta_{in}(\beta_{out}+N\gamma_{out}) \\ -K_{p,in}K_{p,out}\beta_{in}(N+1) \\ -K_{p,in} \end{bmatrix}^T \begin{bmatrix} x_{pos,ref} \\ x_{pos,meas} \\ \omega_m \end{bmatrix}, \end{aligned} \tag{2.31}$$

where the state vector x represents

$$\begin{aligned} x_1 &= PID_D \\ x_2 &= PID_I \\ x_3 &= PI_I. \end{aligned} \tag{2.32}$$

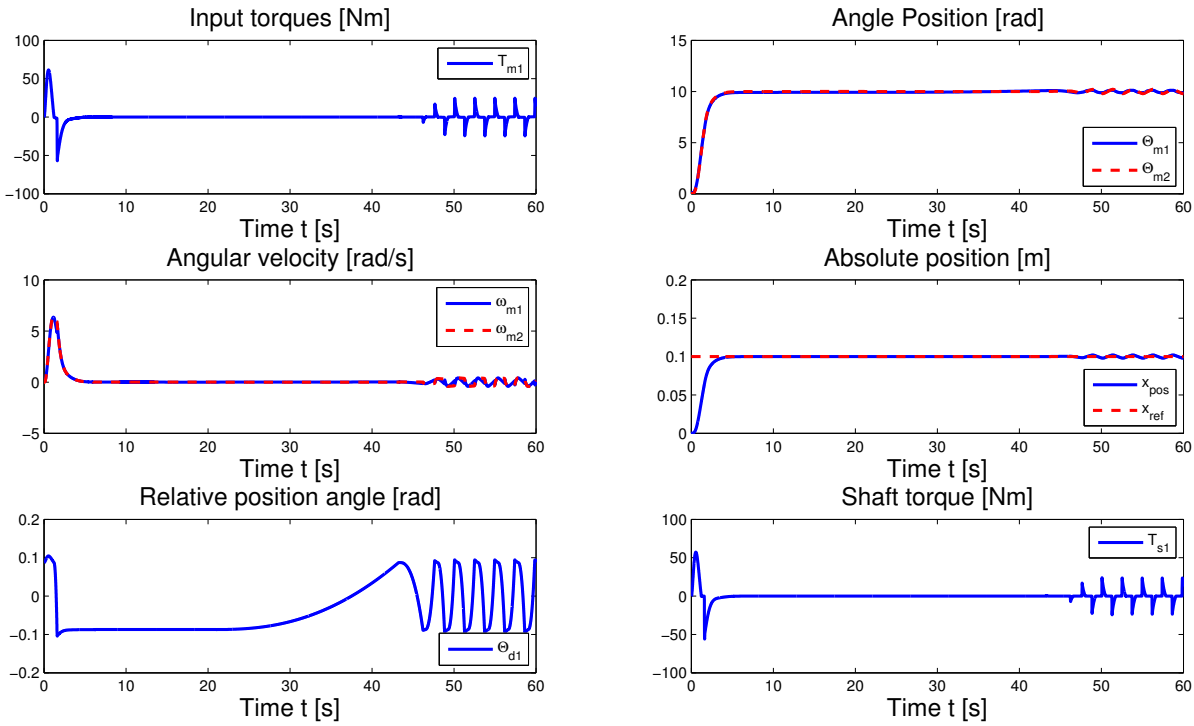

Figure 2.6: Step response of the nonlinear two-mass system using a cascade control structure. As expected the system undergoes limit cycles after some time as consequence of the backlash element.

2.2.3 Control performance on a nonlinear two-mass system

Now the control structure is tested on a nonlinear two-mass system including backlash. The step height is set to 0.1 [m] and the system is assumed to be in contact in the beginning of the motion, that is $\Theta_d(t = 0) = \alpha$. This setup will be used in most of the further simulations as it corresponds to the estimated starting position in the real application.

As expected the system undergoes limit cycles after some time as consequence of the backlash element, see step response in Fig. 2.6. The beginning of the limit cycles can be influenced by the size of the backlash angle. For instance a larger backlash angle leads to a faster generation of limit cycles.

2.3 Stability analysis of a two-mass system containing a dead-zone nonlinearity

This section analyzes the existence of equilibrium points and the stability of a nonlinear system containing a dead-zone nonlinearity. As derived in the previous sections, the system consists of a two-mass system exhibiting backlash and a cascaded control structure containing PID- and PI-control. Additionally, the system has a constant, but controllable torque acting directly on the load.

Note that in the following analysis, the exact backlash model is substituted with a dead-zone, which according to [2], [3] is a common way to model backlash. The shaft twist is then denoted with $\Theta_s = \Theta_d - \Theta_b$ [rad]. In the present analysis, no shaft-damping is considered. Thus, the shaft torque reduces to a function of Θ_d and Θ_b. However, neglecting the shaft-damping does not represent a change for the analysis, as for a possible equilibrium point of the system it must hold $\omega_m = \omega_l = 0$.

In [2] it is stated, that the dead-zone model does not reflect the exact physical behavior of the backlash. However, for the analysis of equilibrium points and stability the difference between the exact model proposed in [2] and the dead-zone model is negligible, as their main difference lays in the fact that the dead-zone model can predict physically impossible shaft torques. But this is not crucial in the following remarks.

The analysis is structured as follows: In Subsection 2.3.1 a state-space model is presented. In Subsection 2.3.2 a controllable canonical form of the system is derived, which is used in 2.3.3 to determine the equilibrium points of the system. In Subsection 2.3.4 the stability of the equilibrium points is analyzed. At last, some physical aspects concerning the model and its equilibrium points are discussed in Subsection 2.3.5.

2.3.1 State-space model

A model describing the closed-loop system can be formulated as follows

$$\begin{aligned} \dot{\overline{x}} &= \overline{A}\overline{x} + \overline{B}dz_{2\alpha}(y) + \overline{H}u_2, \quad \overline{x}(t=0) = \overline{x}_0 \\ y &= \overline{C}\overline{x}, \end{aligned} \tag{2.33}$$

where

$$\Theta_s = dz_{2\alpha}(\Theta_d) = \begin{cases} \Theta_d - \alpha, & \Theta_d > \alpha, \\ 0, & |\Theta_d| < \alpha, \\ \Theta_d + \alpha, & \Theta_d < -\alpha \end{cases} \tag{2.34}$$

and

$$\begin{aligned} \overline{x} &= \begin{bmatrix} \Theta_l & \omega_l & \Theta_m & \omega_m & PI_I & PID_D & PID_I \end{bmatrix}^T, \\ u_2 &= T_{m2}, \\ y &= \Theta_d = \Theta_m - \Theta_l. \end{aligned} \tag{2.35}$$

The states PI_I, PID_D and PID_I correspond to the state-space representation in Section 2.2. The system matrices are given as

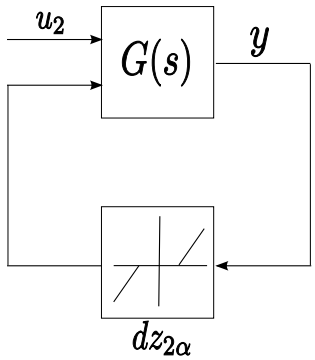

Figure 2.7: Block diagram of the dead-zone-based backlash model with $G(s) = \overline{C}(sI - \overline{A})^{-1}\overline{B}$ and u_2 as constant input on the load side.

$$\overline{A} = \begin{bmatrix} 0 & 0.1786 & 0 & 0 & 0 & 0 & 0 \\ 0 & -0.1786 & 0 & 0 & 0 & 0 & 0 \\ 0 & 0 & 0 & 2.5 & 0 & 0 & 0 \\ 0 & 0 & 0 & -125.3 & 50 & 0 & 0 \\ -105 & 0 & 0 & -6.25 & 0 & -2 \cdot 10^4 & 2.5 \\ -2 & 0 & 0 & 0 & 0 & -400 & 0 \\ -1.333 & 0 & 0 & 0 & 0 & 0 & 0 \end{bmatrix},$$

$$\overline{B} = \begin{bmatrix} 0 \\ 3300 \\ 0 \\ -3300 \\ 0 \\ 0 \\ 0 \end{bmatrix}, \tag{2.36}$$

$$\overline{H} = \begin{bmatrix} 0 \\ 1 \\ 0 \\ 0 \\ 0 \\ 0 \\ 0 \end{bmatrix},$$

$$\overline{C} = \begin{bmatrix} -1 & 0 & 1 & 0 & 0 & 0 & 0 \end{bmatrix}.$$

2.3.2 Transformation into controllable canonical form

Now, the system $(\overline{A}, \overline{B}, \overline{H}, \overline{C})$ is transformed into a controllable canonical form via a transformation matrix T, [14]. The new system description is given as

$$\begin{aligned} x =& T\overline{x}, \\ A =& T\overline{A}T^{-1}, \\ B =& T\overline{B}, \\ H =& T\overline{H}, \\ C =& \overline{C}T^{-1}. \end{aligned} \tag{2.37}$$

Thus, the system matrices have the form:

$$\begin{aligned} A &= \begin{bmatrix} 0 & 1 & \cdots & 0 \\ \vdots & \vdots & \cdots & \vdots \\ 0 & 0 & \cdots & 1 \\ -a_0 & -a_1 & \cdots & -a_{n-1} \end{bmatrix}, \\ B &= \begin{bmatrix} 0 \\ \vdots \\ 0 \\ 1 \end{bmatrix}, \\ H &= \begin{bmatrix} h_0 \\ \vdots \\ h_{n-1} \end{bmatrix}, \\ C &= \begin{bmatrix} c_0 & c_1 & \dots & c_{n-1} \end{bmatrix}. \end{aligned} \tag{2.38}$$

2.3.3 Equilibrium points

The equilibrium points for the original, untransformed system are given as

$$\dot{\overline{x}} = 0 = \overline{A}\overline{x} + \overline{B}dz_{2\alpha}(y) + \overline{H}u_2. \tag{2.39}$$

As this nonlinear set of equations is difficult to solve, equally the following set can be considered

$$\begin{aligned} y &= -\overline{CA}^{-1}(\overline{B}\Theta_s + \overline{H}u_2) \\ \Theta_s &= dz_{2\alpha}(y). \end{aligned} \tag{2.40}$$

In the present case, $\overline{A}$ is not invertible. Thus, we make use of the transformed system equations in controllable canonical form obtained before. In the following the transformed system will be again denoted as (A, B, H, C). The equilibria of the system have then the form

$$\begin{aligned} 0 = \dot{x} &= \begin{bmatrix} 0 & 1 & \cdots & 0 \\ \vdots & \vdots & \cdots & \vdots \\ 0 & 0 & \cdots & 1 \\ -a_0 & -a_1 & \cdots & -a_{n-1} \end{bmatrix} x + \begin{bmatrix} 0 \\ \vdots \\ 0 \\ 1 \end{bmatrix} dz_{2\alpha}(y) + \begin{bmatrix} h_0 \\ \vdots \\ h_{n-1} \end{bmatrix} u_2 \\ y &= \begin{bmatrix} c_0 & c_1 & \dots & c_{n-1} \end{bmatrix} x. \end{aligned} \tag{2.41}$$

In this representation, one can see that the equilibrium states $x_2 \dots x_n$ only depend on the constant input u_2, whereas x_1 depends on all other states, the constant input u_2 and the system output y.

In explicit form the equilibrium conditions can be written as

$$\begin{aligned}
\dot{x}_1 = 0 = x_2 + h_0 u_2 \quad &\Rightarrow \quad x_2 = -h_0 u_2 \\
&\vdots \\
\dot{x}_{n-1} = 0 = x_n + h_{n-2} u_2 \quad &\Rightarrow \quad x_n = -h_{n-2} u_2 \\
\dot{x}_n = 0 = -a_0 x_1 - \ldots - a_{n-1} x_n - h_{n-1} u_2 + dz_{2\alpha}(y).&
\end{aligned} \tag{2.42}$$

The equation for $\dot{x}_n = 0$ can be formulated in dependency of x_1 and u_2 as

$$\begin{aligned}
\dot{x}_n = 0 &= -a_0 x_1 + a_1 h_0 u_2 + \ldots + a_{n-1} h_{n-2} u_2 - h_{n-1} u_2 + dz_{2\alpha}(Cx) \\
\dot{x}_n = 0 &= -a_0 x_1 + a_1 h_0 u_2 + \ldots \\
&\quad + a_{n-1} h_{n-2} u_2 - h_{n-1} u_2 + dz_{2\alpha}(c_0 x_1 - c_1 h_0 u_2 \ldots - c_{n-1} h_{n-2} u_2).
\end{aligned} \tag{2.43}$$

Next, we introduce two constants K_1 and K_2

$$K_1 = a_1 h_0 + \ldots + a_{n-1} h_{n-2} - h_{n-1}, \tag{2.44}$$

$$K_2 = -c_1 h_0 - \ldots - c_{n-1} h_{n-2}. \tag{2.45}$$

Assume, that there is at least one pair $a_i h_{i-1} \neq 0$ and one pair $c_i h_{i-1} \neq 0$.

So we can write

$$\dot{x}_n = 0 = -a_0 x_1 + K_1 u_2 + dz_{2\alpha}(c_0 x_1 + K_2 u_2). \tag{2.46}$$

The equilibria of the system depend only on x_1 and u_2, as well as the dead-zone width α. Now, assume $u_2 = const.$ In the present case it is furthermore $a_0 = 0$, thus the last equation reduces to

$$\dot{x}_n = 0 = K_1 u_2 + dz_{2\alpha}(c_0 x_1 + K_2 u_2). \tag{2.47}$$

Summarizing, the equilibrium equations are given as

$$\dot{x}_n = 0 = K_1 u_2 + dz_{2\alpha}(c_0 x_1 + K_2 u_2) \tag{2.48}$$
$$x_i = -h_{i-2} u_2, \quad i = 2 \dots 6.$$

For the determination of the equilibria, we can distinguish two main cases:

- Case 1: $u_2 = 0$.
- Case 2: $u_2 \neq 0$.

Equilibrium points for $u_2 = 0$

Then equation (2.47) reduces to

$$0 = dz_{2\alpha}(c_0 x_1), \tag{2.49}$$

where the only possible solution is $|\frac{x_1}{c_0}| < \alpha$. Then all possible equilibria of x_1 lay inside the dead-zone. If we solve this inequality, we have to consider:

1. $\frac{x_1}{c_0} < \alpha$. Then for x_1 it holds

$$x_1 < \frac{\alpha}{c_0}. \tag{2.50}$$

All other states become 0, as they depend only on u_2 and $u_2 = 0$. Thus, we can express the system output y as

$$y = c_0 x_1. \tag{2.51}$$

From equation (2.50) it follows that $y < \alpha$. Thus, the system output lays inside the dead-zone for all possible equilibria.

2. $\frac{x_1}{c_0} > -\alpha$. According to the previous discussed case, obviously it is $y > -\alpha$ and therefor all possible equilibrium points lay again inside the dead-zone.

Summarizing, in case $u_2 = 0$ there exist numerous equilibrium points for $-\alpha < y < \alpha$.

Equilibrium points for $u_2 \neq 0$

In the case $u_2 \neq 0$ solutions of (2.47) exist for:

1. $c_0 x_1 + K_2 u_2 < -\alpha$. In this case equation (2.47) leads to

$$\dot{x}_n = 0 = K_1 u_2 + c_0 x_1 + K_2 u_2 + \alpha \tag{2.52}$$

and

$$x_1 = \frac{-(K_2 + K_1)u_2 - \alpha}{c_0}. \tag{2.53}$$

Thus, there is only one possible equilibrium point for a fixed value of u_2.

Inserting the result in

$$dz_{2\alpha}(c_0 x_1 + K_2 u_2), \tag{2.54}$$

gives the condition

$$-K_1 u_2 - \alpha < -\alpha \equiv -K_1 u_2 < 0. \tag{2.55}$$

An interpretation of the latter equation is that an equilibrium point on the left contact side only exists if $u_2 > 0$ and $K_1 > 0$ or if $u_2 < 0$ and $K_1 < 0$.

2. $c_0 x_1 + K_2 u_2 > \alpha$. In this case equation (2.47) leads to

$$\dot{x}_n = 0 = K_1 u_2 + c_0 x_1 + K_2 u_2 - \alpha \tag{2.56}$$

and

$$x_1 = \frac{-(K_2 + K_1)u_2 + \alpha}{c_0}. \tag{2.57}$$

Inserting the result in

$$dz_{2\alpha}(c_0 x_1 + K_2 u_2), \tag{2.58}$$

gives the condition

$$-K_1 u_2 + \alpha > \alpha \equiv -K_1 u_2 > 0. \tag{2.59}$$

Thus, there exists only one possible equilibrium point for a fixed u_2 and it can only lay on the right contact side for $u_2 > 0$ and $K_1 < 0$ or $u_2 < 0$ and $K_1 > 0$.

Consequently, an equilibrium point outside the dead-zone can be achieved by setting $u_2 \neq 0$. By choosing the sign of u_2 one can even determine on which contact side, the equilibrium lays. For every $u_2 \neq 0$ there exists only one equilibrium point.

An interesting observation can be made, when transforming the equilibrium point obtained for (A, B, H, C) and $u_2 \neq 0$ into the original coordinates. The state vector has then only entries unequal 0 on the states representing the motor position and the integrator of the inner-loop PI-controller, that is

$$\overline{x}_{eq} = \begin{bmatrix} 0 & 0 & \Theta_{m,eq} & 0 & PI_{I,eq} & 0 & 0 \end{bmatrix}^T. \tag{2.60}$$

Furthermore, reconstructing the state vector in the original variables at an equilibrium point obtained for $u_2 \neq 0$ leads to

$$\overline{x}_{eq} = T(:,1)^{-1} x(1) + T(:,2:7)^{-1} x(2:7). \tag{2.61}$$

By inserting the equations holding at an equilibrium one obtains

$$\overline{x}_{eq} = -T(:,1)^{-1} \frac{K1 + K2}{c_0} u_2 + T(:,1)^{-1} \frac{\alpha}{c_0} sign(u_2) - T(:,2:7)^{-1} H(1:6) u_2. \tag{2.62}$$

Inserting the numerical values, one obtains

$$\overline{x}_{eq} = \begin{bmatrix} 0 \\ 0 \\ -0.0155 \\ 0 \\ 0 \\ 0 \\ 0 \end{bmatrix} u_2 + \begin{bmatrix} 0 \\ 0 \\ 0.0873 \\ 0 \\ 0 \\ 0 \\ 0 \end{bmatrix} sign(u_2) + \begin{bmatrix} 0 \\ 0 \\ 0.0161 \\ 0 \\ -0.0200 \\ 0 \\ 0 \end{bmatrix} u_2. \tag{2.63}$$

Thus, in an equilibrium point only the values of Θ_m and PI_I are different from 0 and are directly influenced by the choice of u_2. All the other states remain 0, which is physically traceable, as in an equilibrium the angular velocities should be 0. Additionally, the load position should be 0, as no input reference is considered and therefore $PID_D = 0$ and $PID_I = 0$.

The system output y is given as

$$y = \overline{C}\overline{x}. \tag{2.64}$$

Remember, in the present case $\overline{C}$ has the form

$$\overline{C} = \begin{bmatrix} -1 & 0 & 1 & 0 & 0 & 0 & 0 \end{bmatrix}. \tag{2.65}$$

Making use of equation (2.63), we can write the stationary value of y as a function of u_2

$$y = c_2\overline{x}_3 = -0.0155u_2 + 0.0873sign(u_2) + 0.0161u_2. \tag{2.66}$$

Thus, as the used nominal parameters give $K_1 < 0$, for every $u_2 > 0$ the equilibrium point lays on the right side of the dead-zone and y becomes

$$y = K_3u_2 + \alpha. \tag{2.67}$$

Whereas for every $u_2 < 0$, the equilibrium point lays on the left side of the dead-zone and y becomes

$$y = K_3 u_2 - \alpha, \tag{2.68}$$

where K_3 is a constant with $K_3 = 0.0006$.

2.3.4 Stability analysis

In the previous subsection, the existence of equilibrium points in the system was shown. Now, their local stability is analyzed. The analysis is carried out in the original system representation $\overline{A}, \overline{B}, \overline{H}, \overline{C}$. This is possible as there exists an unique transformation T from $\overline{x}$ to x and therefor also from x to $\overline{x}$ with $\overline{x} = T^{-1}x$.

Local stability for $u_2 = 0$

We have shown, that for $u_2 = 0$ there exist multiple equilibria inside the dead-zone. If we linearize the system around one arbitrary chosen equilibrium point, which satisfies the above condition, e.g. $y = \frac{\alpha}{2}$, we obtain

$$\begin{aligned} \dot{\overline{x}} &= \overline{A}\overline{x} \\ y &= \overline{C}\overline{x}. \end{aligned} \tag{2.69}$$

As A has several eigenvalues with $Re(\lambda) = 0$, the system is unstable. This statement holds for all possible equilibrium points obtained when $u_2 = 0$.

Local stability for $u_2 \neq 0$

For every $u_2 \neq 0$ an equilibrium point is defined. If we linearize the system around the equilibrium obtained by choosing an arbitrary value of $u_2 \neq 0$, we obtain

$$\begin{aligned} \dot{\overline{x}} &= \overline{A}\overline{x} + \overline{B}(y \pm \alpha) + \overline{H}u_2 \\ y &= \overline{C}\overline{x}. \end{aligned} \tag{2.70}$$

So we can write

$$\dot{\overline{x}} = (\overline{A} + \overline{BC})\overline{x} + \overline{B}(\pm\alpha) + \overline{H}u_2 \tag{2.71}$$
$$y = \overline{C}\overline{x}.$$

Let us denote $\overline{A}_{cl} = \overline{A} + \overline{BC}$. All poles of $\overline{A}_{cl}$ lay in the LHP, with being $\max(Re\lambda_i) = -0.9317$, $i = 1 \ldots 7$. Thus the system is local asymptotically stable.

The analysis shows that local stability can be achieved by any $u_2 \neq 0$. However, for making sure the stable performance around the equilibrium point some $|u_2| > |\delta| > 0$ is required. This is emphasized by simulations, which show that u_2 has to have a certain magnitude for stabilizing the system. An interpretation would be, that the region of attraction of the equilibrium point increases with increasing magnitude of $|u_2|$.

2.3.5 Physical aspects to consider

In the previous lines, it was shown that there exists a locally stable equilibrium point for every $u_2 \neq 0$. A remarkable point, is that every equilibrium point obtained with some $u_2 \neq 0$ leads to a relative position angle $|\Theta_d| > \alpha$. The higher the magnitude of u_2, the higher the difference $|\Theta_d| - \alpha$.

This is explainable by considering again the formula defining the shaft torque

$$T_s = k_s(\Theta_m - \Theta_l). \tag{2.72}$$

In the present case, k_s and Θ_l are constant, as the latter is the control variable and is set to a desired but fixed value. Thus for increasing the shaft torque, the only possibility is to increase Θ_m. Even for the 'normal' case, where $\Theta_l \neq const$ the relative position angle has to increase in order to increase the transmitted shaft torque.

This observation can also be made in simulations with a Simulink model, which includes a more sophisticated backlash-model, proposed by Nordin *et. al* e.g., in [2]. A gratifying fact is that the equilibrium points obtained by simulations with this model correspond quite precisely with these of the analytical analysis based on the dead-zone model.

For relatively small differences $|\Theta_d| - \alpha < \epsilon$ this fact is physically logical, as one could interpret the additional deformation $\Theta_s = \Theta_d - \Theta_b = \Theta_d - \alpha$ as a consequence of the shaft-elasticity. For higher differences, it must be noted that the model does not completely reflect the real physical behavior of the system, as there is no constrained on $\Theta_d = \Theta_m - \Theta_l$ which represents the blocking/braking of the shaft after its maximum deformation. However, this is a minor aspect as it does not query the results of the analysis.

2.4 Dual motor control with constant load torque

Now, simulations with the nonlinear two-mass model are presented to verify the results of Section 2.3. Thus, the limit cycles are intended to be avoided and the system to be stabilized by applying a constant torque T_{m2} on the load side. In a first step, this can be carried out in two different ways: Either using a constant torque from the beginning of the motion on, that is $t = 0$ or to apply the constant torque not until a to defining point in time on with $t > 0$. An example for the selection of such a point in time would be the beginning of oscillations in the system, when no torque at all is applied.

The sign of the torque, which should be opposite to the main driving direction of the system is defined by the following function

$$v = \text{sign}(x_{ref,old} - x_{ref,new}). \tag{2.73}$$

The torque can then be defined as

$$u_2 = |T_{m2}|\text{sign}(v). \tag{2.74}$$

The remaining parameter to choose is the magnitude of the constant torque T_{m2}. In Fig. 2.8 simulation results for different magnitudes of T_{m2} applied at $t = 0$ [s] are presented. One can observe, that for low values of T_{m2} the backlash effect cannot be avoided completely and there still exist limit cycles. A low torque even speeds up their appearance.

On the other side, one can see that high values of T_{m2} lead to a negative response behavior of the system, since in the beginning $T_{m2} > T_{m1}$. But for certain values of

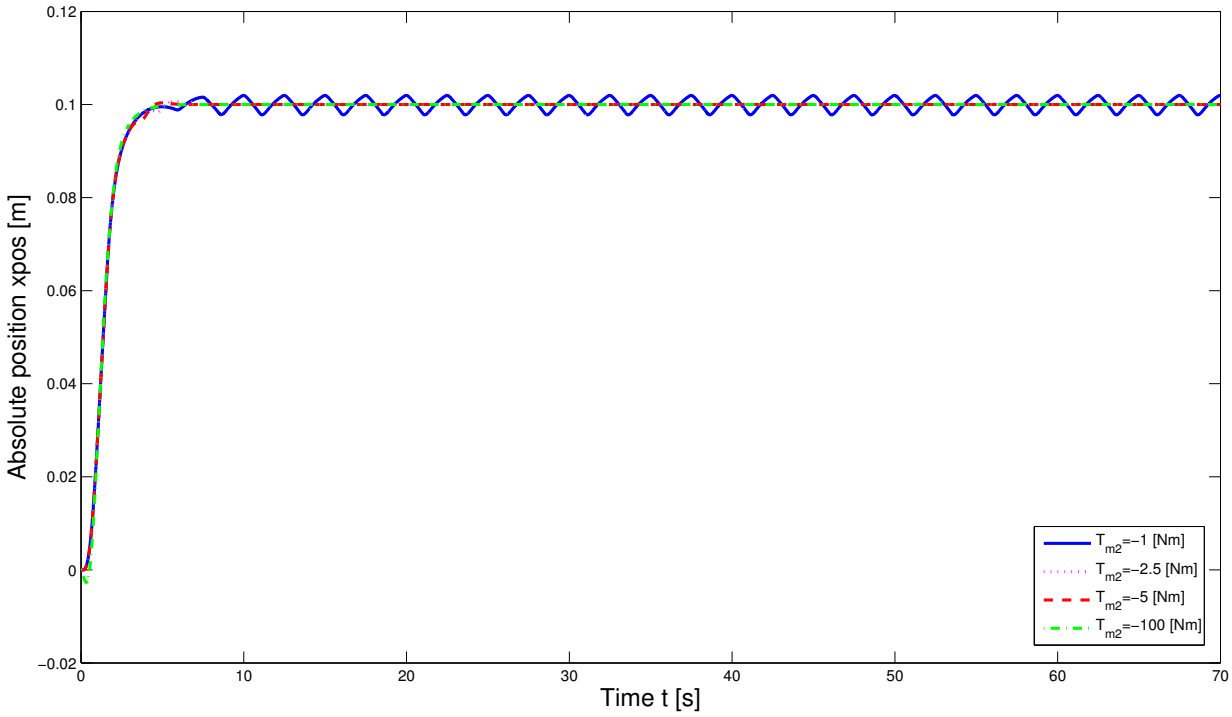

Figure 2.8: Performance of the nonlinear two-mass system for different magnitudes of T_{m2} applied at $t = 0$ [s]. The limit cycles can be oppressed with a torque magnitude of $T_{m2} \geq -2.5$ [Nm].

intermediate magnitude the limit cycles can be completely eliminated without a strong negative response behavior. For the considered nominal system, e.g. a constant torque of $T_{m2} = -5$ [Nm] leads to satisfactory results.

In Fig. 2.9 the torque is not applied until $t = 65$ [s], that is when limit cycles already exist. The behavior of the system is similar to the one described before, but no negative response behavior can be observed.

Another parameter to define is the sign of the torque, which should be opposite to the main driving direction of the system. A function achieving this is given by

$$v = \text{sign}(x_{ref,old} - x_{ref,new}). \tag{2.75}$$

Two simulation results for a constant torque starting at $t = 0[s]$ with $T_{m2} = -5[Nm]$ and $t = 60[s]$ with $T_{m2} = -5[Nm]$ are shown in Fig. 2.10 and Fig. 2.11 respectively. As

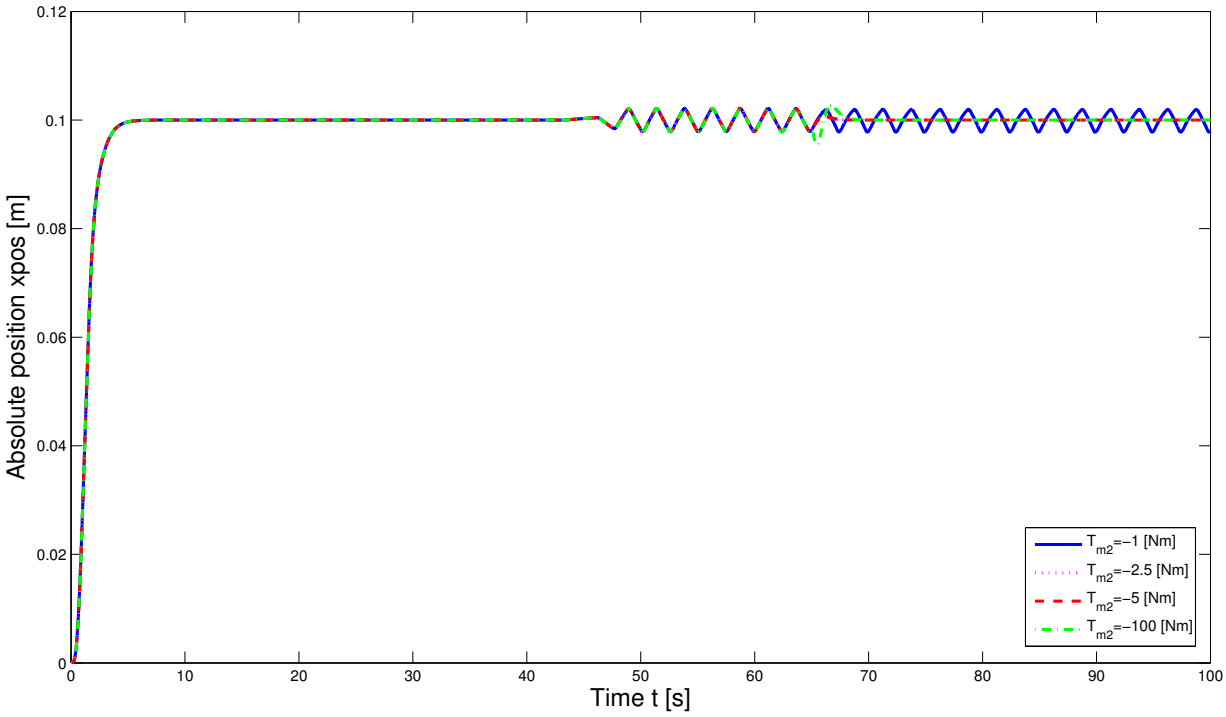

Figure 2.9: Performance of the nonlinear three-mass system for different magnitudes of T_{m2} applied at $t = 65$ [s]. The limit cycles can again be oppressed with a torque magnitude of $T_{m2} \geq -2.5$ [Nm] and no negative response behavior is observed.

before, the step height is set to 0.01 [m] and the system is assumed to be in contact in the beginning of the motion, that is $\Theta_d(t = 0) = \alpha$.

Concluding, the results obtained in Section 2.3 are verified in the simulations. The system is stabilizable by acting with an additional constant torque on the load side. However, as this operation mode only influences the equilibrium point of the system and thus its local stability, a certain magnitude of the torque is required for a stable performance. This also corresponds to the remarks made in Section 2.3, where an increasing torque magnitude is interpreted as an increasing region of attraction of the equilibrium point.

Thus, the approach of using a dual motor control strategy to reduce the backlash effects in a robot actuator seems feasible. Applying a torque from $t = 0[s]$ on, leads to a smoother response of the system, but requires a higher controller output. Additionally, a

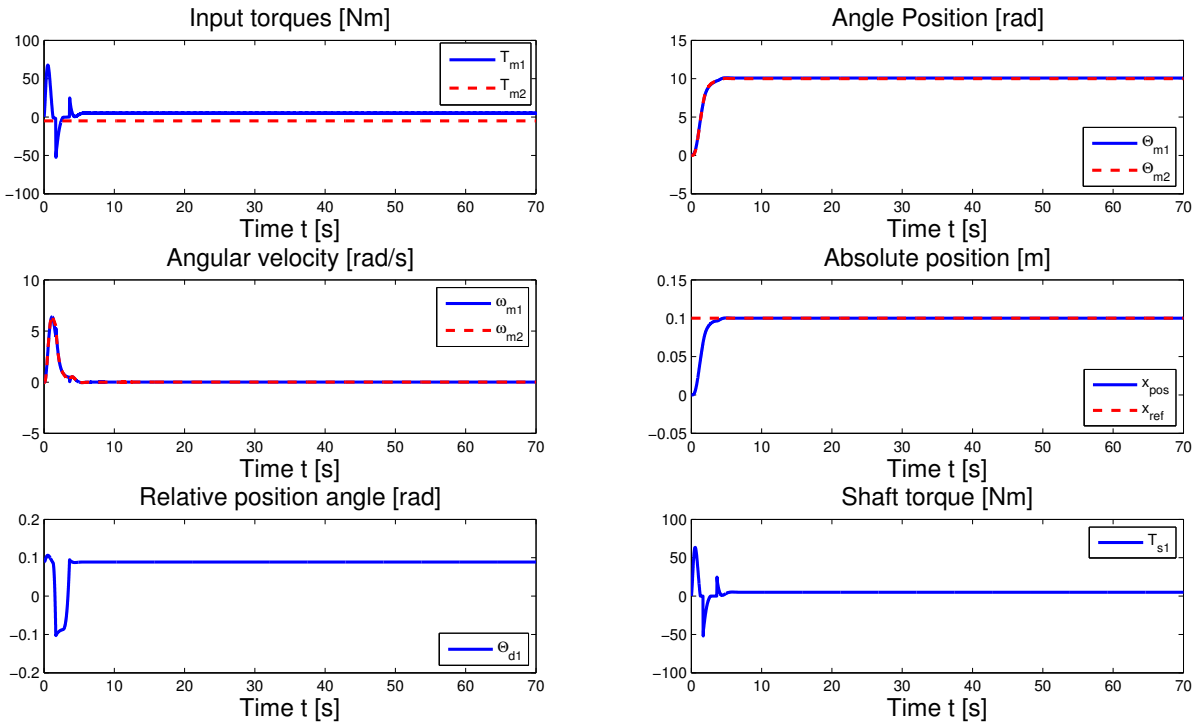

Figure 2.10: Dual motor control with constant torque $T_{m2} = -5$ [Nm] at $t = 0$ [s]. As consequence of the constant torque, no limit cycles appear and the system reaches its desired final position.

negative response behavior can be observed in the beginning of the motion. When applying the torque on a later point in time, the already existing limit cycles are also eliminated and no negative response behavior is observed. The latter observation, leads to the idea of developing strategies to control the operation of the constant torque T_{m2} in order to reduce the required input energy. One way to achieving this, is by trying to act only with T_{m2} when limit cycles would occur in the system for $T_{m2} = 0$.

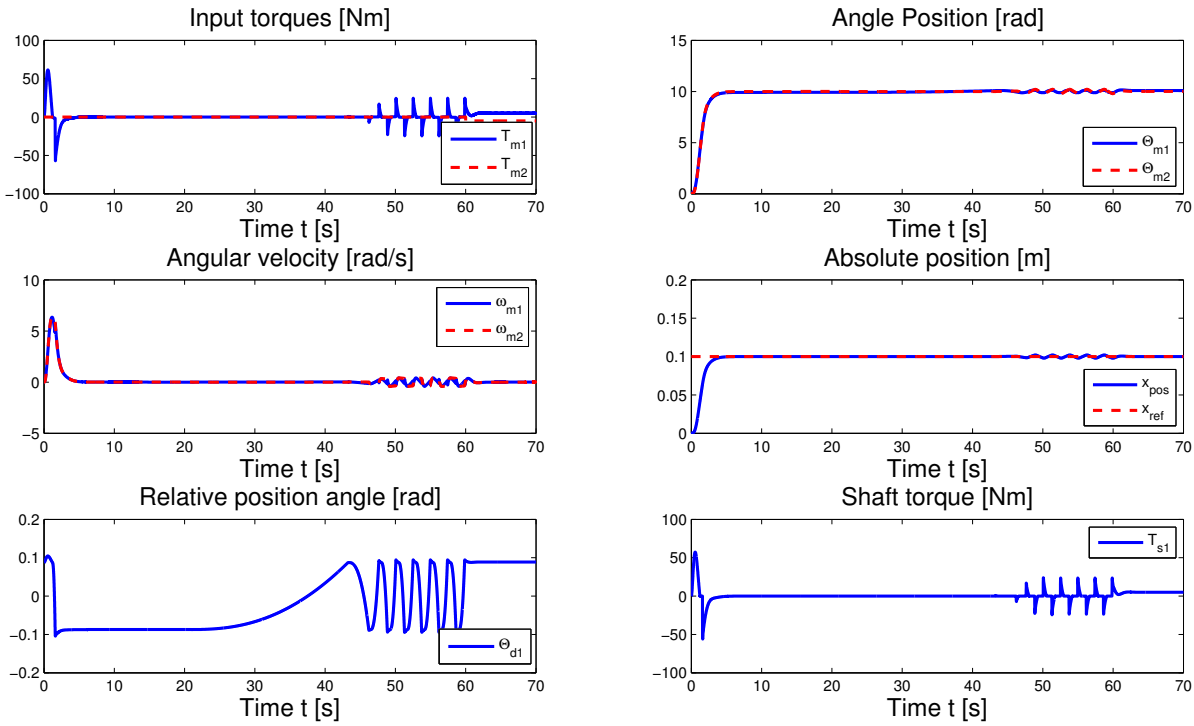

Figure 2.11: Dual motor control with constant torque $T_{m2} = -5$ [Nm] at $t = 60$ [s].The limit cycles appear approximately after 60 [s] and can be oppressed by a constant torque, which starts acting after 60 [s].

2.5 Nonlinear dual motor control of a two-mass system

For improving the performance and energy consumption of the system it is desirable, to use the constant torque opposite to the driving direction only when the system would undergo limit cycles without it.

As can be seen in the simulations in Subsection 2.2.3, this is mainly the case, when the load reaches its final desired position. Then the second motor should be used to act in the opposite direction of the driving motor in order to close the backlash gap. But before one can operate without it and obtains a comparably good performance.

As consequence of these facts, more sophisticated operating strategies are developed in order to reduce the required total input power of the system. The aim is to use the second motor for fast closing the backlash gap and avoiding limit cycles, but only when the system gets into backlash.

All strategies have the following characteristics in common:

- For determining T_{m2} the following function is defined:

$$u_2 = K_{T_{const}} v = 5v, \tag{2.76}$$

  where $v \in [0, 1]$ is the respective switching variable. This implementation follows an approach for a switched controller given in [4], but with a varied determination of v. Different definitions for v are given in equations (2.75), (2.77), (2.78) and (2.79). The gain is chosen according to the results of Section 2.4.

  The first function for v determines T_{m2} regarding the relative position angle Θ_d, whereas the second function does the same but depending on the relative error e_{abs}. The third and last approach represents a combination of the first and the second option. All implementations lead to a nonlinear, smooth switching mode for T_{m2}.

  As the torque is not constantly applied from the beginning on in all cases a magnitude of $|T_{m2}| = 5$ may be sufficiently high according to the simulation results shown of Section 2.4. That is why $K_{T_{const}}$ is set to $u_2 = K_{T_{const}} v = 5v$ for the upcoming operating strategies, where v represents the switching variable.

- The values $x_{ref,old}$ and $x_{ref,new}$ refer to the actual and to the desired final position. Their difference allows to determine whether the motion occurs in positive or negative direction, as $x_{ref,old} < x_{ref,new}$ means a motion in positive direction and $x_{ref,old} > x_{ref,new}$ means a motion in negative direction. The sign of the torque of the second motor should always be opposite to the motion direction.

The step height is set to 0.1 [m] and the system is assumed to be in contact in the beginning of the motion, that is $\Theta_d(t = 0) = \alpha$. The plots for illustrating the simulation

results do normally not cover the same time period as the one for demonstrating the arise of limit cycles in the nonlinear system of the previous section($t = [0, 70]$ [s]), but a shorter one. This is due, to a better presentation of the performance of each switching strategy. Of course, all strategies are tested for longer time periods up to 500 [s].

2.5.1 Switching-strategy for dual motor control depending on Θ_d

The proposed control strategy in this section is based on the relative position angle between then motor and the load $\Theta_d = \Theta_m - \Theta_l$, as this is an indicator whether the system is actually operating in backlash mode or not. If the system is not in backlash, that is $|\Theta_d| > \alpha$, no opposite torque should be used. But if the system is in backlash, that is $|\Theta_d| < \alpha$, the second motor on the load side should act in opposite direction of the motion, as presented in Section 2.4.

The switching variable v is defined as

$$v = \begin{cases} 0, & |\Theta_{d1}| > \alpha \\ \text{sign}(x_{ref,old} - x_{ref,new}) \frac{\alpha - |\Theta_d|}{\frac{\alpha}{2}}, & \frac{\alpha}{2} \leq |\Theta_d| \leq \alpha \\ \text{sign}(x_{ref,old} - x_{ref,new}), & |\Theta_d| < \frac{\alpha}{2}. \end{cases} \tag{2.77}$$

The function is illustrated in Fig. 2.12. This strategy leads to the result presented in Fig. 2.13. One can observe, that the result is not satisfactory as there show up some outliers. This might be mainly due to a sporadic switching between the backlash and non-backlash case. Additionally, no constant torque is continuously applied in the final position what makes the system sensible to disturbances and referring to the stability analysis carried out in Section 2.3 no local stability can be stated. However, this strategy might be hard to apply in practice as normally measuring of Θ_l is not possible.

Conclusions:

- No elimination of limit cycles, when disturbances are present.
- Advantage: Closing backlash gap when existing, even in the beginning.

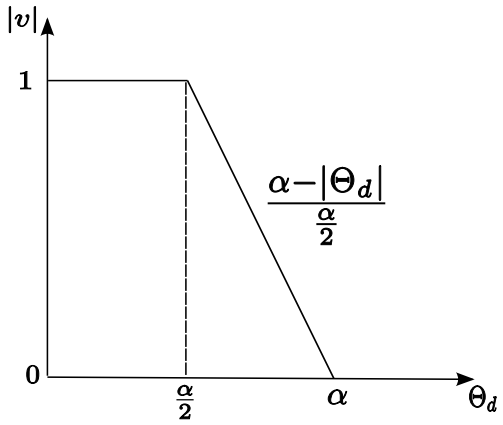

Figure 2.12: Switching function $v = f(\Theta_d)$. $|v|$ takes the value 1, when $|\Theta_d| < \frac{\alpha}{2}$. If $|\Theta_d| > \alpha$, v takes the value 0 and for all other cases $v \in [0, 1]$.

- Disadvantage: Negative response behavior can occur, information about backlash gap size needed.
- Requirements cannot be fulfilled.
- No local stability guaranteed according to the analysis of Section 2.3.

2.5.2 Switching-strategy for dual motor control depending on e_{abs}

Now, the switching-strategy is oriented on the relative error $e_{abs} = \frac{|x_{ref,new} - x_{meas}|}{|x_{ref,new} - x_{ref,old}|}$. This option utilizes the knowledge, that the main influence of the backlash angle occurs when the cart is reaching its final position. This is manifested by the arise of limit cycles. Thus, the relative error may be used as an indicator, when the second motor should act with a constant torque. The function $v = f(e_{abs})$ is implemented as follows

$$v = \begin{cases} 0, & e_{abs} > e_{max} \\ \text{sign}(x_{ref,old} - x_{ref,new}) \frac{e_{abs} - e_{max}}{e_{min} - e_{max}}, & e_{min} \leq e_{abs} \leq e_{max} \\ \text{sign}(x_{ref,old} - x_{ref,new}), & e_{abs} < e_{min}, \end{cases} \tag{2.78}$$

with the free parameters e_{max}, e_{min}.

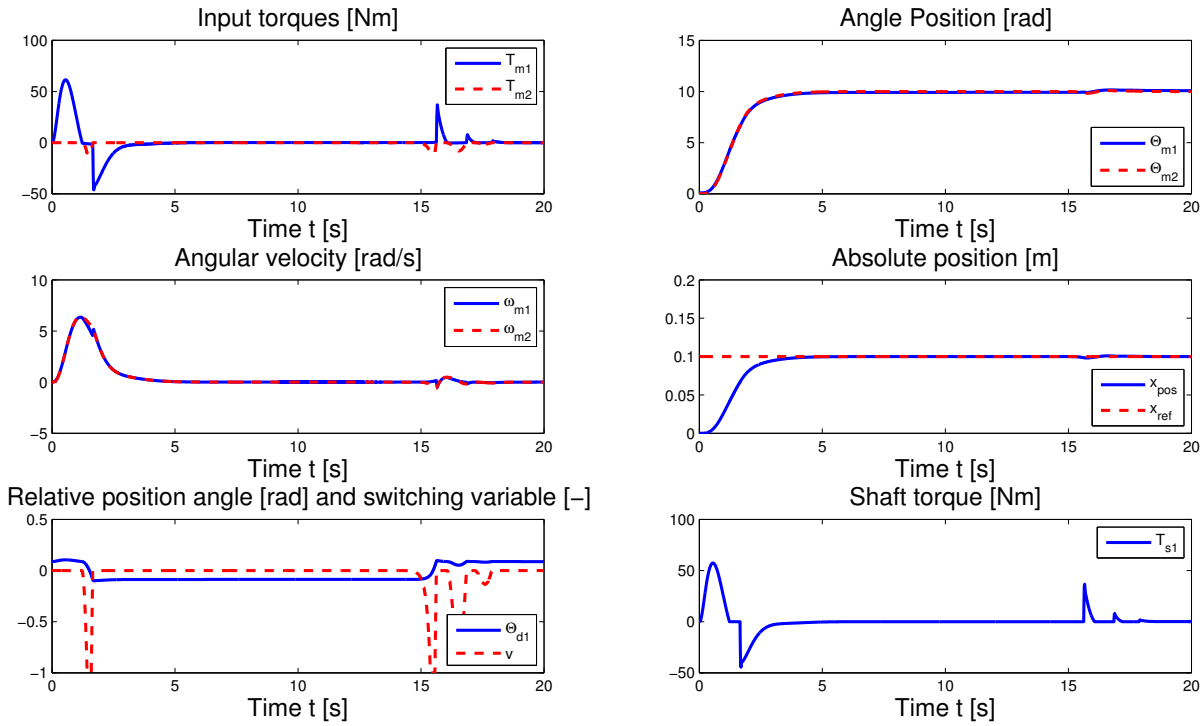

Figure 2.13: Dual motor control with $v = f(\Theta_d)$. No constant torque is continuously applied in the final position which makes the system sensible to disturbances and referring to the stability analysis carried out in Section 2.3 no local stability can be stated.

The function is illustrated in Fig. 2.14 and the performance of this set is shown in Fig. 2.15. The parameters were set to: $e_{max} = 0.25$ and $e_{min} = 0.01$. The limit cycles are oppressed and a smooth response is obtained.

Using this strategy, a constant torque is continuously applied in the final position what makes the system robust against disturbances and referring to the stability analysis carried out in Section 2.3 local stability can be stated.

One important aspect to consider is the system performance for position changes with a path length $l_{path} \leq \alpha r_l$. In such cases no stable performance is achieved as the desired positioning inside the backlash gap leads to a continuous on/off-switching of T_{m2}.

This can be avoided by operating with a constant pretorque on the second motor for reference trajectories with $l_{path} \leq \alpha r_l$.

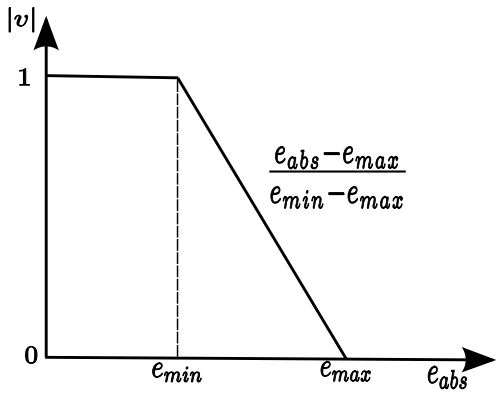

Figure 2.14: Switching function $v = f(e_{abs})$. $|v|$ takes the value 1, when $e_{abs} < e_{min}$. If $e_{abs} > e_{max}$, v takes the value 0 and for all other cases $v \in [0, 1]$.

Another solution for that problem could be to completely avoid small values of l_{path} by artificially increasing the trajectory path for position changes, which are too close together. This can be achieved e.g. by changing the trajectory path from $x_{pos,old} = 0 \rightarrow x_{pos,new} = 0.001$ into $x_{pos,old} = 0 \rightarrow x_{pos,artificial} = -0.1 \rightarrow x_{pos,new} = 0.001$. Then, the positioning can be effectuated in a satisfactory manner, as the implementation has no problem regarding the accuracy for high resoluted reference values, but for trajectory paths $l_{path} \leq \alpha r_l$.

Conclusions:

- Strategy fulfills requirements.
- Local stability can be stated referring to the analysis of Section 2.3.
- Switching dependent on relative error with respect to final position, not on backlash.
- Therefore, no reaction if system is in backlash while $e_{abs} < e_{max}$.
- Strategy is robust against load disturbances and does not lead to negative response behavior.

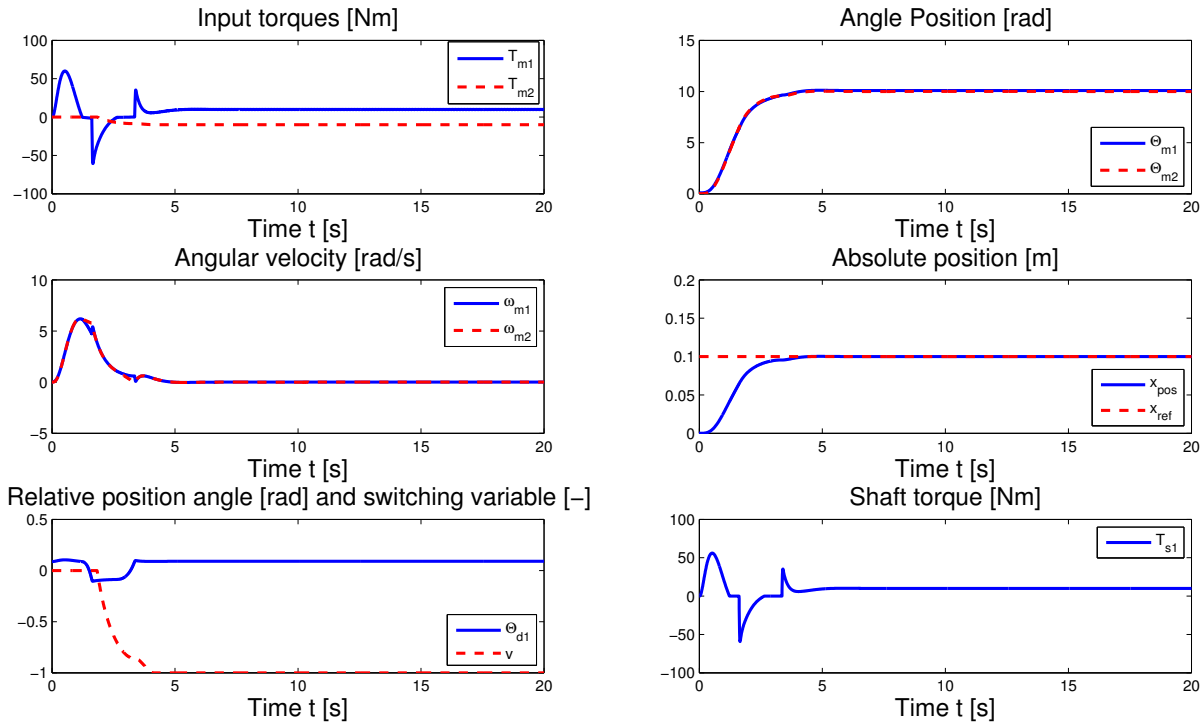

Figure 2.15: Control strategy with $v = f(e_{abs})$. Here, the limit cycles are oppressed. Furthermore a smooth response is obtained and the strategy is robust against disturbances. Referring to the stability analysis carried out in Section 2.3 local stability can be stated as a constant torque is continuously applied in the final position.

2.5.3 Switching-strategy for dual motor control depending on Θ_d and e_{abs}

The last switching-version is a combination of the first and the second. It aims to join both switching reference values Θ_d and e_{abs} in order to be able to react to backlash-situations during the motion and especially avoid limit cycles when reaching the final position. Therefore v is defined as

$$v = \begin{cases} 0, & |\Theta_{d1}| > \alpha \; and \; e_{abs} > e_{max} \\ \text{sign}(x_{ref,old} - x_{ref,new}) \frac{\alpha - |\Theta_d|}{\frac{\alpha}{2}}, & \frac{\alpha}{2} \leq |\Theta_d| \leq \alpha \; and \; e_{abs} > e_{max} \\ \text{sign}(x_{ref,old} - x_{ref,new}), & |\Theta_d| < \frac{\alpha}{2} \; and \; e_{abs} > e_{max} \\ \text{sign}(x_{ref,old} - x_{ref,new}) \frac{e_{abs} - e_{max}}{e_{min} - e_{max}}, & e_{min} \leq e_{abs} \leq e_{max} \\ \text{sign}(x_{ref,old} - x_{ref,new}), & e_{abs} < e_{min}, \end{cases} \tag{2.79}$$

with e_{max}, e_{min} to be chosen appropriately.

This strategy leads to the behavior presented in Fig. 2.16. It shows a satisfactory behavior, similar to the case when $v = f(e_{abs})$. But it could possibly lead to an inverse response behavior, when the system is in backlash at the beginning of the motion. For this strategy, local stability in the final position can be achieved.

Conclusions:

- Satisfactory behavior, similar to case when $v = f(e_{abs})$.
- Local stability can be stated referring to the analysis of Section 2.3.
- Closing of eventual backlash gaps during transition.
- Robust against load disturbances.
- Possibly inverse response behavior.
- Information about backlash gap size needed.

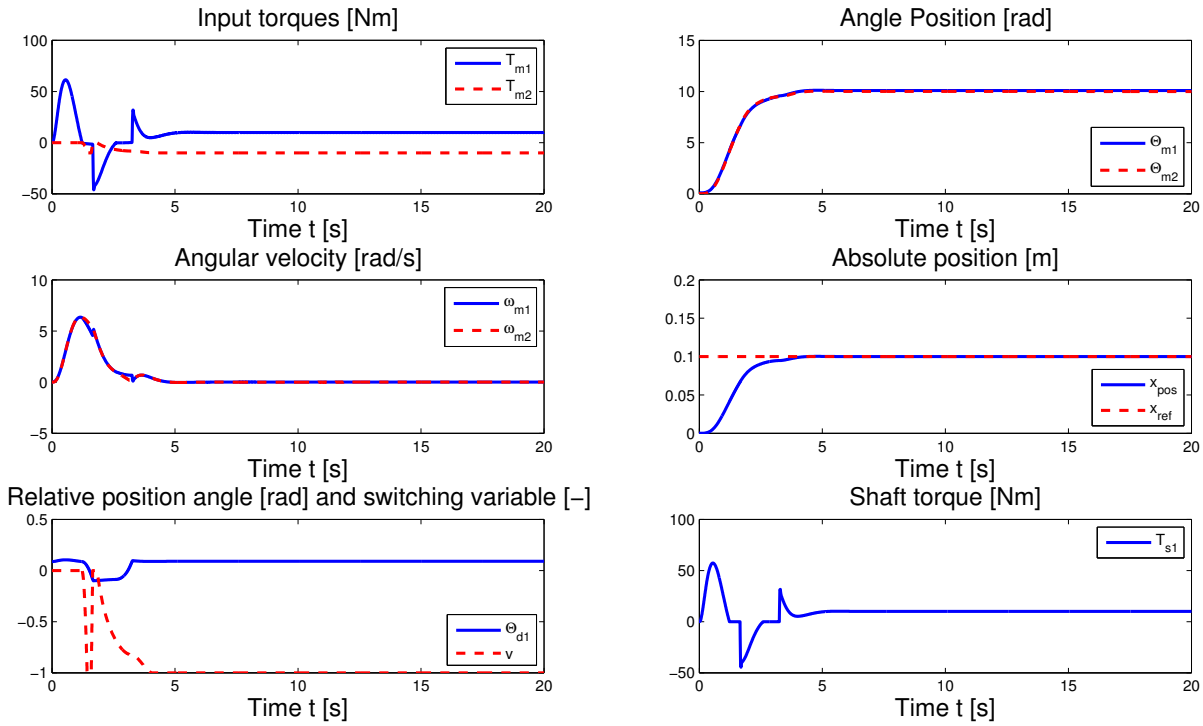

Figure 2.16: Control strategy with $v = f(\Theta_d, e_{abs})$. This alternative shows a satisfactory behavior, similar to the case when $v = f(e_{abs})$. However, it could eventually lead to an inverse response behavior.

2.6 Summary

In this chapter a model of a nonlinear two-mass system has been introduced and analyzed regarding its characteristics when operating with a control structure for the load position and an additional constant torque acting directly on the load.

For this setup, equilibrium points and local stability criteria have been presented, showing that the system is locally stabilizable by introducing this additional constant torque.

Subsequently, different operating modes for the system have been presented and analyzed in simulations in order to improve the system performance. Of these, defining $v = f(e_{abs})$ seems to achieve the best performance in meanings of a smooth and efficient motion, as well as stability. Determining the action of the torque T_{m2} via $v = f(\Theta_d)$ does not lead to satisfactory results. Additionally it might be difficult to estimate the size of

the backlash gap in practice.

Operating with a switching-function based on both variables (e_{abs} and Θ_d), also leads to a less advantageous performance as determining v only depending on the relative error e_{abs}. The main disadvantages of the combination are higher input and shaft torques, which might be provoked by the intention of closing the backlash gap in the beginning of a position change. In that situation, the motors are forced to act against each other.

In conclusion, the most promising strategy seems to be the one based on $v = f(e_{abs})$. Another advantage of this variant is that measuring the position angles Θ_m of motor and Θ_l of the load becomes unnecessary.

Chapter 3

Experimental tests on a nonlinear two-mass system exhibiting backlash

In this chapter, the proposed ideas to reduce and control the backlash-effect in the robot actuators, which have been presented in Chapter 2, are investigated on an experimental plant representing a nonlinear two-mass system exhibiting backlash.

The outline of the chapter is as follows: In the first section (3.1), the laboratory setup is described and a model of the process is derived. Subsequently, the required transfer functions are identified. Afterwards, a position control for the load position Θ_l is designed in Section 3.2 based on a linear model neglecting the backlash. In Section 3.3 the different strategies for defining the torque on the second motor are implemented according to the ones presented in Chapter 2. The control structure is enhanced with the defined functions and subsequently the resulting configurations are tested on the real plant with the backlash element.

3.1 Laboratory setup and modeling

The present laboratory setup could represent e.g., [13] an automotive power-train system. It consists of two equal rotating masses, the backlash element and two equal DC motors of which one is used as driving motor and the other one is used on the load side. The shaft

is rather stiff and does not include a spring element e.g., unlike in [13]. The backlash gap size α is approximately 30°. Furthermore the system features two encoders for position and velocity measurements. The measured values are the motor position Θ_m, the motor velocity ω_m, the load position Θ_l and the load velocity ω_l.

As already stated in Chapter 2, the second motor on the load side may generally be used to simulate load-disturbance effects. But in our case, it will be used to simulate the second motor of the desired dual-motor-drive aiming to close the backlash gap with a torque acting in opposite direction of the driving torque.

No shaft damping nor shaft elasticity is present in the laboratory setup, thus a nonlinear model describing the process is given as

- System in backlash: $|\Theta_d| < \alpha$

$$\begin{aligned} L\frac{di}{dt} &= k_u u_1 - k_G\omega_m - Ri \\ J_m\omega_m &= -c_m\omega_m + k_m i \\ J_l\omega_l &= -c_l\omega_l - T_L \end{aligned} \tag{3.1}$$

- System in contact: $|\Theta_d| > \alpha$ and thus $\Theta_l = \Theta_m \pm \alpha$

$$\begin{aligned} L\frac{di}{dt} &= k_u u_1 - k_G\omega - Ri \\ (J_m + J_l)\omega &= -(c_m + c_l)\omega + k_m i - T_L, \end{aligned} \tag{3.2}$$

where

$$\Theta_d = \Theta_m - \Theta_l \tag{3.3}$$

and

$$T_L = k_m k_I u_2. \tag{3.4}$$

The first equation models the electrical circuit and the second and third model the mechanical part of the process. The latter two are reduced to one equation in the contact-case. Fig. 3.1 shows a picture of the setup.

According to [23], u_1 [V] represents the input voltage of the driving motor, i [A] the resulting current, ω_m [rad] the motor velocity, ω_l [rad] the load velocity and T_L [Nm] an input torque on the load side. The parameter L [Vs/A] reflects the inductivity, R [V/A] the resistance, k_u [-] the power amplifier amplifying coefficient, k_G [Vs/rad] the electro-motor feedback coefficient, J_m [kgm^2/rad] and J_l [kgm^2/rad] the inertias of the masses, c_m [Nm/rad/s] and c_l [Nm/rad/s] the viscous friction on the load and motor side, k_I [A/V] and k_m [Nm/V] the load motor current amplifying factor and the moment of inertia of the servo and load motor respectively.

3.1.1 Stiction analysis

For the purpose of parameter identification the system is first analyzed concerning its stiction and friction, while performing in the different operating conditions mentioned above. The results are shown in Fig. 3.2. As input signals sawtooth-sequences of relatively low amplitudes were used.

One can observe that the stiction differs significantly in all operating points. Sometimes it can be overcome quite easily by low input signals, while other times the process does not move at all even with the highest input signal. As expected the stiction is higher when operating with both masses instead of using just one mass, because of the higher inertia. Furthermore when using both masses, the stiction is higher when the system is stiffly connected than when it operates including the backlash element.

3.1.2 Transfer function identification

For the purpose of controller design a first order model for the linear relation $G_{u_1\omega_l}$ between the input u_1 and the load velocity w_l is identified.

For the identification procedure, the system is stiffly connected and operated with

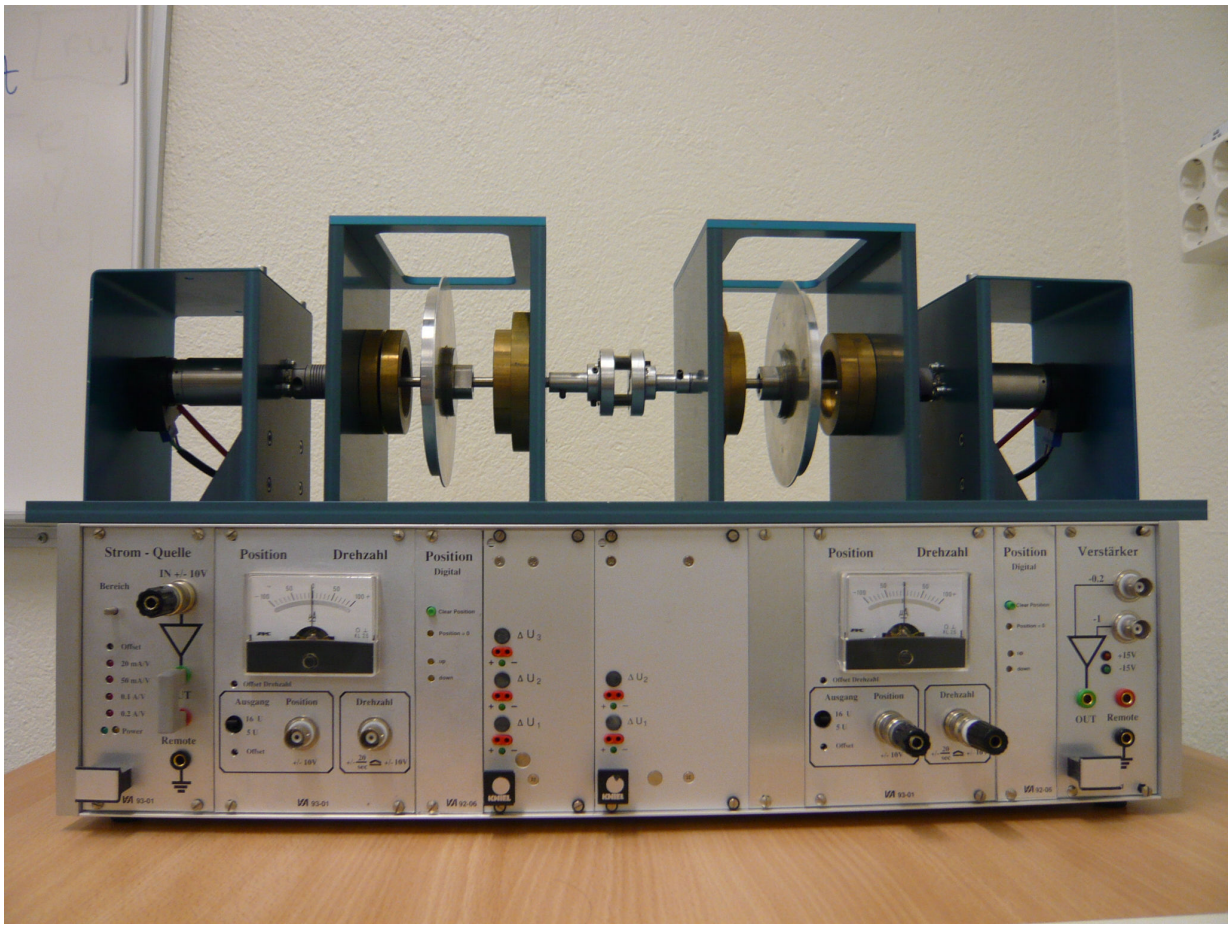

Figure 3.1: Experimental setup with the mass representing the motor on the right and the load on the left side. The backlash element is situated in the middle.

a constant input torque as offset to overcome static influences like stiction. From this configuration on, the system is excited with steps between $[0, 0.3]$ [V]. The obtained data is evaluated using the Matlab-function `pem`.

As result of the identification procedure, a transfer function describing the desired relation is given as

$$G_{u_1\omega_l} = \frac{0.7345}{s + 0.04091}. \tag{3.5}$$

Furthermore, the transfer function describing the relation between u_1 and the load position Θ_l is obtained by enhancing $G_{u_1\omega_l}$ with an integrator, what gives

$$G_{u_1\Theta_l} = \frac{1}{s} G_{u_1\omega_l}. \tag{3.6}$$

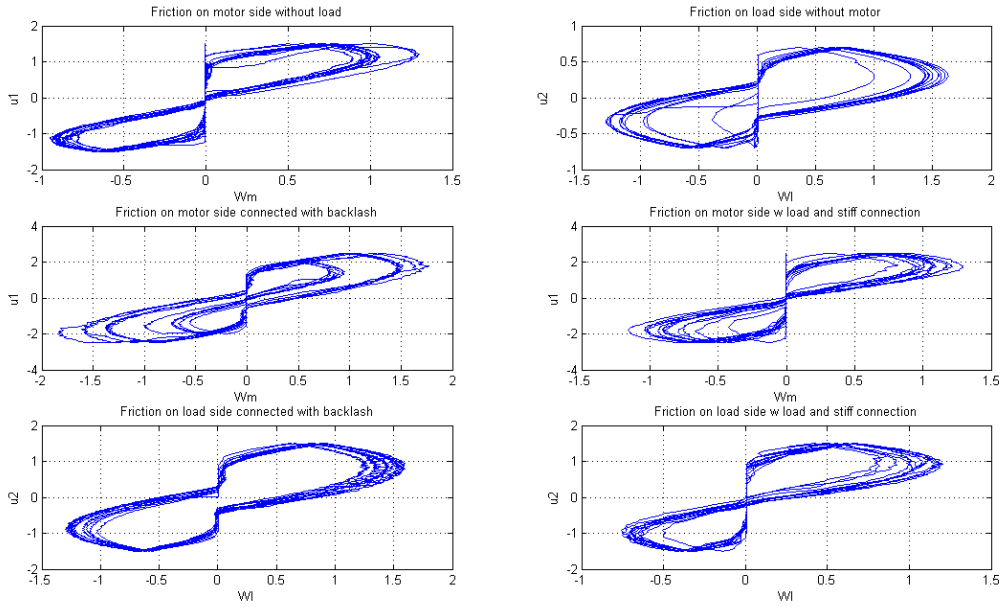

Figure 3.2: The stiction differs significantly in all operating points. Sometimes it can be overcome quite easy by low input signals, while other times the process does not move at all even with the highest input signal.

The first order relation between u_1 and the velocity ω_m of the first mass corresponding to the motor is identified as

$$G_{u_1\omega_m} = \frac{0.8113}{s + 0.3492}. \tag{3.7}$$

One can observe, how the pole of $G_{u_1\omega_l}$ changes due to the additional mass representing the load in comparison to the pole of $G_{u_1\omega_m}$.

An indicator for the matching between the model and the real plant is the correlation between measured and simulated data. Fig. 3.3 shows a step response of both, the experimental plant and the identified transfer function as stated in Eq.(3.5) for a reference step height of 0.1 [V]. The correlation of the error between the measured and simulated data is shown in Fig. 3.4. One can conclude, that the model seems to fit the real system behavior in a quite accurate way.

This is supported by looking at the correlation coefficient, which is defined as [20]

$$r_{X,Y} = \frac{cov(X,Y)}{\sigma_X \sigma_Y}. \tag{3.8}$$

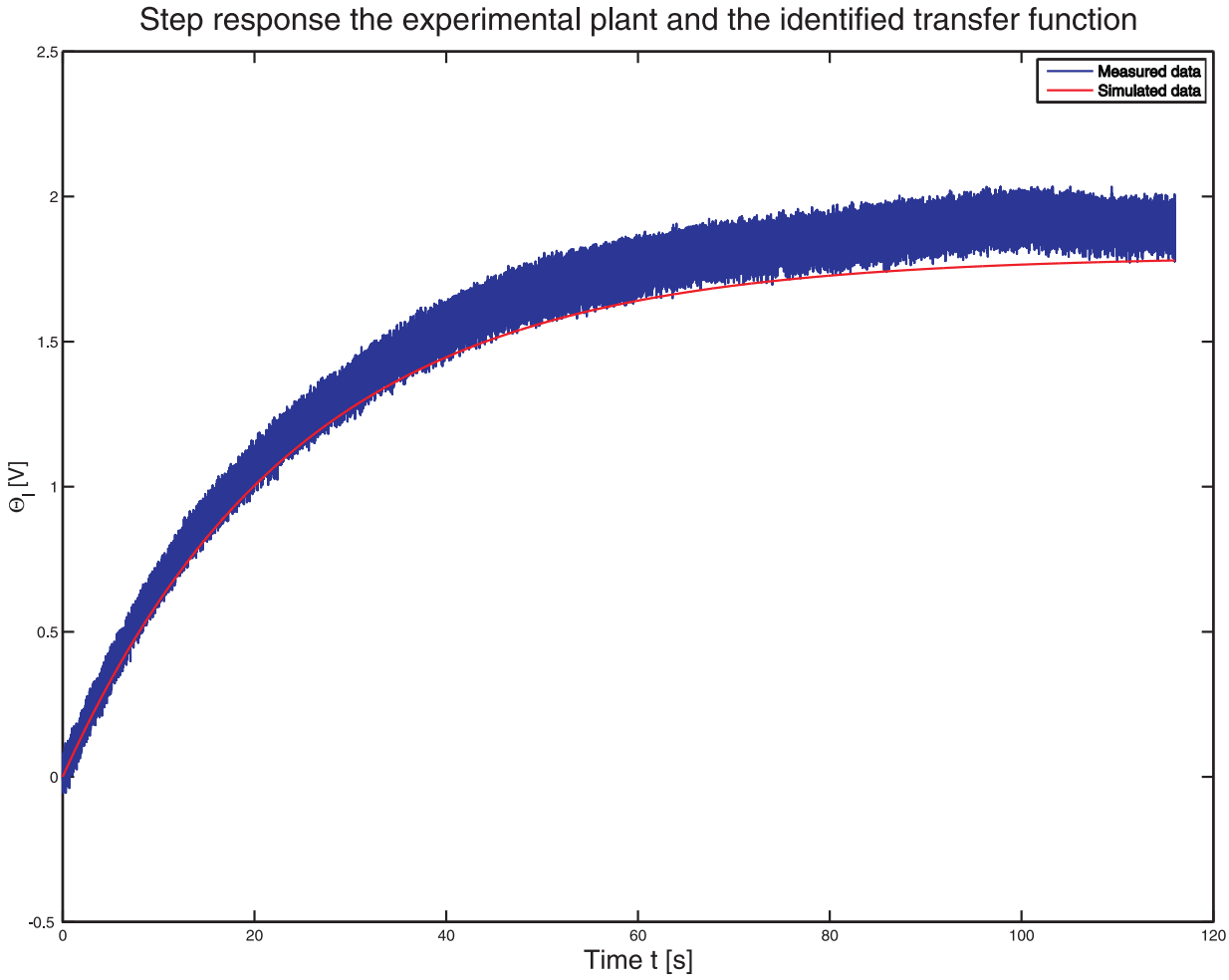

Figure 3.3: Step response of experimental plant and identified transfer function of Eq.(3.5) for a step height of 0.1 [V].

The correlation coefficient gives an indication about the relationship of data columns e.g., values close to 1 suggest a positive linear relationship, values close to -1 suggest a negative linear relationship, whereas values around 0 indicate that there is no linear relationship between the data or random variables.

In the present case $r_{X,Y} = 0.9945$, thus there seems to be a high linear relationship between the measured and simulated data, which underlines the validity of the model.

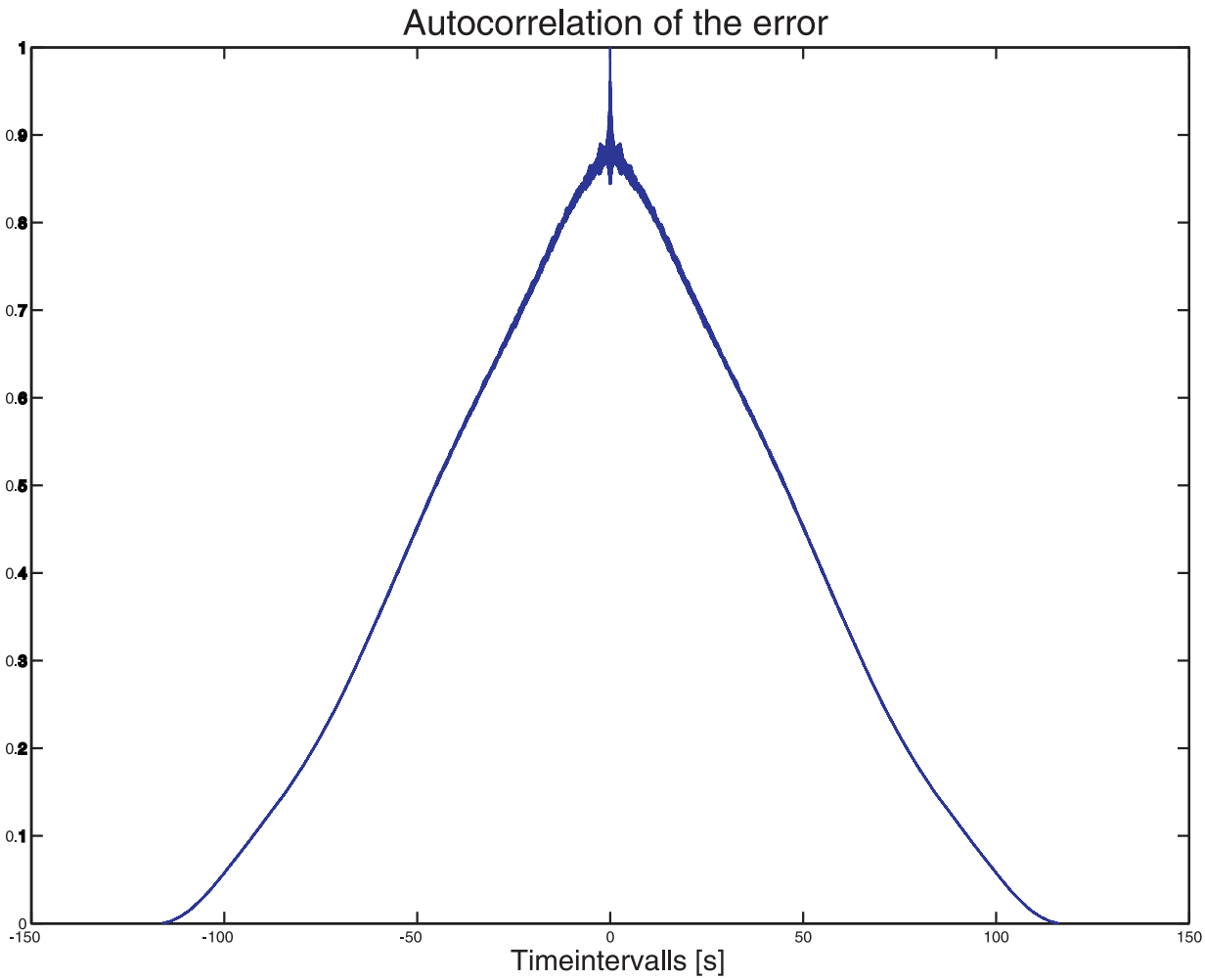

Figure 3.4: Autocorrelation of the error between the step response of experimental plant and identified transfer function of Eq.(3.5) for a step height of 0.1 [V].

3.2 Linear position controller design

Now, a controller for the load position Θ_l is designed. Therefore, at first the identified transfer function $G_{u_1\Theta_l}$ for the stiff connected system is used for a linear controller design with the following requirements:

- No overshoot
- Fast response (rise time$<$ 5[s]).

The chosen structure and parameters are

$$U(s) = K_P((\beta Y_{ref}(s) - Y_{meas}(s)) + \frac{1}{T_i s}E(s) + \frac{T_d s}{1 + \frac{T_d s}{N}}(\gamma Y_{ref}(s) - Y_{meas}(s))), \tag{3.9}$$

and

$$K_P = 100 \tag{3.10}$$

$$\beta = 0 \tag{3.11}$$

$$T_i = 0.8[s] \tag{3.12}$$

$$T_d = 0.15[s] \tag{3.13}$$

$$\gamma = 0 \tag{3.14}$$

$$N = 20. \tag{3.15}$$

For the same reasons as stated in Chapter 2, the controller includes modifications on the setpoint weighting and the limitation of the derivative gain. Furthermore, the control structure includes an anti-windup, as the input voltage is limited to $\pm 15V$, see Fig. 3.5.

To compensate part of the measurement noise, a low-pass filter G_{low} is added at the process output. The filter time constant has been determined by analyzing the Fourier spectrum of measurements obtained of the process output Θ_l. The filter corresponds to the transfer function

$$G_{low} = \frac{1}{1 + \frac{1}{20}s}. \tag{3.16}$$

In Fig. 3.6 and Fig. 3.7 experimental results for the performance of the designed controller on the real linear and nonlinear system are shown. One can clearly appreciate how the backlash element makes the system undergo limit cycles. Therefore, the control action should be supported and improved by using the second motor to avoid this behavior.

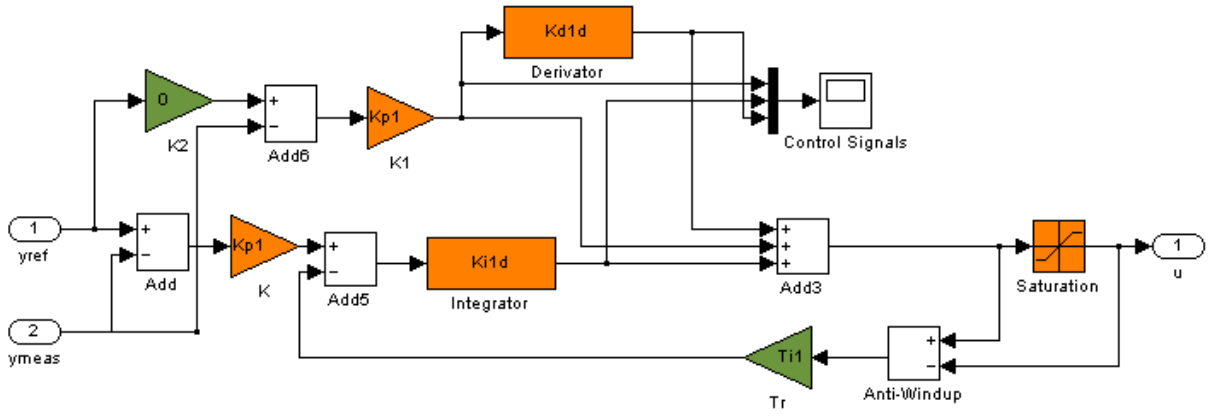

Figure 3.5: Control structure for experimental plant. The controller includes modifications on the setpoint weighting and the limitation of the derivative gain. Furthermore, the control structure includes an anti-windup, as the input voltage is limited to $\pm 15V$.

3.3 Operating strategies for the second motor

In this section, four different approaches to define the torque on the second motor are presented and experimentally tested. Mainly, the approaches are equal to the ones presented in Chapter 2 except the function $K_{constTorque}$, which is replaced by K_{u2} and defined as

$$K_{u2} = 2v, \tag{3.17}$$

where $v \in [0, 1]$ is the respective switching variable, which is defined in different manners in equations (3.18), (3.19), (3.20) and (3.21).

The following examples were obtained with a reference step $y_{ref,new} = \Theta_{l,new} = 2[V] \equiv 41.8879$ [rad] and the starting position $y_{ref,old} = 0$. The backlash angle is estimated experimentally to $\alpha = 0.42$ [rad], which is equivalent to $\alpha = 24$ [deg]. Thus, the backlash gap is quite large relatively to the one used previously in the simulations in Chapter 2. $y_{ref,old}$ refers to the previous final position and $y_{ref,new}$ refers to the actual desired final position. The difference of the latter two values allows again to determine whether the motion occurs in positive or negative direction. Furthermore is $e_{abs} = \frac{|y_{ref,new} - y_{meas}|}{|y_{ref,new} - y_{ref,old}|}$.

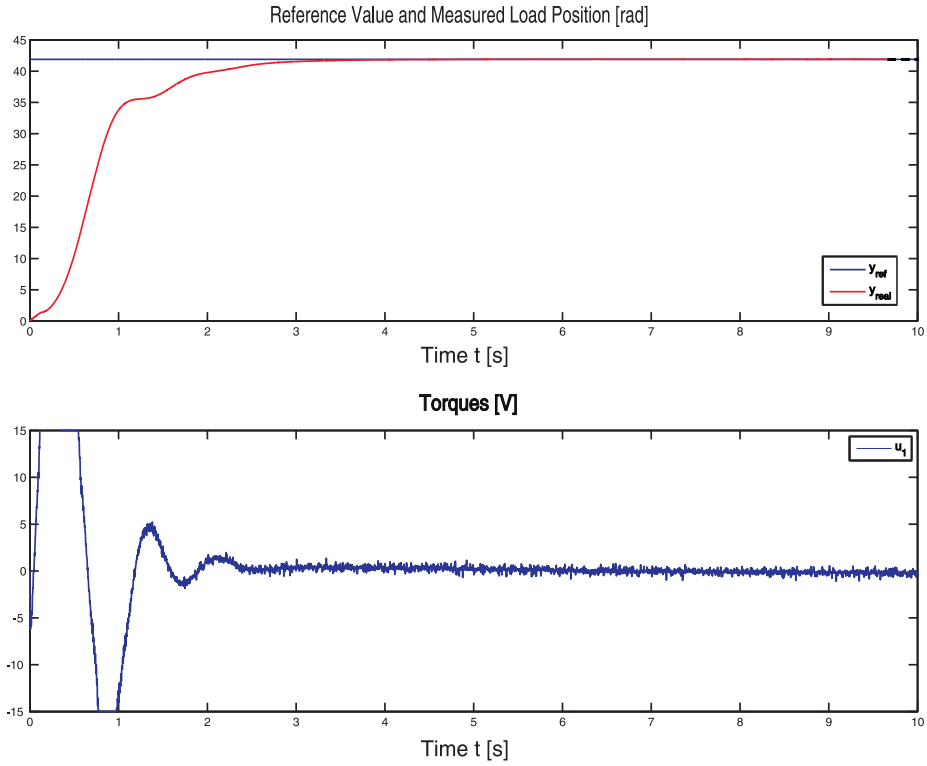

Figure 3.6: Experimental step response of the linear system of Section 3.2.

3.3.1 Constant load torque

The first and most simple approach is to operate from the beginning of the motion on with a constant torque in opposite direction of the desired motion. In this case v is defined as

$$v = \text{sign}(y_{ref,old} - y_{ref,new}). \tag{3.18}$$

Numerous experiments have shown, that on this system a reasonable torque T_L to avoid limit cycles is achieved by setting $u_2 = \pm 2$ [V] depending on the direction of the motion. A lower torque cannot yield to a satisfactory performance as it is to weak to close the backlash gap effectively. Whereas a too high torque forces a high control action, which also does not lead to the desired result. Furthermore, it is not desired to apply a higher torque than necessary in order to keep the required energy as low as possible. This is

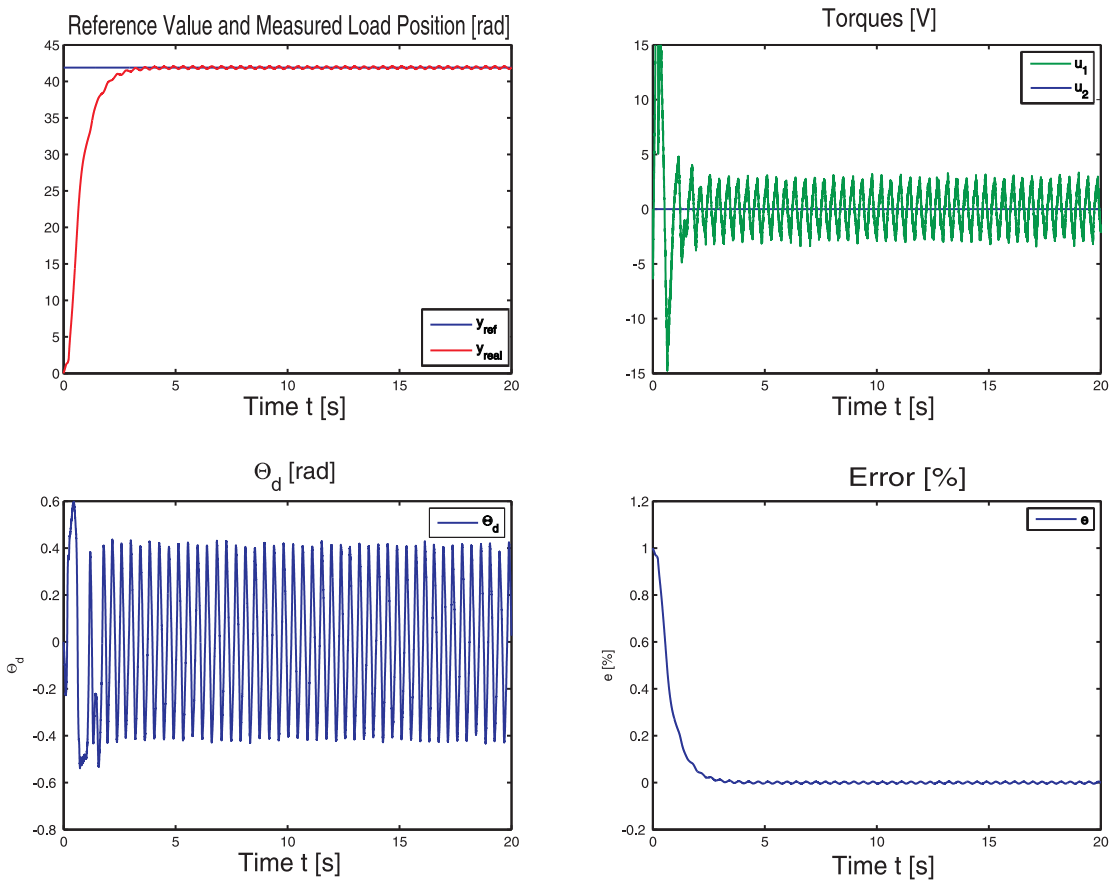

Figure 3.7: Experimental step response of the nonlinear system of Section 3.2. The backlash element makes the system undergo limit cycles.

concordant with the results of Chapter 2, in which the need of a certain magnitude of the constant torque is stated in order to stabilize the system.

In Fig. 3.8 a step response of the system for an input reference $\Theta_l = 2[V] \equiv 41.8879$ [rad] and a constant torque T_L with $u_2 = -2$ [V] is shown. Effectively, the limit cycles disappear and the system behaves as desired. But due to T_L the input power of the first motor increases in comparison to the case with $T_L = 0$. The performance applying the same constant torque from a point in time $t = 5[s]$ on is illustrated in Fig. 3.9.

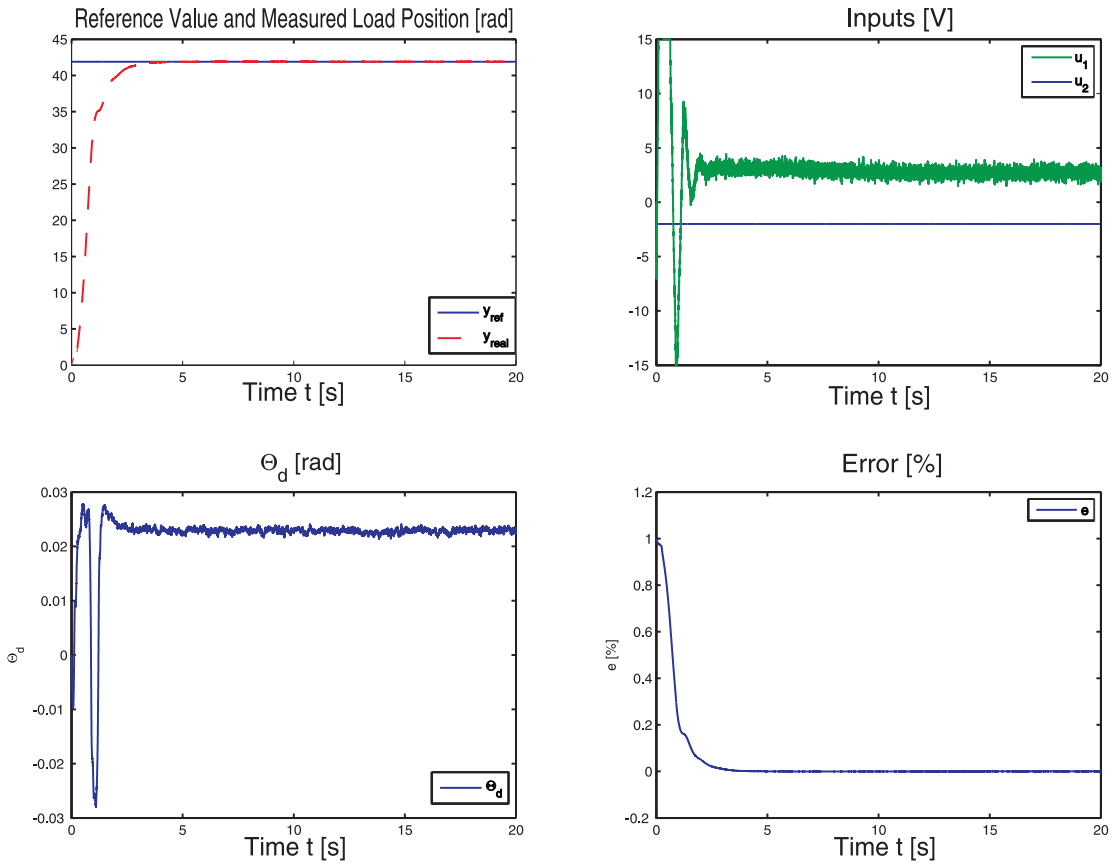

Figure 3.8: Experimental step response applying a constant torque T_L with $u_2 = -2$ [V] at $t = 0$ [s]. Effectively, the limit cycles disappear and the system behaves as desired.

Conclusions:

- Applying a constant torque in opposite direction of motion allows to avoid limit cycles.

- By applying T_L from the beginning on, a higher control signal is needed and it may lead to a negative response behavior if the system is not in backlash at $t = 0$.

- Applying T_L from a time in point later than $t = 0$ leads to more jitter.

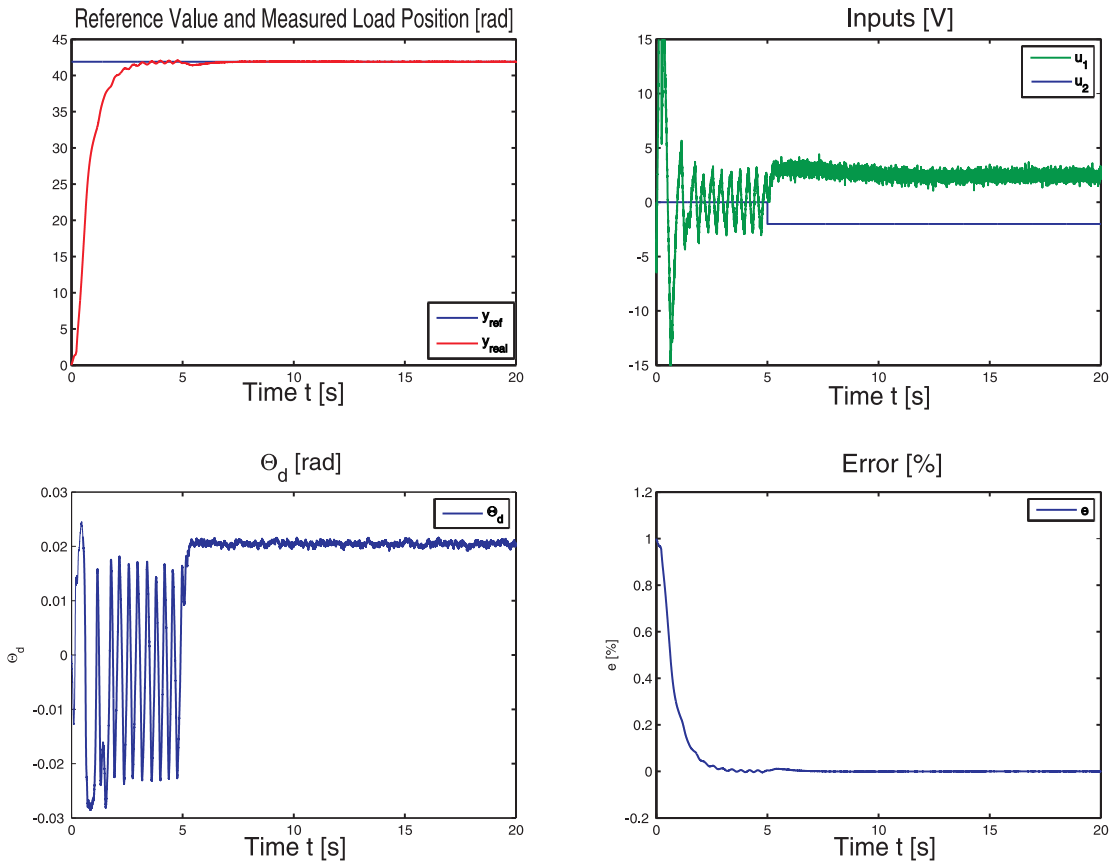

Figure 3.9: Experimental step response applying a constant torque T_L with $u_2 = -2$ [V] at $t = 5$ [s]. Also in this case the limit cycles are oppressed.

3.3.2 Load torque determination using Θ_d

This approach aims to use the relative position angle Θ_d to determine the action of the second motor. Therefore the following function is defined according to Subsection 2.5.1

$$v = \begin{cases} 0, & |\Theta_d| > \alpha \\ \text{sign}(y_{ref,old} - y_{ref,new}) \frac{\alpha - |\Theta_d|}{\frac{\alpha}{2}}, & \frac{\alpha}{2} \leq |\Theta_d| \leq \alpha \\ \text{sign}(y_{ref,old} - y_{ref,new}), & |\Theta_d| < \frac{\alpha}{2}. \end{cases} \tag{3.19}$$

The performance of this approach can be seen in Fig. 3.10. As already observed in the simulations in Subsection 2.5.1, the constant torque tends to be 0 in the final position. This might lead to problems when disturbances appear. Furthermore, an accurate estimate and

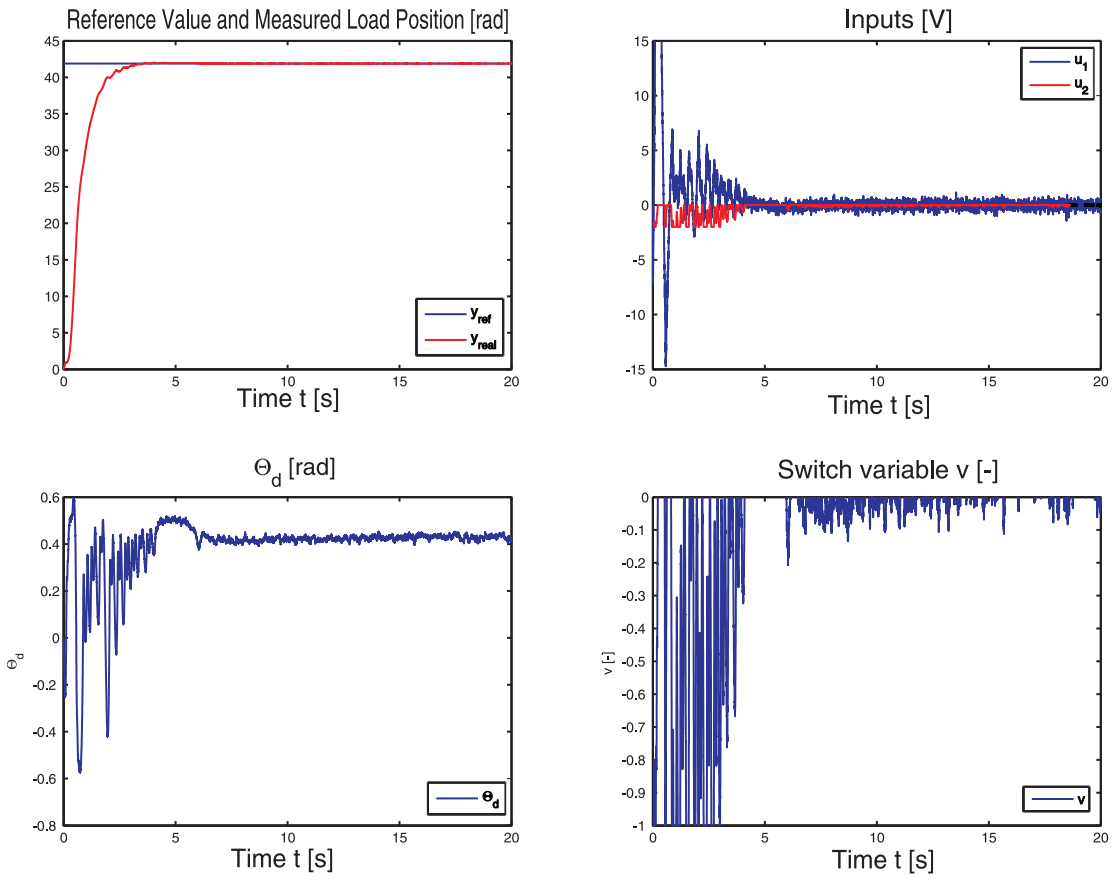

Figure 3.10: Experimental step response with $T_L = f(\Theta_d)$. The performance of this approach does not fulfill the requirements.

calibration of the process is essential for a right performance of the switching. Particularly, the calibration, that is positioning motor and load exactly in the middle of the backlash gap at the beginning of the experiment, is quite hard.

Conclusions:

- The theoretical and simulated results of Chapter 2 concerning the performance of this strategy are confirmed.

- In practice, a good estimation of α might be difficult or not accurate enough.

3.3.3 Load torque determination using e_{abs}

Now the relative error difference between the reference value and the actually measured value e_{abs} is taken in consideration. Therefore the following function is implemented (see also Subsection 2.5.2)

$$v = \begin{cases} 0, & e_{abs} > e_{max} \\ \text{sign}(y_{ref,old} - y_{ref,new}) \frac{e_{abs} - e_{max}}{e_{min} - e_{max}}, & e_{min} \leq e_{abs} \leq e_{max} \\ \text{sign}(y_{ref,old} - y_{ref,new}), & e_{abs} < e_{min}, \end{cases} \tag{3.20}$$

with $e_{max} = 0.1, e_{min} = 0.001$.

This strategy leads to the performance of Fig. 3.11.

Conclusions:

- No limit cycles, no negative response behavior.
- The strategy is not based on whether the system is in backlash or not, but it is based on the knowledge that the worst effects will occur, when reaching the final reference value.
- Small jitter appear when entering the error-bound.
- Less control power needed than in first case.

3.3.4 Load torque determination using Θ_d and e_{abs}

This last option intends to combine the advantages of the previous approaches, by using Θ_d to determine T_L, when the system is not close to the desired reference value and e_{abs}, when the system is reaching the final reference position. According to Subsection 2.5.3, this can be achieved by defining v as

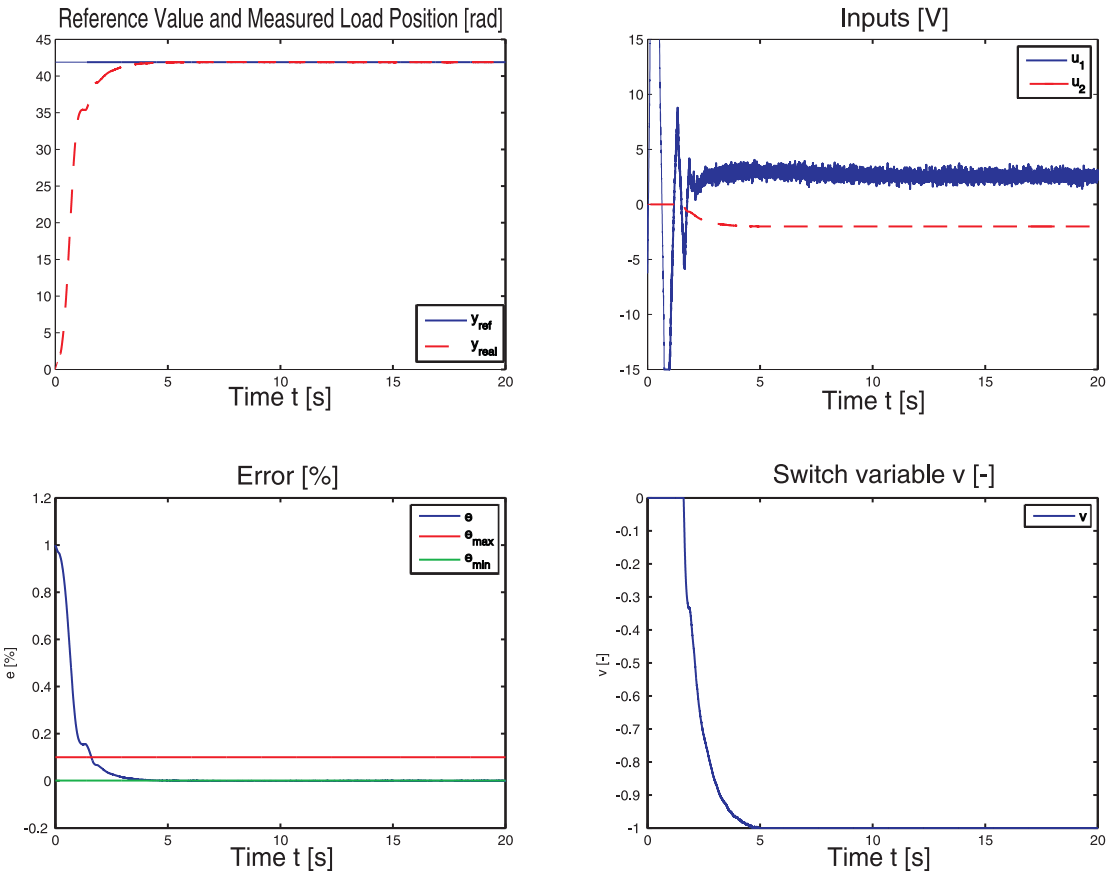

Figure 3.11: Experimental step response with $T_L = f(e_{abs})$. The strategy is not based on whether the system is in backlash or not, but it is based on the knowledge that the worst effects will occur, when reaching the final reference value. Actually, it conduces to oppress the limit cycles and maintain the desired step-response behavior.

$$v = \begin{cases} 0, & |\Theta_d| > \alpha \; and \; e_{abs} > e_{max} \\ \text{sign}(y_{ref,old} - y_{ref,new}) \frac{\alpha - |\Theta_d|}{\frac{\alpha}{2}}, & \frac{\alpha}{2} \leq |\Theta_d| \leq \alpha \; and \; e_{abs} > e_{max} \\ \text{sign}(y_{ref,old} - y_{ref,new}), & |\Theta_d| < \frac{\alpha}{2} \; and \; e_{abs} > e_{max} \\ \text{sign}(y_{ref,old} - y_{ref,new}) \frac{e_{abs} - e_{max}}{e_{min} - e_{max}}, & e_{min} \leq e_{abs} \leq e_{max} \\ \text{sign}(y_{ref,old} - y_{ref,new}), & e_{abs} < e_{min}, \end{cases} \tag{3.21}$$

with $e_{max} = 0.1, e_{min} = 0.001$.

The experimental results with this strategy, lead to the results presented in Fig. 3.12.

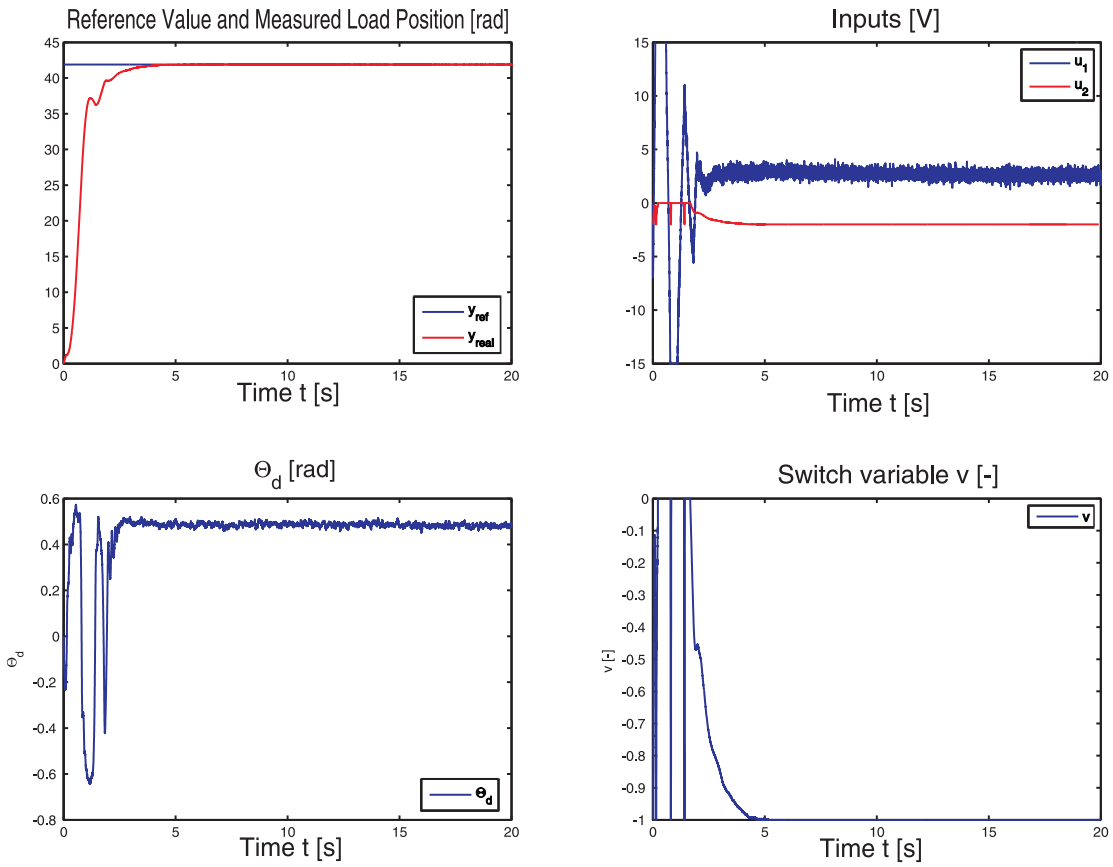

Figure 3.12: Experimental step response with $T_L = f(\Theta_d, e_{abs})$. Here, the strategy is more dependent on e_{abs} than on backlash/non-backlash situation of the system. Thus, the accuracy of the estimate of α is not that relevant as when using only Θ_d.

Conclusions:

- No limit cycles. No jitter.
- Accuracy of estimate of α not that relevant as when using only Θ_d.
- Higher energy input required than with $v = f(e_{abs})$.
- Strategy more dependent on e_{abs} than on backlash/non-backlash situation of the system.

3.4 Further observations

The following topics have been additionally investigated:

- System behavior in steady-state neighborhood

  No limit cycles could be detected even by long experimenting times.

  Stable behavior.

- Switching between different controllers depending on operation point

  A similar switching strategy for the controller was used for the controller as for the load torque depending on e_{abs}. It is based on the same function for determining v, only the boundaries e_{max} ans e_{min} are different. The control strategy can be expressed as follows:

  $$G_{con} = G_{fast} + v(G_{slow} - G_{fast}), \tag{3.22}$$

  where G_{fast} is a PID-controller with the nominal integral part and G_{slow} a PID-controller with a slower integral part with respect to the nominal controller.

  Results were not satisfactory. It seems due to two main reasons:

  - If $e_{max} - e_{min}$ is chosen too large, the lower time constant of the second controller leads to a slow steady-state-reaching.
  - If $e_{max} - e_{min}$ is chosen too small the switching is continuous and the region, where $0 < v < 1$ is overcrossed quite frequently and will cause many switches between the controllers.

3.5 Summary

This chapter evaluates the theoretical results of the previous Chapter 2 on an experimental setup. A model of the process and a control structure with the load position Θ_l as main control variable are presented. The different operating modes developed in Chapter 2 are picked up and tested.

In general, the results obtained in the previous Chapter 2 are confirmed in experiments. The nonlinear system can be stabilized with a constant torque acting in opposite driving direction. The different strategies lead to similar performances in the experiments as in simulations.

Thus, by defining $v = f(e_{abs})$ one achieves the best performance in meanings of a smooth and efficient motion, as well as stability.

Determining the action of the constant torque via $v = f(\Theta_d)$ does not lead to satisfactory results. Additionally it is difficult to estimate the size of the backlash gap in practice and to position the motor and load masses exactly in the middle of the backlash gap in the beginning of the experiments.

Operating with a switching-function based on both variables (e_{abs} and Θ_d), also leads to a less advantageous performance as determining v only depending on the relative error e_{abs}. The main disadvantages of the combination are again higher input and shaft torques.

Chapter 4

Dual motor control of a nonlinear three-mass system

In this chapter the treated model is extended to a nonlinear three-mass system representing two driving motors and one load. The load represents the cart of the robot actuator and therefore its absolute position is the main control variable.

The modeling is carried out according to the common two-mass models which can be found in literature [4] and have already been discussed in Chapter 2 and Chapter 3. The additional motor will be used to decrease the backlash-effects, namely limit cycles, by acting in opposite direction of the main driving motor.

This extension of the setup is necessary, as in the case of the parallel-kinematic robot it is not possible to have a motor which is directly acting on the load as it was assumed in the previous Chapter 2. However, it is aimed to use the additional motor to support the main driving motor in the forward motion and only to counteract, when the system is in backlash.

The chapter is structured in a similar way to the previous ones:

In Section 4.1 a model of the process with its respective parameters is introduced. Next, a control structure for a linear three-mass model, which is equivalent to the contact-case of the nonlinear one, is designed (Section 4.2).

In Section 4.3 the equilibrium points and stability characteristics of the system are

analyzed, assuming one motor to operate with the designed control law, whereas the other one acts with a constant torque. Hereby, is the backlash again modeled by a dead-zone. As consequence of the setup extension, now two dead-zones are incorporated to represent the backlash gaps between each motor and the load. Furthermore, the stability analysis is extended to global stability in Section 4.4 and conditions for the constant input under which the system is globally stable are derived.

Subsequently, the system behavior is analyzed in simulations in Matlab/Simulink (Section 4.5). In the following Section 4.6 switching strategies for the operating of the second motor are presented in analogy to Chapter 2. But now, they lead to nonlinear, smooth switching control laws for the additional motor. The different approaches are tested and compared based on simulations in Matlab/Simulink.

In Section 4.7 the different approaches are implemented and tested in Dymola in order to recheck the results obtained in Matlab/Simulink. Then the controller and switching parameters for the best switching control strategy are optimized in Section 4.8. Finally, in Section 4.9 a nonlinear, switching MIMO control law is introduced by including an additional switching between the master/slave-assignment of the motors.

4.1 Modeling of a nonlinear three-mass system

In analogy to Chapter 2 a model describing the extended process can be formulated as follows

$$\begin{aligned} J_{m1}\dot{\omega}_{m1} &= -c_{m1}\omega_{m1} - T_{s1} + T_{m1} \\ J_{m2}\dot{\omega}_{m2} &= -c_{m2}\omega_{m2} - T_{s2} + T_{m2} \\ J_l\dot{\omega}_l &= -c_l\omega_l + T_{s1} + T_{s2} - T_d \\ x_{pos} &= r_l\Theta_l \\ \omega_{d1} &= \omega_{m1} - \omega_l \\ \omega_{d2} &= \omega_{m2} - \omega_l \end{aligned} \tag{4.1}$$

with

$$\dot{\Theta}_{mi} = \omega_{mi},\ \dot{\Theta}_{l} = \omega_{l},\ \dot{\Theta}_{di} = \omega_{di},$$

$$T_{si} = \begin{cases} k_s(\Theta_{di} - \Theta_{bi}) + c_s\omega_{di}, & \text{contact} \\ 0, & \text{backlash} \end{cases} \tag{4.2}$$

and

$$\dot{\Theta}_{bi} = \begin{cases} \max(0, \Delta\dot{\Theta}_{di} + \frac{k_s}{c_s}(\Theta_{di} - \Theta_{bi})), & \Theta_{bi} = -\alpha \\ \dot{\Theta}_{di} + \frac{k_s}{c_s}(\Theta_{di} - \Theta_{bi}), & |\Theta_{bi}| < \alpha \\ \min(0, \Delta\dot{\Theta}_{di} + \frac{k_s}{c_s}(\Theta_{di} - \Theta_{bi})), & \Theta_{bi} = \alpha, \end{cases} \tag{4.3}$$

where $i = \{1, 2\}$.

Thus, the main difference of the model with respect to the one presented in Chapter 2, is the additional ODE representing the dynamics of the second motor. As consequence, an additional shaft torque is acting on the load and to describe the physical behavior the following variables are needed:

- The position of the second motor Θ_{m2} [rad], with $\omega_{m2} = \dot{\Theta}_{m2}$ and $\Theta_{d2} = \Theta_{m2} - \Theta_{l}$.
- The shaft torque T_{s2} [Nm] between Motor_2 and the load.
- The backlash angle Θ_{b2} [rad] between Motor_2 and the load.

In the present case, both motors are considered to be equal. Thus, according to Chapter 2 the used set of parameters is

$$\begin{aligned} J_{m1} = J_{m2} = 0.4 \quad & [kgm^2] \\ c_{m1} = c_{m2} = 0.1 \quad & [Nm/(rad/s)] \\ J_l = 5.6 \quad & [kgm^2] \\ c_l = 1 \quad & [Nm/(rad(s)] \\ k_s = 3300 \quad & [Nm/rad] \\ c_s = 1 \quad & [Nm/(rad/s)] \\ r_l = 0.01 \quad & [m] \\ \alpha = 5 \quad & [deg]. \end{aligned}$$

Now, the distinction between the operation modes of the system is a bit more complicated (see equation (4.2)): When the system is in contact, torque transmission between at least one motor and the load is possible, whereas there is no torque transmission in the backlash case. The conditions for the backlash case, can be summarized as follows

$$\text{backlash} = \begin{cases} \Theta_{bi} = (-\alpha) \wedge \omega_{bi} > 0 \\ |\Theta_{bi}| < \alpha \\ \Theta_{bi} = \alpha \wedge \omega_{bi} < 0, \end{cases} \tag{4.4}$$

where $i = \{1, 2\}$.

For all other cases at least one part of the system is in contact mode, that is

$$\text{contact} = \begin{cases} \Theta_{bi} = \alpha \wedge \omega_{bi} \geq 0 \\ \Theta_{bi} = (-\alpha) \wedge \omega_{bi} \leq 0, \end{cases} \tag{4.5}$$

where $i = \{1, 2\}$.

The impact when the backlash gap closes is again assumed to be inelastic, [7].

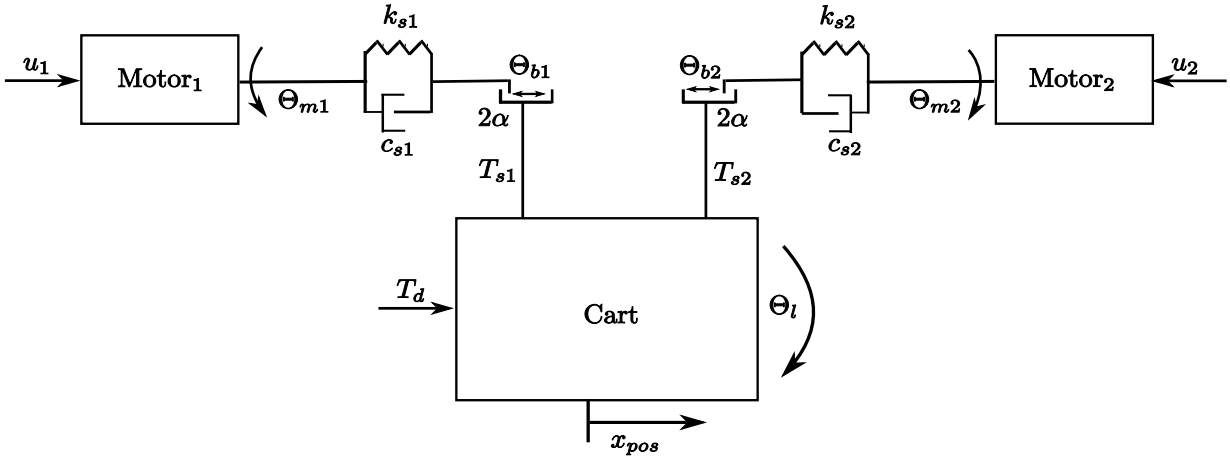

Figure 4.1: Schematic representation of a three-mass system exhibiting backlash or gear-play between the motors and the load.

The model will be studied in two different simulation environments: Matlab/Simulink and Dymola. The first one will mainly be used for controller design, whereas the Dymola model should reflect the real physical behavior of the process in a more accurate way and is used to verify the results obtained with Matlab/Simulink.

4.1.1 Matlab/Simulink model

The implemented model is shown in Fig. 4.2. The model has two inputs, which are the torques of the driving motors and several outputs including the angle positions of motors and load and its respective velocities. Additionally the shaft torques and the absolute position are available.

Nevertheless, only the absolute position of the load (x_{pos}), the motor and load angle positions (Θ_{m1}, Θ_{m2}, Θ_l) and the motor velocities (ω_{m1}, ω_{m2}) are considered to be measurable, as this represents the given situation on the real robot.

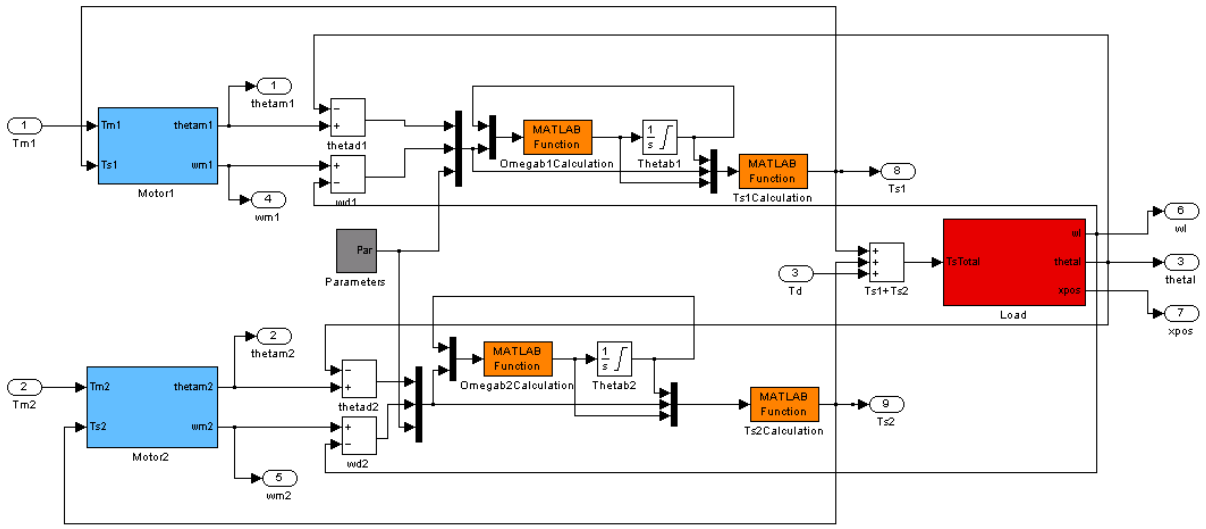

Figure 4.2: Three-mass system in Simulink as described in Eq.(4.1).

4.2 Linear dual motor position control of a nonlinear three-mass system

In this section a linear controller for the absolute position x_{pos} of the considered process is designed. Therefore, at first the controller for the linear two-mass system of Chapter 2 is added on the master motor of the three-mass system. For the slave motor a separate controller is designed.

Again the design is carried out formulating some rather weak requirements on the step response of the system, which does not reflect the commonly used input references in robotics. But as before the control-design task is regarded as a minor point compared to the analysis of the system performance under backlash effects.

4.2.1 Controller design

In the linear case, the three-mass model presented in Section 4.1 reduces to

$$J_{m1}\dot{\omega}_{m1} = -c_{m1}\omega_{m1} - T_{s1} + T_{m1} \tag{4.6}$$

$$J_{m2}\dot{\omega}_{m2} = -c_{m2}\omega_{m2} - T_{s2} + T_{m2} \tag{4.7}$$

$$J_l\dot{\omega}_l = -c_l\omega_l + T_{s1} + T_{s2} - T_d \tag{4.8}$$

$$x_{pos} = r_l\Theta_l \tag{4.9}$$

$$\omega_{d1} = \omega_{m1} - \omega_l \tag{4.10}$$

$$\omega_{d2} = \omega_{m2} - \omega_l \tag{4.11}$$

with

$$\dot{\Theta}_{mi} = \omega_{mi},\ \dot{\Theta}_l = \omega_l,\ \dot{\Theta}_{di} = \omega_{di},$$

and

$$T_{si} = k_s\Theta_{di} + c_s\omega_{di} \tag{4.12}$$

The meaning and nominal values of the parameters are equal to those in Section 4.1. The measured variables are x_{pos}, Θ_{m1}, Θ_{m2}, ω_{m1} and ω_{m2}.

At first, the characteristics of the linear system are analyzed. Therefore, the following six dimensional state-space representation is derived

$$\dot{x} = Ax + Bu + Gd \tag{4.13}$$

$$y = Cx, \tag{4.14}$$

where

$$x = \begin{bmatrix} \Theta_l & \Theta_{m1} & \Theta_{m2} & \omega_l & \omega_{m1} & \omega_{m2} \end{bmatrix}^T, \tag{4.15}$$

$$u = \begin{bmatrix} T_{m1} & T_{m2} \end{bmatrix}^T, \tag{4.16}$$

$$d = T_d, \tag{4.17}$$

$$A = \begin{bmatrix} 0 & 0 & 0 & 1 & 0 & 0 \\ 0 & 0 & 0 & 0 & 1 & 0 \\ 0 & 0 & 0 & 0 & 0 & 1 \\ -\frac{2k_s}{J_l} & \frac{k_s}{J_l} & \frac{k_s}{J_l} & -\frac{c_s+c_l}{J_l} & -\frac{c_s}{J_l} & -\frac{c_s}{J_l} \\ 0 & 0 & 0 & 0 & -\frac{c_{m1}}{J_{m1}} & 0 \\ 0 & 0 & 0 & 0 & 0 & -\frac{c_{m2}}{J_{m2}} \end{bmatrix}, \tag{4.18}$$

$$B = \begin{bmatrix} 0 \\ 0 \\ 0 \\ 0 \\ \frac{1}{J_{m1}} \\ \frac{1}{J_{m2}} \end{bmatrix}, \tag{4.19}$$

$$G = \begin{bmatrix} 0 \\ 0 \\ 0 \\ \frac{1}{J_l} \\ 0 \\ 0 \end{bmatrix}, \tag{4.20}$$

$$C = \begin{bmatrix} rl & 1 & 1 & 0 & 1 & 1 \end{bmatrix}. \tag{4.21}$$

Now it can be easily shown, that the system has 5 poles in the LHP, but two poles at the origin. It is controllable and observable. Thus, a control law, which stabilizes the system is desired. A logical approach would be to implement the designed controller for the two-mass system on the linear three-mass system by implementing the same control

law on both input motors.

Regarding simulations, the system seems to behave equal to the two-mass system, unless the fact that the generated control signal on each motor is half of the value of the two-mass system with only one motor. But analyzing its characteristics, it turns out to be unstable. This is a result of the chosen control structure, which locates to integral parts in parallel.

The present case, which models a linear drive system connected in parallel is discussed in [12]. As main difficulties, which may arise when using parallel integral action, the arise of unstable subsystems as well as loss of observability and controllability in the system are stated. One loses controllability on the integrators, as they cannot be influenced independently from the control error. For instance, they may not go to zero after a disturbance, but drift away from each other, which cannot be detected. As possible solutions, the authors propose to use only one integrator in the control strategy. Its output might then be distributed among all available motors. An alternative is to provide only one motor with an integral part and the others just with proportional controllers.

Latter is the alternative chosen for the inner-loop controllers in the present case, as there is no common variable, which might be used as control variable for the inner loop control of both motors. If we would just deal with linear systems, the velocities of the motors could be considered to be equal and therefore used as common control variable, see [12]. But when introducing the nonlinearity represented by the backlash elements, this equality cannot be guaranteed.

For the outer-loop controller the same statements apply, if we would connect the outer PID controllers in parallel. But differently from the inner-loop, the outer-loop has a common control variable, which is x_{pos}. Consequently, the output signal of the PID controller is used as reference input signal on both inner-loop controllers.

Thus, in order to achieve stability and controllability the inner-loop PI-controller of Motor_2 is redesigned into a pure P-controller. This may reduce the control performance on the second motor, but is reasonable as idem is regarded as slave-motor and additionally the main control variable is the absolute position of the cart x_{pos} and not the veloci-

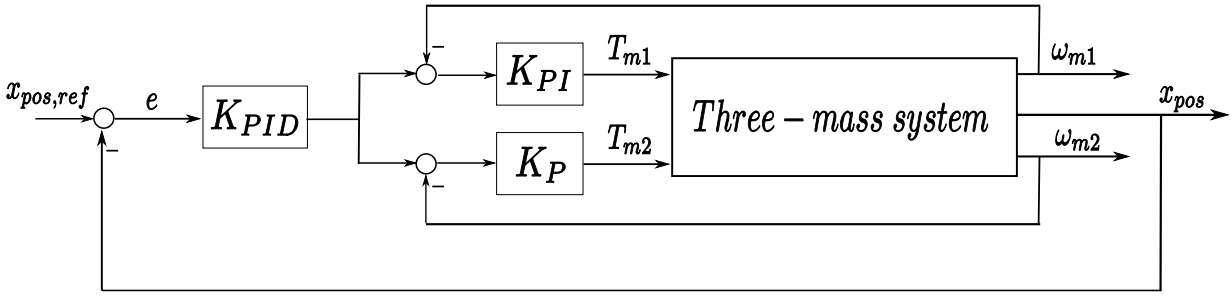

Figure 4.3: Schematic representation of dual motor control for a linear three-mass system. On both sides a cascade structure is implemented, but for stability reasons only one inner-loop controller contains an integrator-part.

ties of the motors.

Besides the performance of the speed control of w_{m2}, the overall performance of the whole closed-loop system is analyzed. It would be desirable to have an equal power distribution on both motors. Including this aspect, the P-control needs to be adapted reducing its gain. The used structure for the inner-loop controller of Motor_2 is then

$$U_2(s) = K_{P,in2}E(s), \tag{4.22}$$

with

$$K_{P,in2} = 10.3. \tag{4.23}$$

With this configuration the closed-loop system is stable, as for all eigenvalues λ_i it holds $Re(\lambda_i) < 0$. Its realization is minimal and all modes are controllable. The controllability is analyzed using the Hautus-criteria. A schematic overview of the implemented structure is shown in Fig. 4.3. The step response of the linear three-mass system using the designed cascade control structure on both motors is shown in Fig 4.4. The generated control signal on each motor is rather equally distributed and half of the value of the two-mass system with only one motor, which was analyzed in Chapter 2.

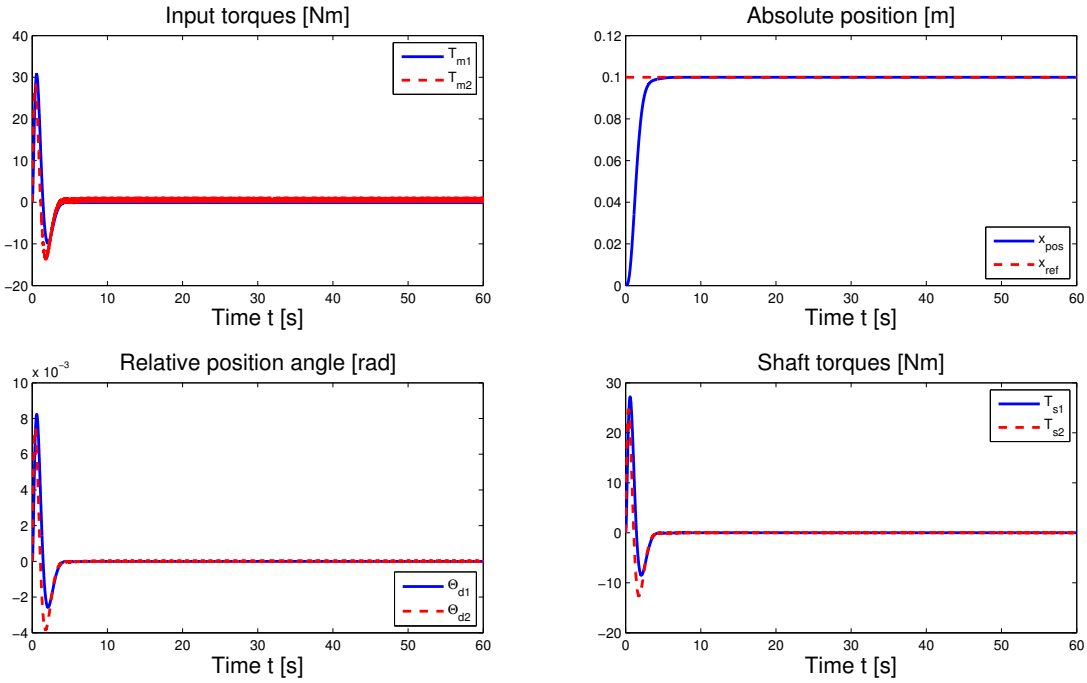

Figure 4.4: Step response of the linear three-mass system using a cascade control structure on both motors. The generated control signal on each motor is rather equally distributed and half of the value of the two-mass system with only one motor.

4.2.2 Control performance on a nonlinear three-mass system

Now the same control structure is tested on a nonlinear three-mass system including a backlash gap between each motor and the load. The step height is set to 0.1 [m] and the system is assumed to be in contact in the beginning of the motion, that is $\Theta_{d1}(t=0) = \alpha$ and $\Theta_{d2}(t=0) = -\alpha$.

As expected the system undergoes limit cycles after some time as consequence of the backlash element, see step response in Fig. 4.5. The beginning of the limit cycles can be influenced by the size of the backlash angle.

For instance a bigger backlash angle leads to a faster generation of limit cycles. For the nonlinear system the reduction on the magnitudes of the input torques is not as high as on the linear system, but it still exists.

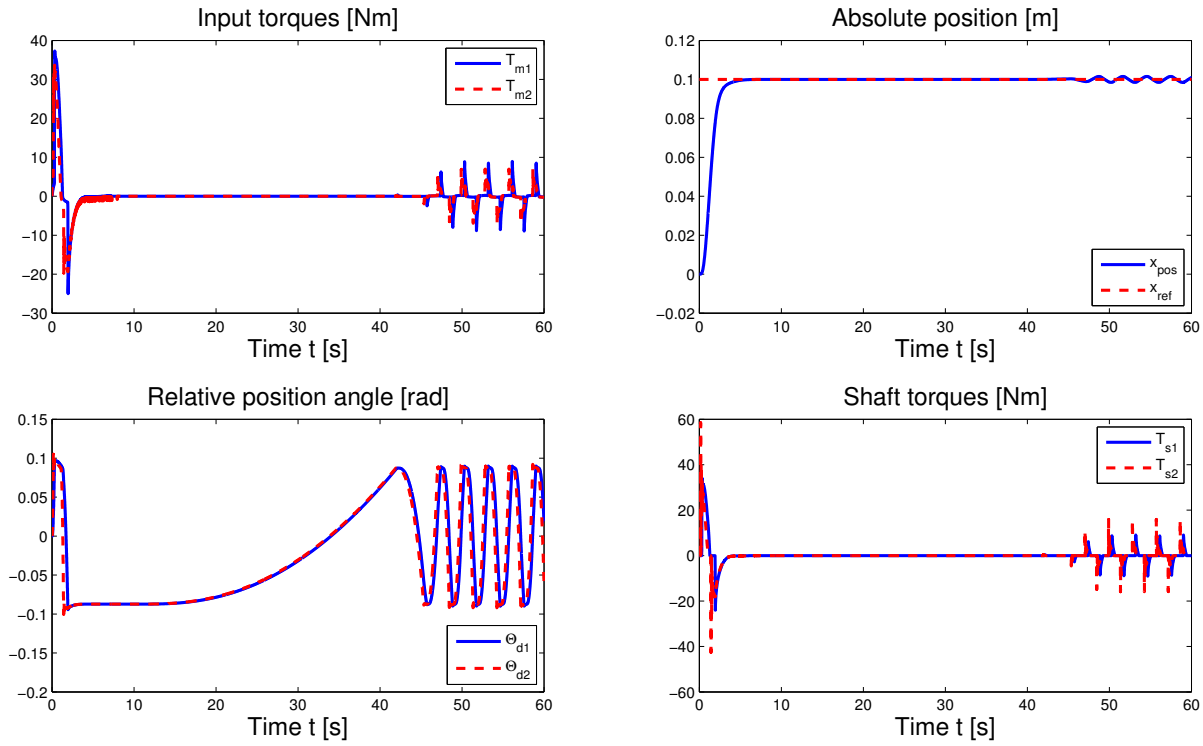

Figure 4.5: Step response of the nonlinear three-mass system using a cascade control structure on both motors. As expected the system undergoes limit cycles after some time as consequence of the backlash element.

4.3 Stability analysis of a three-mass system containing two dead-zone nonlinearities

This section analyzes the existence of equilibrium points and the stability of a nonlinear system containing two dead-zone nonlinearities. The system consists of a three-mass system exhibiting backlash and a cascaded control structure containing PID- and PI-control acting on the input of the first motor, as it was developed in Sections 4.1 and 4.2. The PID-design includes a low-pass filter for high-frequencies in the derivative part. Additionally, the system has a constant, but controllable torque acting directly on the input of the second motor. The system structure is shown in Fig. 4.6.

The proceeding is analogue to the one of the analysis in Chapter 2. Thus, the structure

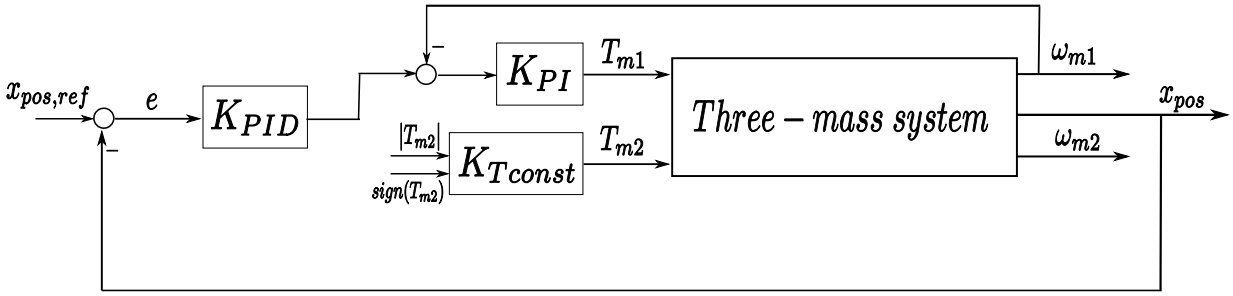

Figure 4.6: Schematic representation of dual motor control with constant torque. The first motor is the main driving motor, whereas the second motor acts as a brake in order to close the backlash gap.

is as follows: In Subsection 4.3.1 a state-space model is presented. In Subsection 4.3.2 a controllable canonical form of the system is derived, which is used in Subsection 4.3.3 to determine the equilibrium points of the system. In Subsection 4.3.4 the stability of the equilibrium points is analyzed.

4.3.1 State-space model

A state-space model describing the closed-loop system can be formulated as follows

$$\begin{aligned} \dot{\overline{x}} &= \overline{A}\overline{x} + \overline{B}\begin{bmatrix} u_1 \\ u_2 \end{bmatrix} + \overline{H}u_3, \quad \overline{x}(t=0) = \overline{x}_0 \\ y &= \overline{C}\overline{x}, \end{aligned} \tag{4.24}$$

where

$$\begin{aligned} \overline{x} &= \begin{bmatrix} \Theta_l & \omega_l & \Theta_{m1} & \omega_{m1} & \Theta_{m2} & \omega_{m2} & PI_I & PID_D & PID_I \end{bmatrix}^T, \\ u_1 &= dz_{2\alpha}(y_1), \\ u_2 &= dz_{2\alpha}(y_2), \\ u_3 &= T_{m2}, \\ y &= \begin{bmatrix} \Theta_{d1} & \Theta_{d2} \end{bmatrix}^T. \end{aligned} \tag{4.25}$$

and

$$\Theta_s = dz_{2\alpha}(\Theta_d) = \begin{cases} \Theta_d - \alpha, & \Theta_d > \alpha, \\ 0, & |\Theta_d| < \alpha, \\ \Theta_d + \alpha, & \Theta_d < -\alpha. \end{cases} \tag{4.26}$$

The states PI_I, PID_D and PID_I refer to the states of the cascaded control structure given in Eq.(2.30) in Subsection 2.2.2.

A schematic representation of the system is given in Fig. 4.3.1. The system matrices are given in Eq.(4.27).

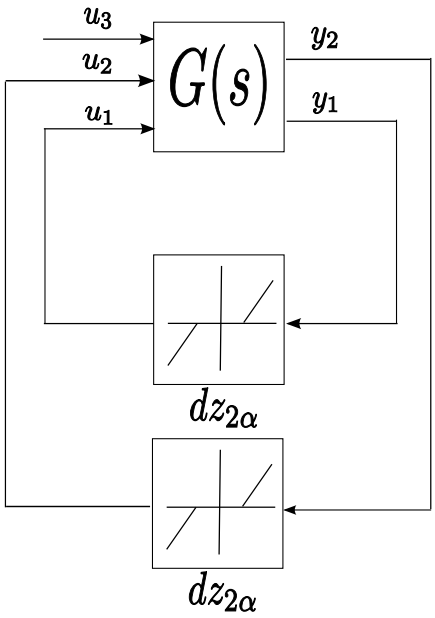

Figure 4.7: Schematic representation of a three mass system with backlash represented by the two dead-zones.

$$\overline{A} = \begin{bmatrix} 0 & 0.1786 & 0 & 0 & 0 & 0 & 0 & 0 & 0 \\ 0 & -0.1786 & 0 & 0 & 0 & 0 & 0 & 0 & 0 \\ 0 & 0 & 0 & 2.5 & 0 & 0 & 0 & 0 & 0 \\ 0 & 0 & 0 & -125.3 & 0 & 0 & 50 & 0 & 0 \\ 0 & 0 & 0 & 0 & 0 & 2.5 & 0 & 0 & 0 \\ 0 & 0 & 0 & 0 & 0 & -0.25 & 0 & 0 & 0 \\ -105 & 0 & 0 & -6.25 & 0 & 0 & 0 & -2 \cdot 10^4 & 2.5 \\ -2 & 0 & 0 & 0 & 0 & 0 & 0 & -400 & 0 \\ -1.333 & 0 & 0 & 0 & 0 & 0 & 0 & 0 & 0 \end{bmatrix},$$

$$\overline{B} = \begin{bmatrix} 0 & 0 \\ -3300 & -3300 \\ 0 & 0 \\ 3300 & 0 \\ 0 & 0 \\ 0 & 3300 \\ 0 & 0 \\ 0 & 0 \\ 0 & 0 \\ 0 & 0 \end{bmatrix}, \tag{4.27}$$

$$\overline{H} = \begin{bmatrix} 0 \\ 0 \\ 0 \\ 0 \\ 0 \\ -1 \\ 0 \\ 0 \\ 0 \end{bmatrix},$$

$$\overline{C} = \begin{bmatrix} -1 & 0 & 1 & 0 & 0 & 0 & 0 & 0 & 0 \\ -1 & 0 & 0 & 0 & 1 & 0 & 0 & 0 & 0 \end{bmatrix}.$$

4.3.2 Transformation into controllable canonical form

Now, the system $(\overline{A}, \overline{B}, \overline{H}, \overline{C})$ is transformed into a controllable canonical form via a transformation matrix T. The new system description is given as

$$\begin{aligned} x =& T\overline{x}, \\ A =& T\overline{A}T^{-1}, \\ B =& T\overline{B}, \\ H =& T\overline{H}, \\ C =& \overline{C}T^{-1}. \end{aligned} \tag{4.28}$$

For MIMO systems the controllable canonical form is generally not unique, but its structure can be influenced by the engineer, [16]. As in the SISO case, the system is required to be controllable in order to be transformable into a controllable canonical form. The canonical form used in the present case, is the one called 'second type of canonical form' in [16]. The transformation matrix T is obtained via the Matlab-function `MI\_ctrb` [15].

Note, that this representation is only obtained when inserting the given numerical values for the parameters. Therefore, the analysis in this section is more specific as the one described in Chapter 2, which can be seen as a more general approach for determining equilibrium points of nonlinear systems.

The system matrices have the form

$$A = \begin{bmatrix} 0 & 1 & 0 & 0 & 0 & 0 & 0 & 0 & 0 \\ 0 & 0 & 1 & 0 & 0 & 0 & 0 & 0 & 0 \\ 0 & 0 & 0 & 1 & 0 & 0 & 0 & 0 & 0 \\ 0 & 0 & 0 & 0 & 1 & 0 & 0 & 0 & 0 \\ 0 & 0 & a_{53} & a_{54} & a_{55} & 0 & 0 & 0 & 0 \\ 0 & 0 & 0 & 0 & 0 & 0 & 1 & 0 & 0 \\ 0 & 0 & 0 & 0 & 0 & 0 & 0 & 1 & 0 \\ 0 & 0 & 0 & 0 & 0 & 0 & 0 & 0 & 1 \\ 0 & a_{92} & a_{93} & a_{94} & 0 & 0 & a_{97} & a_{98} & a_{99} \end{bmatrix},$$

$$B = \begin{bmatrix} 0 & 0 \\ 0 & 0 \\ 0 & 0 \\ 0 & 0 \\ 1 & 1 \\ 0 & 0 \\ 0 & 0 \\ 0 & 0 \\ 0 & 1 \end{bmatrix}, \tag{4.29}$$

$$H = \begin{bmatrix} 0 \\ 0 \\ 0 \\ 0 \\ 0 \\ h_6 \\ h_7 \\ h_8 \\ h_9 \end{bmatrix},$$

$$C = \begin{bmatrix} c_{11} & c_{12} & c_{13} & c_{14} & 0 & 0 & c_{17} & c_{18} & 0 \\ c_{11} & c_{12} & c_{13} & c_{14} & 0 & c_{16} & c_{17} & c_{18} & 0 \end{bmatrix}.$$

4.3.3 Equilibrium points

The equilibrium points for the original, untransformed system are given as

$$\dot{\overline{x}} = 0 = \overline{A}\overline{x} + \overline{B}\begin{bmatrix} u_1 \\ u_2 \end{bmatrix} + \overline{H}u_3. \tag{4.30}$$

As this nonlinear set of equations is difficult to solve, equally the following set can be considered

$$y = -\overline{CA}^{-1}(\overline{B}\begin{bmatrix} \Theta_{s_1} \\ \Theta_{s_2} \end{bmatrix} + \overline{H}u_3) \tag{4.31}$$
$$\Theta_{s_{1,2}} = dz_{2\alpha}(y_{1,2}).$$

In the present case, $\overline{A}$ is not invertible. Thus, we make use of the transformed system equations in controllable canonical form obtained before. In the following the transformed system will be again denoted as (A, B, H, C). The equilibria of the system have then the form

$$0 = \dot{x} = Ax + B\begin{bmatrix} u_1 \\ u_2 \end{bmatrix} + Hu_3 \tag{4.32}$$
$$y = Cx.$$

This representation, gives a set of equations which is easier to solve. Indeed, the set can be divided in the following subsets of equations for the equilibrium points of the system:

1. Subset 1: Conditions for x_2 to x_5

$$\begin{aligned} \dot{x}_1 = 0 \quad &\Rightarrow \quad x_2 = 0, \\ \dot{x}_2 = 0 \quad &\Rightarrow \quad x_3 = 0, \\ \dot{x}_3 = 0 \quad &\Rightarrow \quad x_4 = 0, \\ \dot{x}_4 = 0 \quad &\Rightarrow \quad x_5 = 0, \end{aligned} \tag{4.33}$$

2. Subset 2: Conditions for x_7 to x_9

$$\begin{aligned} \dot{x}_6 = 0 \quad &\Rightarrow \quad x_7 = -h_6 u_3, \\ \dot{x}_7 = 0 \quad &\Rightarrow \quad x_8 = -h_7 u_3, \\ \dot{x}_8 = 0 \quad &\Rightarrow \quad x_9 = -h_8 u_3, \end{aligned} \tag{4.34}$$

3. Subset 3: Condition for u_1 and u_2. The equilibrium condition for $\dot{x}_5$ is

$$\dot{x}_5 = 0 = a_{53}x_3 + a_{54}x_4 + a_{55}x_5 + u_1 + u_2$$

From this equation and making use of subset 1 we obtain the equilibrium condition for the shaft torques u_1 and u_2

$$u_1 + u_2 = 0. \tag{4.35}$$

4. Subset 4: Condition for $\dot{x}_9$

$$\dot{x}_9 = 0 = a_{92}x_2 + a_{93}x_3 + a_{94}x_4 + a_{97}x_7 + a_{98}x_8 + a_{99}x_9 + u_2 + h_9 u_3.$$

Using subset 1 and 2, this equation can be expressed as follows

$$0 = (-a_{97}h_6 - a_{98}h_7 - a_{99}h_8 + h_9)u_3 + u_2. \tag{4.36}$$

5. Subset 5: Explicit representation for the determination of u_1 and u_2

$$\begin{aligned} u_1 &= dz_{2\alpha}(C(1,:)x), \\ u_2 &= dz_{2\alpha}(C(2,:)x). \end{aligned}$$

Making use of subset 1 and subset 2, latter equations can be rewritten as

$$u_1 = dz_{2\alpha}(c_{11}x_1 + (-c_{17}h_6 - c_{18}h_7 - c_{19}h_8)u_3), \tag{4.37}$$
$$u_2 = dz_{2\alpha}(c_{21}x_1 + c_{26}x_6 + (-c_{27}h_6 - c_{28}h_7 - c_{29}h_8)u_3).$$

Note that u_1 only depends on x_1 and u_3, whereas u_2 contains a dependency of x_6, too.

For simplification, we introduce three constants K_1, K_2 and K_3

$$K_1 = -c_{17}h_6 - c_{18}h_7 - c_{19}h_8, \tag{4.38}$$
$$K_2 = -c_{27}h_6 - c_{28}h_7 - c_{29}h_8, \tag{4.39}$$
$$K_3 = -a_{97}h_6 - a_{98}h_7 - a_{99}h_8 + h_9. \tag{4.40}$$

Note that all three constants have negative sign.

Summarizing, the described set gives already explicit definitions for the states x_1 to x_5 and x_7 to x_9. There are two remaining equations for $\dot{x}_6$ and $\dot{x}_9$, which in combination with the definitions of u_1 and u_2 allow us to find solutions for the remaining states x_1 and x_6. For this purpose the concerning equations are rewritten as

$$0 = K_3u_3 + u_2 = K_3u_3 - u_1, \tag{4.41}$$
$$u_1 = -u_2. \tag{4.42}$$

Here, we take advantage of the non-dependency of u_1 of x_6 by first finding possible solutions for x_1 and then using the equilibrium condition for the shaft torques to define x_6.

For the determination of the equilibria, we can distinguish two main cases:

- Case 1: $u_3 = 0$.
- Case 2: $u_3 \neq 0$.

Equilibrium points for $u_3 = 0$

Then equation (4.41) reduces to

$$0 = -u_1, \tag{4.43}$$

where the only possible solution is $|\frac{x_1}{c_{11}}| < \alpha$. Then all possible equilibria of x_1 lay inside the dead-zone.

Furthermore, equation (4.42) gives

$$u_2 = 0. \tag{4.44}$$

From what follows

$$|c_{21}x_1 + c_{26}x_6| < \alpha. \tag{4.45}$$

Using the triangle inequality and inserting then the previous result for x_1 we obtain

$$\begin{aligned} |c_{21}x_1 + c_{26}x_6| \leq |c_{21}x_1| + |c_{26}x_6| < \alpha, \\ |c_{26}||x_6| < \alpha - |c_{21}||x_1| \\ |x_6| < \frac{1}{|c_{26}|}(1 - \frac{|c_{21}|}{|c_{11}|})\alpha. \end{aligned} \tag{4.46}$$

All other states become 0, as they depend only on u_3 and $u_3 = 0$.

The output y can then be expressed as

$$|y| = |Cx| = \begin{bmatrix} |c_{11}||x_1| \\ |c_{21}||x_1| + |c_{26}|x_6| \end{bmatrix} < \begin{bmatrix} \alpha \\ \alpha \end{bmatrix} \tag{4.47}$$

Summarizing, in case $u_3 = 0$ there exist numerous equilibrium points for $|y| < \alpha$.

Equilibrium points for $u_3 \neq 0$

In the case $u_3 \neq 0$ solutions of (4.41) exist for

1. $u_1 < 0 \Rightarrow c_{11}x_1 + K_1u_3 < -\alpha$. In this case equation (4.41) leads to:

$$0 = K_3 u_3 - \underbrace{(c_{11} x_1 + K_1 u_3 + \alpha)}_{u_1} \tag{4.48}$$

and the equilibrium point is

$$x_1 = \frac{(K_3 - K_1) u_3 - \alpha}{c_{11}}. \tag{4.49}$$

Inserting the result in

$$dz_{2\alpha}(c_{11} x_1 + K_1 u_3), \tag{4.50}$$

gives the condition

$$\begin{gathered} K_3 u_3 - \alpha < -\alpha \Rightarrow K_3 u_3 < 0 \Rightarrow u_3 > 0 \text{ and } K_3 < 0 \\ \text{or} \\ u_3 < 0 \text{ and } K_3 > 0. \end{gathered} \tag{4.51}$$

As we know that $u_1 = -u_2$ and in the present case $u_1 < 0$, we only must consider the case $u_2 > 0$ for determining x_6. Thus, we have

$$u_2 = c_{21} x_1 + c_{26} x_6 + K_2 u_3 > \alpha, \tag{4.52}$$

$$u_2 = -u_1, \tag{4.53}$$

$$c_{21} + c_{26} x_6 + K_2 u_3 - \alpha = -K_3 u_3 \tag{4.54}$$

and x_6 results to

$$x_6 = \frac{1}{c_{26}}((-K_2 - K_3 - \frac{c_{21}}{c_{11}}(K_3 - K_1)) u_3 + (1 + \frac{c_{21}}{c_{11}})\alpha). \tag{4.55}$$

2. $u_1 > 0 \Rightarrow c_{11} x_1 + K_3 u_3 > \alpha$. In this case equation (4.41) leads to

$$0 = K_3 u_3 - \underbrace{(c_{11}x_1 + K_1 u_3 - \alpha)}_{u_1} \tag{4.56}$$

and the equilibrium point is

$$x_1 = \frac{(K_3 - K_1)u_3 + \alpha}{c_{11}}. \tag{4.57}$$

Inserting the result in

$$dz_{2\alpha}(c_{11}x_1 + K_1 u_3), \tag{4.58}$$

gives the condition

$$\begin{gathered} K_3 u_3 + \alpha > \alpha \Rightarrow K_3 u_3 > 0 \Rightarrow u_3 > 0 \text{ and } K_3 > 0 \\ \text{or} \\ u_3 < 0 \text{ and } K_3 < 0. \end{gathered} \tag{4.59}$$

As we know that $u_1 = -u_2$ and in the present case $u_1 > 0$, we only must consider the case $u_2 < 0$ for determining x_6. Thus, we have

$$\begin{aligned} u_2 &= c_{21}x_1 + c_{26}x_6 + K_2 u_3 < -\alpha, \\ u_2 &= -u_1, \\ c_{21} + c_{26}x_6 + K_2 u_3 + \alpha &= -K_3 u_3 \end{aligned} \tag{4.60}$$

and x_6 results to

$$x_6 = \frac{1}{c_{26}}((-K_2 - K_3 - \frac{c_{21}}{c_{11}}(K_3 - K_1))u_3 + (-1 - \frac{c_{21}}{c_{11}})\alpha). \tag{4.61}$$

Consequently, an equilibrium point outside the dead-zone can be achieved by setting $u_3 \neq 0$. By choosing the sign of u_3 one can even determine on which contact side the equilibrium lays, as K_3 is determined by the system parameters. Note that for every $u_3 \neq 0$ there exists only one equilibrium point.

4.3.4 Stability analysis

In the previous subsection, the existence of equilibrium points in the system was shown. Now, their local stability is analyzed. The analysis is carried out in the original system representation $\overline{A}, \overline{B}, \overline{H}, \overline{C}$. This is possible as their exists a transformation T from $\overline{x}$ to x and therefore also from x to $\overline{x}$ with $\overline{x} = T^{-1}x$.

Local stability for $u_3 = 0$

We have shown, that for $u_3 = 0$ there exist multiple equilibria inside the dead-zone. If we linearize the system around one arbitrary chosen equilibrium point, which satisfies the above condition, e.g. $y = \frac{\alpha}{2}$, we obtain

$$\begin{aligned} \dot{\overline{x}} &= \overline{A}\overline{x} \\ y &= \overline{C}\overline{x}. \end{aligned} \tag{4.62}$$

As $\overline{A}$ has several eigenvalues with $Re(\lambda) = 0$, the system is unstable. This statement holds for all possible equilibrium points obtained when $u_3 = 0$.

Local stability for $u_3 \neq 0$

For every $u_3 \neq 0$ an equilibrium point is defined. If we linearize the system around the equilibrium obtained by choosing an arbitrary value of $u_3 \neq 0$, we obtain

$$\begin{aligned} \dot{\overline{x}} &= \overline{A}\overline{x} + \overline{B}(y \pm \alpha) + \overline{H}u_3 \\ y &= \overline{C}\overline{x}. \end{aligned} \tag{4.63}$$

So we can write

$$\begin{aligned} \dot{\overline{x}} &= (\overline{A} + \overline{BC})\overline{x} + \overline{B}(\pm\alpha) + \overline{H}u_3 \\ y &= \overline{C}\overline{x}. \end{aligned} \tag{4.64}$$

Let us denote $\overline{A}_{cl} = \overline{A} + \overline{BC}$. All poles of $\overline{A}_{cl}$ lay in the LHP, with being $\max(Re\lambda_i) = -0.2880$, $i = 1 \ldots 9$. Thus the system is local asymptotically stable.

As in the case of the two-mass system, local stability can be achieved by any $u_3 \neq 0$. But again, for making sure a stable performance some $|u_3| > |\delta| > 0$ is required. This is emphasized by simulations, which show that u_3 has to have a certain magnitude for stabilizing the system. An interpretation would be, that the region of attraction of the equilibrium point increases with increasing magnitude of $|u_3|$.

4.4 Global stability of a nonlinear three-mass system

In this section the stability analysis of Section 4.3 is extended to global stability. For this purpose we introduce the *multivariable circle criterion* in Subsection 4.4.1. The same nonlinear system containing two dead-zone nonlinearities as presented in Section 4.3 is analyzed.

To apply the *multivariable circle criterion* in the present case some operations on the system are required: In Subsection 4.4.2, the loop shown in Fig. 4.3.1 in Section 4.3 is modified in order to obtain a stable linear part, which is in negative feedback with the nonlinear part. Then in Subsection 4.4.3 the loop is once again transformed to allow a better analysis of the influence of the constant input on the system. As we have shown in Section 4.3 for $u_3 \neq 0$ the equilibrium of the system does not lay in the origin. Subsection 4.4.4 gives a coordinate transformation which shifts the equilibrium in the origin and explains in more detail the influence of that coordinate change on the nonlinearities, especially on their sector bounds.

In Subsection 4.4.5 finally we derive a condition which guarantees global stability for the system depending on the constant input u_3.

4.4.1 Mulivariable Circle Criterion

According to [22] the *multivariable circle criterion* can be formulated as follows:

Theorem *The system*

$$\dot{x} = Ax + Bu \tag{4.65}$$

$$y = Cx + Du \tag{4.66}$$

$$u = -\phi(t, y) \tag{4.67}$$

is absolutely stable if

- $\phi \in [K_1, \infty]$ *and* $G(s)[I + K_1 G(s)]^{-1}$ *is strictly positive real, or*
- $\phi \in [K_1, K_2]$, *with* $K = K_2 - K_1 = K^T > 0$, *and* $[I + K_2 G(s)][I + K_1 G(s)]^{-1}$ *is strictly positive real.*

If the sector condition is satisfied only on a set $Y \subset R^p$, *then the foregoing conditions ensure that the system is absolutely stable with a finite domain.*

The next lemma gives a characterization of a strictly positive transfer function, [22].

Lemma *Let* $G(s)$ *be a* $p \times p$ *proper rational transfer function matrix, and suppose det*$[G(s) + G^T(-s)]$ *is not identical zero. Then,* $G(s)$ *is strictly positive real if and only if*

- $G(s)$ *is Hurwitz; that is poles of all elements of G(s) have negative real parts,*
- $G(j\omega) + G^T(-j\omega)$ *is positive definite for all* $\omega \in R$, *and*
- *either* $G(\infty) + G^T(\infty)$ *is positive definite or it is positive semidefinite and* $\lim_{\omega \to \infty} \omega^2 M^T [G(j\omega) + G^T(-j\omega)] M$ *is positive definite for any* $p \times (p-q)$ *fullrank matrix* M *such that* $M^T [G(\infty) + G^T(\infty)] M = 0$, *where* $q = rank[G(\infty) + G^T(\infty)]$.

4.4.2 Loop transformation to asymptotically stable linear part

A state-space representation $(\overline{A}, \overline{B}, \overline{C}, \overline{H})$ of the system is given in Eq.(4.24) and Eq.(4.27). Let us denote the backlash nonlinearities modeled by a dead-zone as defined in Eq.(4.26) by $\phi(\cdot)$. Then we can write

$$\begin{aligned} \dot{\overline{x}} &= \overline{A}\overline{x} + \overline{B}u + \overline{H}u_3 \\ y &= \overline{C}\overline{x} \\ u &= \phi(y), \end{aligned} \tag{4.68}$$

where

$$\phi(\cdot) = \begin{bmatrix} dz_{2\alpha}(\Theta_{d1}) & 0 \\ 0 & dz_{2\alpha}(\Theta_{d2}) \end{bmatrix} \tag{4.69}$$

with

$$dz_{2\alpha}(\Theta_d) = \begin{cases} \Theta_d - \alpha, & \Theta_d > \alpha, \\ 0, & |\Theta_d| < \alpha, \\ \Theta_d + \alpha, & \Theta_d < -\alpha \end{cases} \tag{4.70}$$

and $(\overline{A}, \overline{B}, \overline{C}, \overline{H})$ as given in Eq.(4.27).

Now the loop can be transformed as shown in Fig.4.8. With this transformation the linear part becomes asymptotically stable and is in negative feedback with the nonlinear part $\tilde{\phi}(\cdot)$. The latter becomes a saturation with a positive slope K and saturation bounds $[-K\alpha, K\alpha]$, see Fig. 4.9. The system can then be written as

$$\begin{aligned} \dot{\overline{x}} &= (\overline{A} + \overline{B}K\overline{C})\overline{x} + \overline{B}\tilde{u} + \overline{H}u_3 \\ y &= \overline{C}\overline{x} \\ \tilde{u} &= -\tilde{\phi}(y), \end{aligned} \tag{4.71}$$

where

$$\tilde{\phi}(\cdot) = \begin{bmatrix} sat_{2\alpha}(\Theta_{d1}) & 0 \\ 0 & sat_{2\alpha}(\Theta_{d2}) \end{bmatrix} \tag{4.72}$$

with

$$sat_{2\alpha}(\Theta_d) = \begin{cases} K\alpha, & \Theta_d > \alpha, \\ K\Theta_d, & |\Theta_d| < \alpha, \\ -K\alpha, & \Theta_d < -\alpha. \end{cases} \tag{4.73}$$

4.4.3 Loop transformation to analyze the influence of the constant input

The system loop as given in Eq.(4.71) is again transformed such that the influence of the constant input is split from the rest of the system as shown in Fig 4.10. This is possible without any restrictions as the poles of the transfer function matrix
$G(s) = \overline{C}[sI - (\overline{A} + \overline{B}K\overline{C})]^{-1}[\overline{B}H]$ lay all in the LHP. The system can thus be written as

$$\begin{aligned} y &= \tilde{G}(s)\tilde{u} + G_{T_{m2}}u_3 \\ \tilde{u} &= -\tilde{\phi}(y). \end{aligned} \tag{4.74}$$

For a slope of both saturation nonlinearities of $K = 1$, one obtains the following transfer function matrices, wchich have the same denominator polynomial with all poles in the LHP

$$\tilde{G}(s) = \begin{bmatrix} \tilde{G}_{11} & \tilde{G}_{12} \\ \tilde{G}_{21} & \tilde{G}_{22} \end{bmatrix} = \overline{C}[sI - (\overline{A} + \overline{BC})]^{-1}\overline{B}, \tag{4.75}$$

and

$$G_{T_{m2}}(s) = \begin{bmatrix} G_{T_{m2}11} \\ G_{T_{m2}21} \end{bmatrix} = \overline{C}[sI - (\overline{A} + \overline{BC})]^{-1}H. \tag{4.76}$$

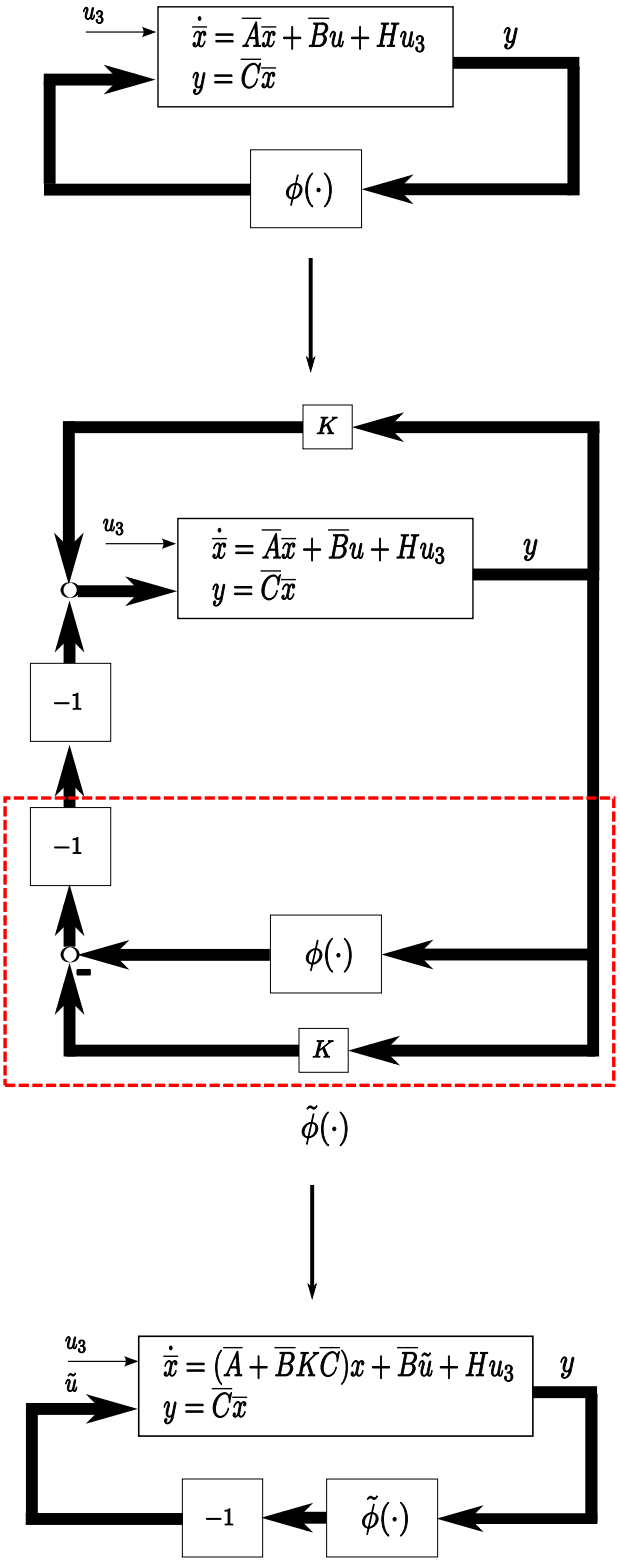

Figure 4.8: Loop-transformation for state-space representation of the nonlinear three-mass system of Eq.(4.68). The transformed loop contains a asymptotically stable linear part, which is in negative feedback with the nonlinearity.

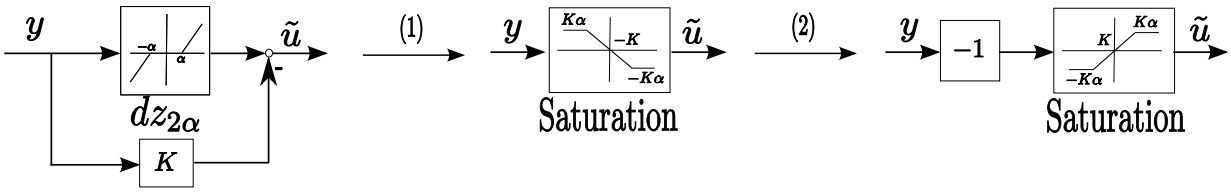

Figure 4.9: Transformation of a dead-zone into a saturation.

4.4.4 Coordinate transformation and sector bound changes under influence of an offset

Now the influence of the constant input u_3 is interpreted as an offset. The equilibrium point of the system given in Eq.(4.74) does not lay in the origin as soon as $u_3 \neq 0$, see Section 4.3. However, the *multivariable circle criterion* can only be applied to analyze stability with respect to the origin. Therefore the system coordinates are transformed for the stability analysis as follows

$$\tilde{x} = x + \Delta x, \tag{4.77}$$

where

$$\Delta x = H u_3. \tag{4.78}$$

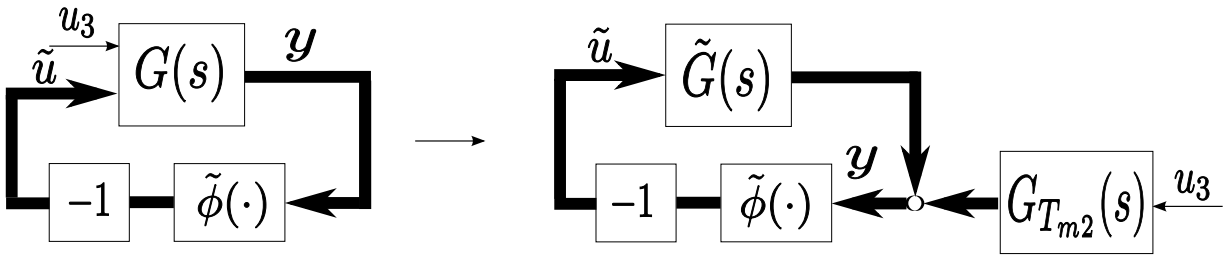

Figure 4.10: Loop transformation of the system given in Eq.(4.71) to analyze the influence of the constant input u_3.

The transformation has no influence on the linear dynamics of the system, but on the nonlinearity. The influence of the offset on a saturation nonlinearity is shown in Fig. 4.11 for a positive offset $G_{T_{m2}} u_3 > 0$. For a negative offset the effect is reflected on the origin of the original coordinate system.

One can observe how the operating range of the nonlinearity changes due to the coordinate transformation, see Fig. 4.11. This affects also the sector bounds of the saturation. In Fig. 4.12 the effects on the sector bounds of the nonlinearity are shown for a positive offset. The upper bound k_2 decreases with increasing magnitude of the offset, while the lower bound remains constant $k_1 = 0$. This fact is crucial for the stability analysis of the system depending on the constant input u_3.

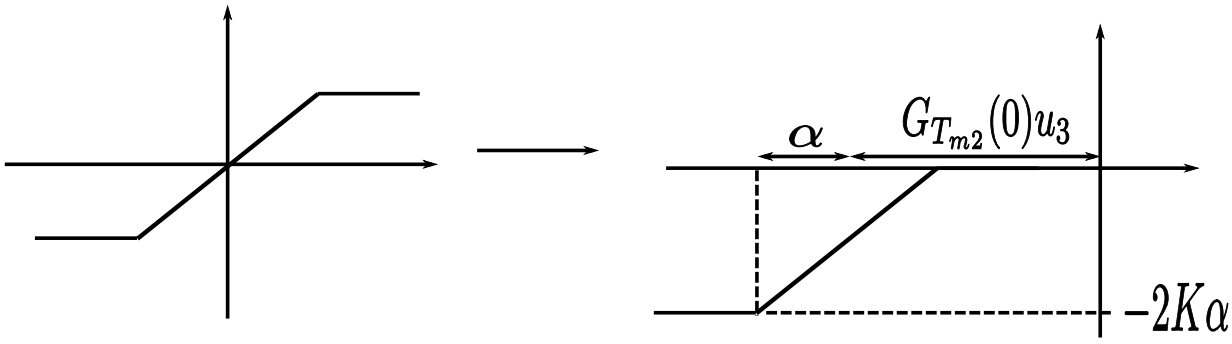

Figure 4.11: Changes in a saturation nonlinearity under coordinate transformation.

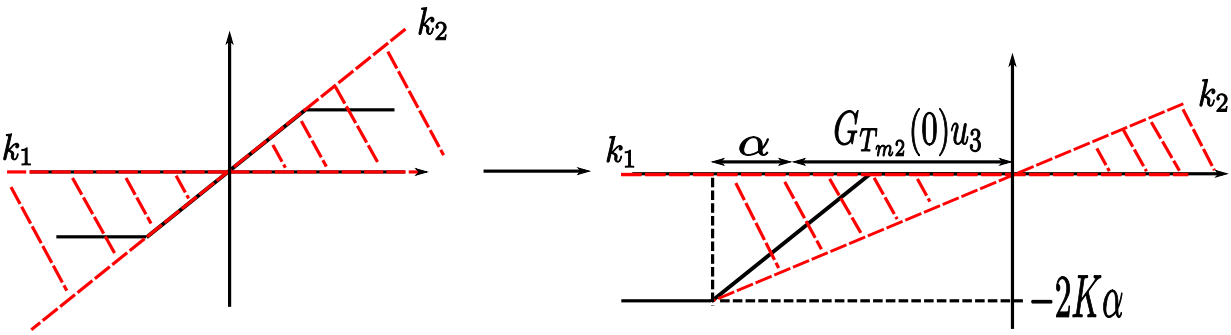

Figure 4.12: This figure illustrates the effects of an offset on sector bounds of a saturation. The upper bound k_2 decreases with increasing magnitude of the offset, while the lower bound k_1 remains constant.

4.4.5 Global stability analysis

As shown in the previous Subsection 4.4.4, the constant input u_3 can be used to influence the upper sector bound of the nonlinearities. To quantify the impact of the constant torque we look at

$$G_{T_{m2}}(0) = \begin{bmatrix} G_{T_{m2}11}(0) \\ G_{T_{m2}21}(0) \end{bmatrix} = \begin{bmatrix} \frac{-2.455e8}{8.103e11} \\ \frac{2.455e8}{8.103e11} \end{bmatrix}. \tag{4.79}$$

Thus, the constant input influences both nonlinearities with the same magnitude, but different signs in the stationary case. The constant input shifts their operating points in opposite directions, but as the magnitude is equal they lay in the same sector. One block is shifted into the upper right quadrant and the other one into the lower left quadrant. Consequently both saturation blocks are bounded by the same sector bounds $[k_1, k_2]$, where the lower bound is always $k_1 = 0$.

This fact is now used in the stability analysis in the following way: We try to find the highest upper bound $k_2 \in (0, 1]$ for which the system is stable according to the *multivariable circle criterion*. Then we are able to determine the minimal necessary magnitude of the constant input needed to achieve global stability.

Stability analysis

In our case the second point of the *multivariable circle criterion* as given in Subsection 4.4.1 applies. As always

$$K_1 = \begin{bmatrix} k_1 & 0 \\ 0 & k_1 \end{bmatrix}$$

with $k_1 = 0$, we simply need to find the maximum

$$K_2 = \begin{bmatrix} k_2 & 0 \\ 0 & k_2 \end{bmatrix}$$

with $k_2 \in (0, 1]$, such that $[I + K_2\tilde{G}(s)]$ is strictly positive real.

To check positive definiteness we use the Lemma given in Subsection 4.4.1. Point 1 and 3 of the Lemma hold for any $k_2 \in (0, 1]$:

- As the original system $(\overline{A}, \overline{B}, \overline{C}, \overline{H})$ was transformed in a way that the linear part $\tilde{G}(s)$ is stable, also $[I + K_2\tilde{G}(s)]$ will always be Hurwitz.

- As the system $(\overline{A}, \overline{B}, \overline{C}, \overline{H})$ is causal, $[I + K_2\tilde{G}](\infty) + [I + K_2\tilde{G}]^T(\infty) = 2I \quad \forall k_2 \in (0, 1]$, which is positive definite.

Thus, we need to check for which k_2 the transfer function matrix $[I+K_2\tilde{G}](j\omega)+ [\, I+ K_2\, \tilde{G}\,]^{\,T}\,(-j\omega)$ is positive definite. If we do so, we obtain the following result:

The system is globally stable for $k_2 \leq 0.7349$.

Determination of required torque magnitude

Using the graphical approach of Fig. 4.11 the following equation for the determination of u_3 can be derived

$$u_3 = \frac{-K\alpha(2 + k_2)}{G_T(0)k_2}, \tag{4.80}$$

where $K = 1$ is the slope of the saturation and $G_T = |G_{T_{m2}11}(0)| = |G_{T_{m2}21}(0)| = |3.0297e - 4|$.

For $k_2 = 0.7349$ this gives $|u_3| = 1.0719e3$. Thus, for $u_3 \geq 1.0719e3$ the system is globally stable.

Note that this result might be conservative as global stability is guaranteed for any nonlinearity in the sector $[0, k_2]$ and not only for the actual considered shifted saturation.

4.5 Dual motor control with constant torque

In order to verify the results of the stability analysis in Section 4.3 and Section 4.4 the system structure as presented in Fig.4.6 in Section 4.3 is now implemented in Matlab/Simulink.

To avoid the systems´ behavior shown in Subsection 4.2.2, the second motor should now be used to act in the opposite direction of the driving motor in order to close the backlash gap.

This approach is implemented using the same transfer function for T_{m2} as in equation (2.74) in Chapter 2. The only parameter which changes, is the magnitude of the constant torque $|T_{m2}|$. For its determination, various simulations with changing magnitude of $|T_{m2}|$ are considered (Fig. 4.13). Thereby, the controller parameters of the first motor remain equal to the ones described in the previous section and the torques are applied at $t = 0$ [s]. The step height is set to 0.1 [m] and the system is assumed to be in contact in the beginning of the motion, that is $\Theta_d(t = 0) = \alpha$ and $\Theta_{d2}(t = 0) = -\alpha$.

For torque magnitudes over $|T_{m2}| = 2$ [Nm] the limit cycles can be oppressed and the system seems to be stable. However, one can observe small overshoots in the step response when the torque magnitude is below $|T_{m2}| = 20$ [Nm]. Thus, a good performance is achieved for magnitudes around $|T_{m2}| = 20 - 25$ [Nm]. Higher magnitudes do not change the performance significantly. This underlines the conservatism of the global stability analysis presented in Section sec:globStabAnalysisThreeMass.

Note however, that the system shows a negative response behavior as consequence of the additional constant torque in opposite driving direction, since in the beginning $T_{m2} > T_{m1}$. This behavior is more distinctive the higher the torque magnitude. Consequently, for an overall satisfying performance a trade-off between the overshoot and the negative response is needed.

Another possibility is to apply the constant torque not until a certain point in time. This is the case for the simulation results shown in Fig. 4.14, where the torque is not applied until $t = 50$ [s], that is when limit cycles already exist.

Also in this case a constant torque can oppress the limit cycles. However, a sparse higher magnitude is required as in the previous simulations. Namely, the limit cycles are not eliminated with a magnitude $|T_{m2}| = 2$ [Nm], but with $|T_{m2}| = 3$ [Nm] and higher. A good performance can be achieved by setting $|T_{m2}| = |5 - 15|$. Higher torques lead to a higher outlier in a first moment.

An advantage compared to the first simulations, is that no negative response behavior is observed. This means a significantly improvement in the performance, as negative response behavior should be avoided in position control.

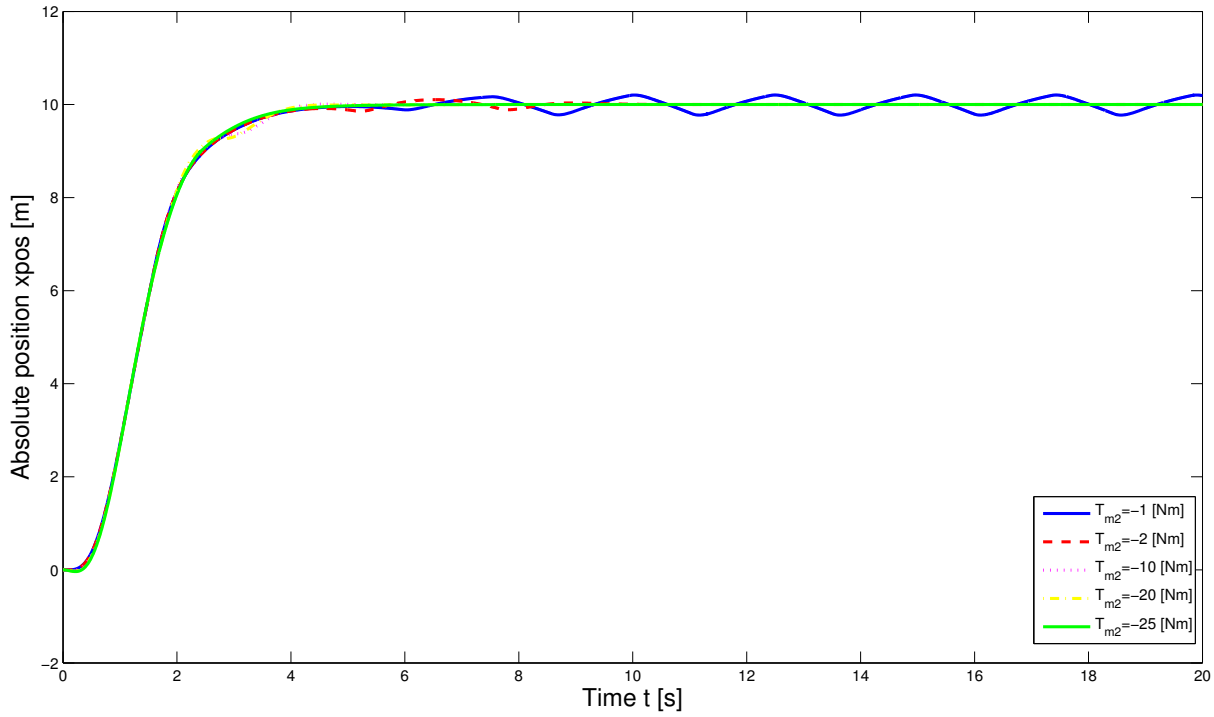

Figure 4.13: Performance of the nonlinear three-mass system for different magnitudes of T_{m2} applied at $t = 0$ [s]. The limit cycles can be oppressed with a torque magnitude of $|T_{m2}| \geq 2$ [Nm].

Two simulation results for a constant torque starting at $t = 0[s]$ with $T_{m2} = -20[Nm]$ and $t = 50[s]$ with $T_{m2} = -10[Nm]$ are shown in Fig. 4.15 and Fig. 4.16 respectively.

One can conclude that the approach of using a dual motor control strategy to reduce the backlash effects in a robot actuator actually works also for the three-mass system. As in the case of the two-mass system, applying a torque from $t = 0[s]$ on requires a higher controller output. Additionally, a negative response behavior can be observed in the beginning of the motion.

Contrary, applying the torque on a later point in time, the already existing limit cycles are eliminated. The difficulty is to determine the optimal point in time, when to start applying the torque. Furthermore, this strategy does not allow a dynamical behavior of the second motor.

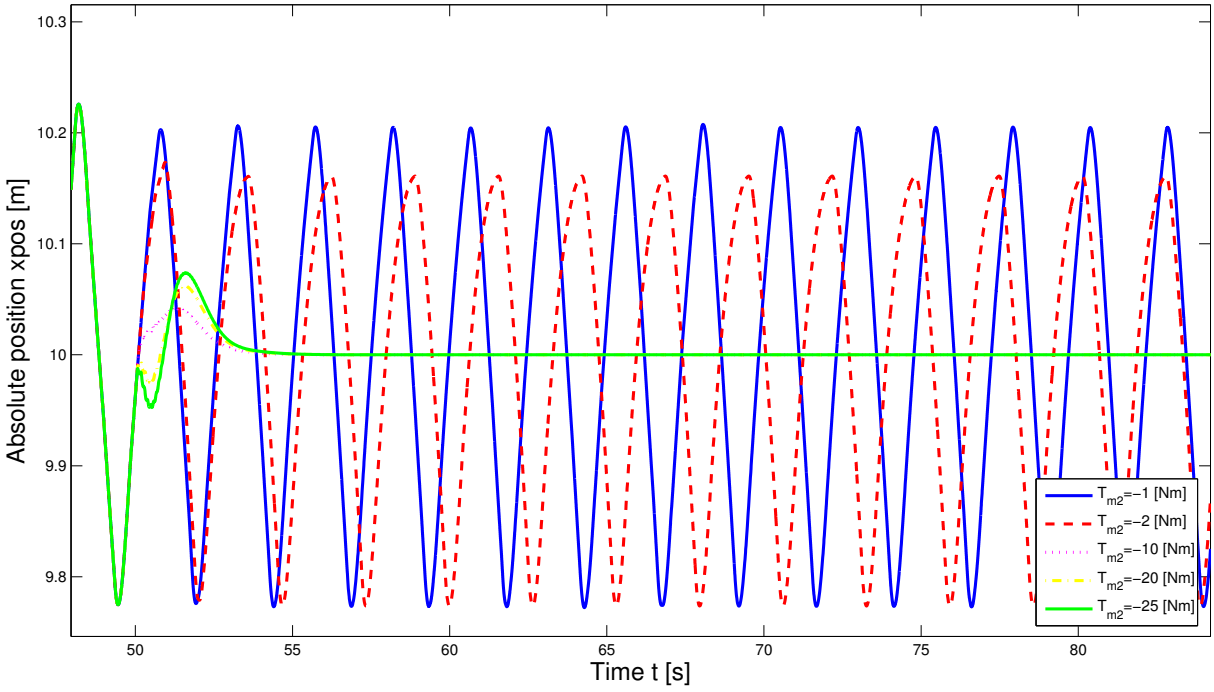

Figure 4.14: Performance of the nonlinear three-mass system for different magnitudes of T_{m2} applied at $t = 50$ [s]. The limit cycles can already be oppressed with a torque magnitude of $|T_{m2}| \geq 3$ [Nm].

4.6 Nonlinear dual motor control of a three-mass system

In the previous Sections 4.3, 4.4 and 4.5 it was shown that the system can be locally stabilized by driving the additional second motor with a constant torque. However, some disadvantages of this operation mode were discussed at the end of Section 4.5.

Therefore, more sophisticated operating strategies are developed in order to reduce the required total input power of the system. The aim is to use both motors for the motion drive while the system is not in backlash and to switch the operating of the second motor when the system gets into backlash for fast closing the backlash gap and avoiding limit cycles. Different approaches are developed and tested in simulations. Here, Motor_1 is always considered to be the main driving or master motor, whereas Motor_2 is regarded as

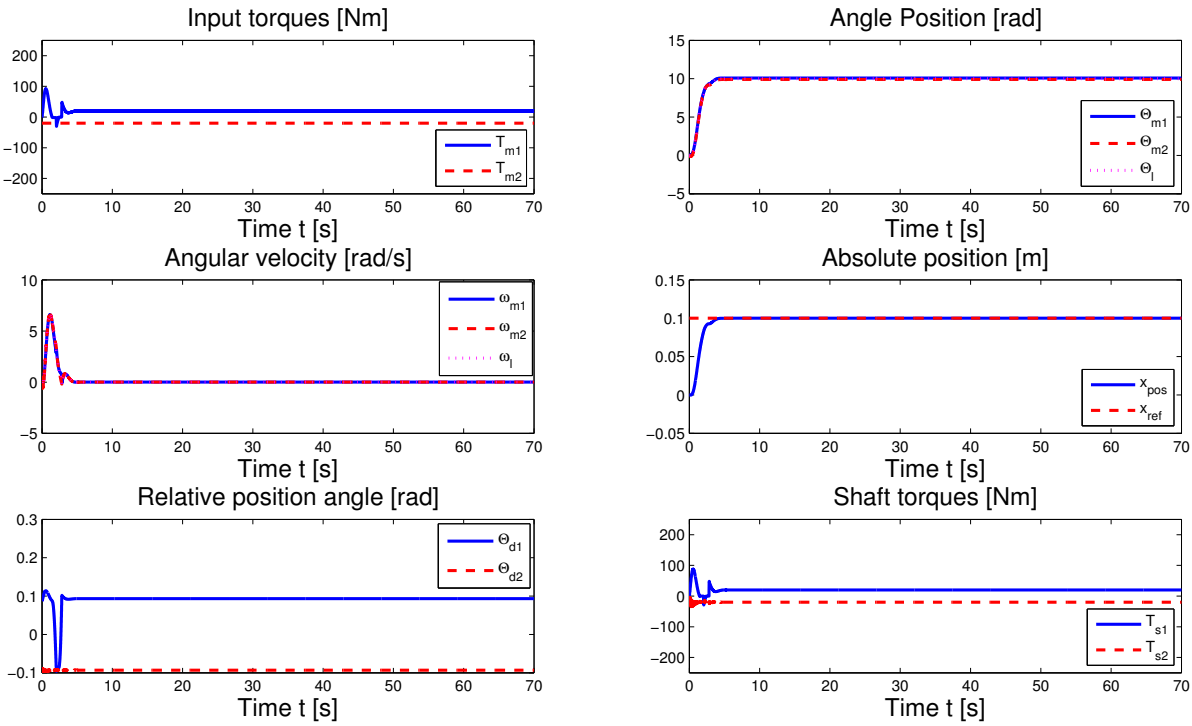

Figure 4.15: Dual motor control with constant torque $T_{m2} = -20$ [Nm] at $t = 0$ [s]. As consequence of the constant torque, no limit cycles appear and the system reaches its desired final position.

switching or slave motor.

As already described in Chapter 2, the first function determines T_{m2} regarding the relative position angle Θ_{d1}, whereas the second function does the same but depending on the relative error e_{abs}. The third and last approach represents a combination of the first and the second option.

In contrast to Chapter 2, the switching modes lead now to a nonlinear, smooth switching control law for the slave motor. This is due to the fact, that the motor is additionally used to support the master motor, when the system is not in backlash. The step height is set to 0.1 [m] and the system is assumed to be in contact in the beginning of the motion, that is $\Theta_d(t = 0) = \alpha$ and $\Theta_{d2}(t = 0) = -\alpha$.

The plots for illustrating the simulation results do normally not cover the same time period as the one for demonstrating the arise of limit cycles in the nonlinear system of the

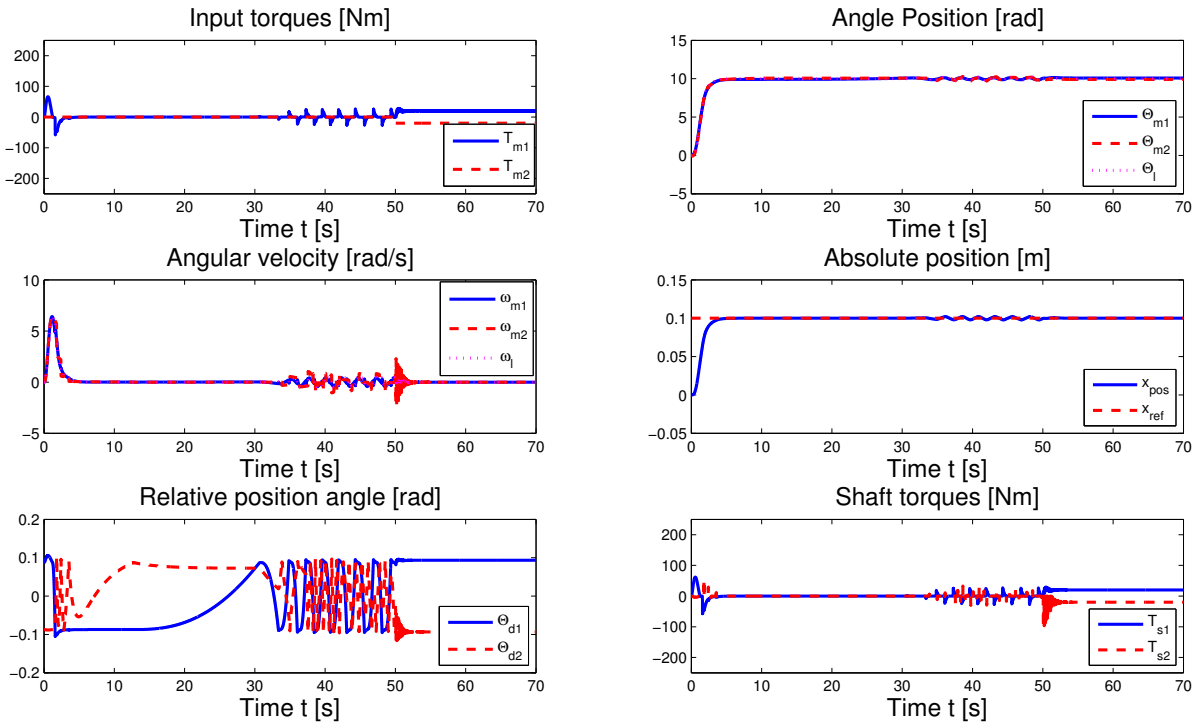

Figure 4.16: Dual motor control with constant torque $T_{m2} = -10$ [Nm] at $t = 50$ [s].The limit cycles appear approximately after 15 [s] and can be oppressed by a constant torque, which starts acting after 50 [s].

previous section($t = [0, 70]$ [s]), but a shorter one. This is due, to a better presentation of the performance of each switching strategy. Of course, all strategies are tested for longer time periods up to 500 [s].

4.6.1 Switching function for the slave motor

To achieve a smoother switching between both operating modes of Motor$_2$, the switching function K_{switch} given below is implemented

$$\begin{aligned} U_2(s) &= K_{switch}(Y_{ref}(s), Y_{meas}(s), v, |T_{m2}|) \\ &= K(K_{PID/P} + |v|(K_{T_{const}} - K_{PID/P}))(Y_{ref}(s), Y_{meas}(s), v, |T_{m2}|), \end{aligned} \tag{4.81}$$

where $v \in [0, 1]$ is the to defining switching variable, $K_{PID/P}$ is the control function

corresponding to the cascaded controller as designed in Section 4.2 for the second motor and $K_{T_{const}}$ is defined analogue to Chapter 2, but with varied gain

$$T_{m2} = K_{T_{const}} v = 10\text{sign}(v). \tag{4.82}$$

As in all cases, the torque is not constantly applied from the beginning on a magnitude of $|T_{m2}| = 10$ may be sufficiently high according to the simulation results shown in Section 4.5. Note that in K_{switch} only the absolute value of v is used, as the sign of the switching variable v is only used to determine the sign of the torque in $K_{T_{const}}$.

This implementation follows an approach for a switched controller given in [4], but with a varied determination of v. Different definitions for v are given in equations (2.75), (2.77), (2.78) and (2.79). A scheme of the switching function is shown in Fig. 4.17.

4.6.2 Feed-forward control for the master motor

Furthermore, a feed-forward structure is implemented to provide the master motor with information about the switching status of the slave motor. The aim is to reduce the impact of the switching of the second motor on the system response. Additionally it should help to avoid an inverse response behavior.

If we rewrite K_{switch} of equation (4.81) into

$$K_{switch} = K_{PID/P}(1 - |v|) + |v| K_{T_{const}}, \tag{4.83}$$

we can see, that the switching function damps $K_{PID/P}$ to 0 with increasing value of $|v|$, whereas the portion of $K_{T_{const}}$ increases with increasing $|v|$. Thus, we can take advantage of the signal $|v|K_{T_{const}}$ for improving the performance of the system by feed-forward control. This is achieved by adding inversely the weighted constant torque signal to the output of the PID/PI-controller of the master motor, that is

$$u_{1,FF} = u_1 - |v| K_{T_{const}}(sign(v), |T_{m2}|). \tag{4.84}$$

An overview of the complete control structure is given in Fig. 4.18. There the calculation of the feed-forward signal is included in the block representing K_{switch}.

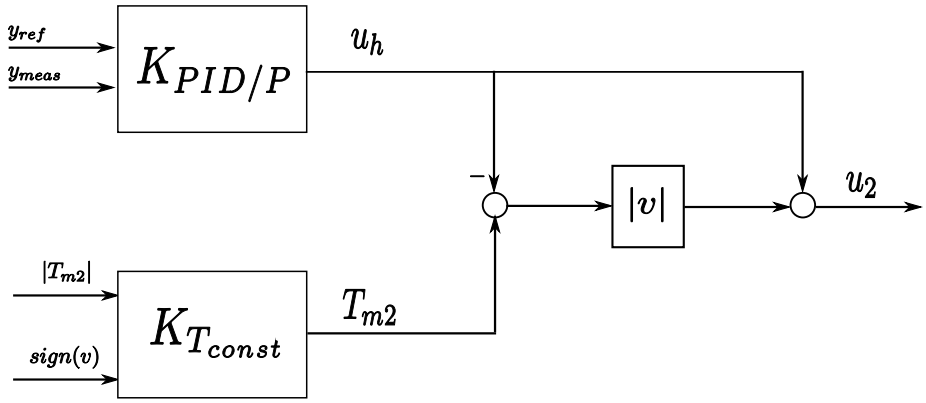

Figure 4.17: Switching function K_{switch}. The function depends on the switching variable v, for which different definitions are given in equations (2.75), (2.77), (2.78) and (2.79).

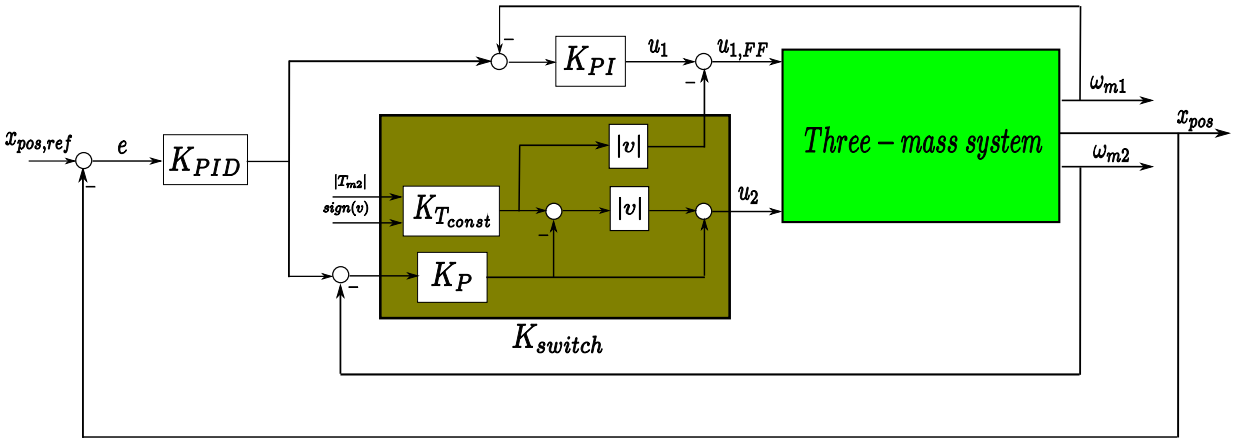

Figure 4.18: Nonlinear dual motor control structure of a three-mass system. K_{switch} defines the switching of the slave motor and provides the master motor with additional information through a feed-forward structure.

4.6.3 Switching-strategy for dual motor control depending on Θ_{d1}

The proposed control strategy in this section is based on the relative position angle between Motor_1 and the load $\Theta_{d1} = \Theta_{m1} - \Theta_l$, as this is an indicator whether the system is actually operating in backlash mode or not. If the system is not in backlash, that is $|\Theta_{d1}| > \alpha$, both motors should be used as driving motors. But if the system is in backlash, that is $|\Theta_{d1}| < \alpha$, the second motor should act in opposite direction of the motion, as presented in Section 4.5.

The backlash state of the second motor with respect to the load is not taken into consideration, as the first motor is seen as the main driving element and it is supposed that the second backlash gap will be automatically closed when the accordant motor is switched into constant torque mode. The switching variable v is defined in equation (2.77) with Θ_{d1} as input argument.

This strategy leads to the result presented in Fig. 4.19. One can observe that the control power of each motor is actually lower than in the previous case and that the second motor takes actively part in the driving task. Unfortunately, this strategy is not robust against disturbances, especially in the final position. This might be mainly due to the then constant switching between the backlash and non-backlash case.

As before, this strategy does not achieve the desired improvement in performance. Again, one can observe that in the undisturbed case, the constant torque is switched to 0 in the final position and thus according to Section 4.3 no stable behavior can be obtained.

However, the negative response behavior observed in the simulations of the two-mass system can be avoided due to the additional feed-forward control.

Conclusions:

- No elimination of limit cycles, when disturbances are present.
- Advantage: Closing backlash gap when existing, even in the beginning.

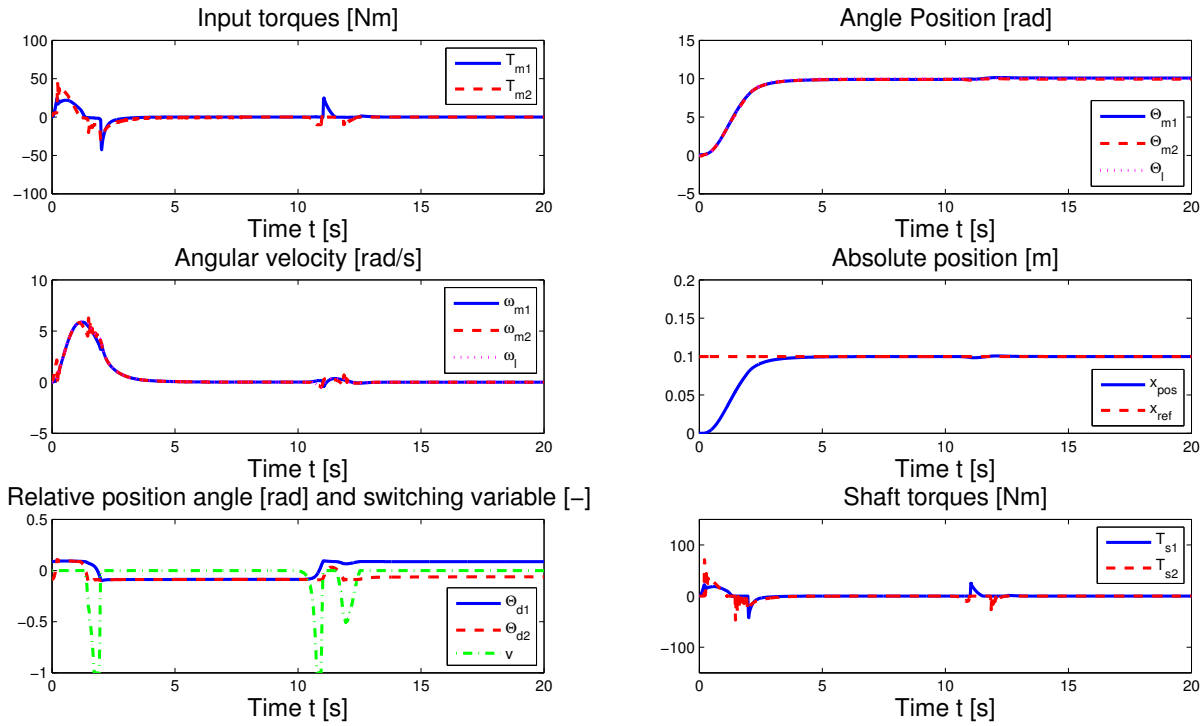

Figure 4.19: Dual motor control with $v = f(\Theta_{d1})$. In the undisturbed case, the strategy does not fulfill the requirements.

- Disadvantage: No local stability as control signals becomes 0 in the final position.
- Requirements cannot be fulfilled.

4.6.4 Switching-strategy for dual motor control depending on e_{abs}

Here, the switching variable v is determined according to Eq.(2.78). The performance of this set is shown in Fig. 4.20. The switching parameters are set to $e_{max} = 0.25$ and $e_{min} = 0.01$. The limit cycles are oppressed and the required controller energy is distributed on both motors in the beginning of the motion. Additionally a smooth response is obtained and the strategy is robust against disturbances. As the second motor is acting with a constant torque in the final position, local stability can be achieved according to Section 4.3.

A small overshoot of 0.3% is observed in the simulation, which was not the case when

acting with a constant torque from the beginning of the motion on. This might be due to the impact of the switching of the second motor on the process. However, the overshoot can be eliminated by e.g. increasing the P-gain on the PID-controller of the outer loop from 200 to 250-300. Then the control signal of the first motor increases and it can faster compensate the impact of the constant torque. Further, the distribution of power when both motors act together remains equal.

Actually, the P-gain has to be increased depending on the desired accuracy of the position trajectory. For small position changes, the control output signals are lower, thus the impact of the constant torque switching are higher and more difficult to compensate for the master motor. A higher controller gain allows to react on this fact.

But as already stated in the discussion for the two-mass case, one has to be careful when the trajectory path is lower than $r_l\alpha$, that is $l_{path} \leq r_l\alpha$. However, the same methods as presented in Subsection 2.5.2 may solve this problem.

Conclusions:

- Strategy fulfills requirements.
- Switching dependent on relative error with respect to final position, not on backlash-state.
- Therefore, no reaction if system is in backlash while $e_{abs} < e_{max}$.
- Strategy is robust against load disturbances.
- Need to adapt parameters e_{max} and e_{min} depending on trajectory path length l_{path}.

4.6.5 Switching-strategy for dual motor control depending on Θ_{d1} and e_{abs}

The last switching-version is a combination of the first and the second. It aims to join both switching reference values Θ_{d1} and e_{abs} in order to be able to react to backlash-situations during the motion and especially avoid limit cycles when reaching the final

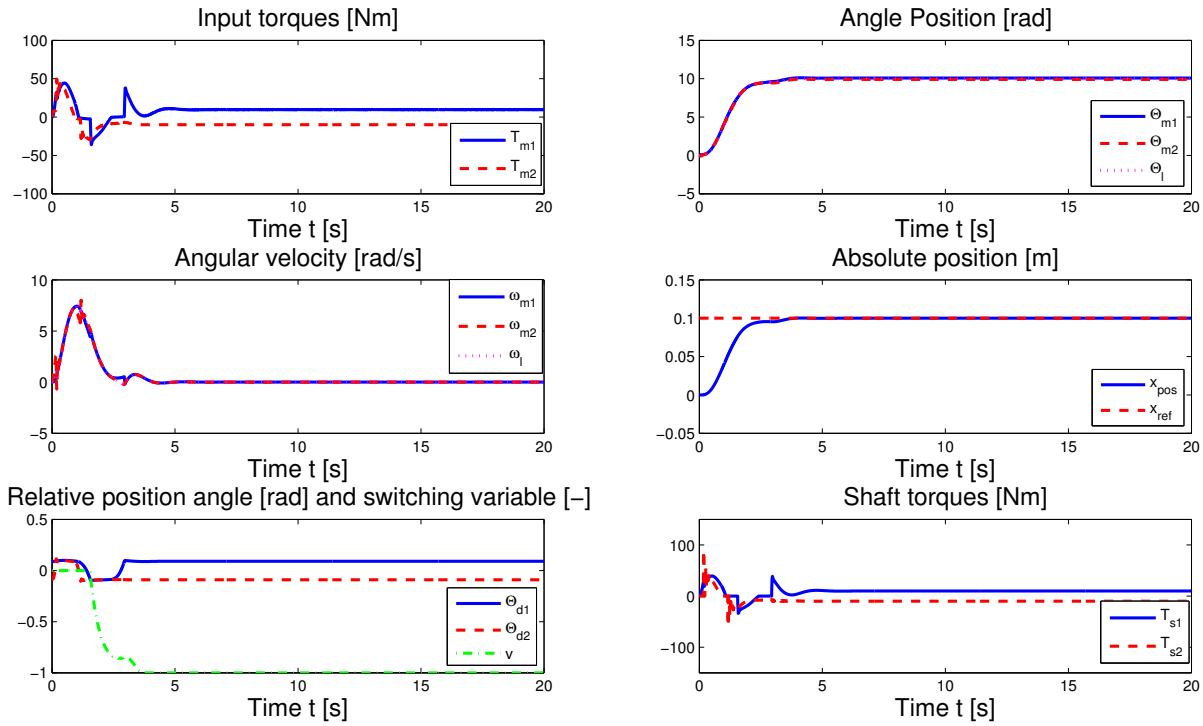

Figure 4.20: Dual motor control with $v = f(e_{abs})$.The limit cycles are oppressed and the required controller energy is distributed on both motors in the beginning of the motion. Furthermore a smooth response is obtained and the strategy is robust against disturbances.

position. Therefore v is defined according to equation (2.79) with Θ_{d1} and e_{abs} as input arguments.

This strategy leads to the behavior presented in Fig. 4.21. It shows a satisfactory behavior, similar to the case when $v = f(e_{abs})$. But it could eventually lead to an inverse response behavior, when the system is in backlash at the beginning of the motion.

Conclusions:

- Satisfactory behavior, similar to case when $v = f(e_{abs})$.
- Closing of eventual backlash gaps during transition.
- Robust against load disturbances.

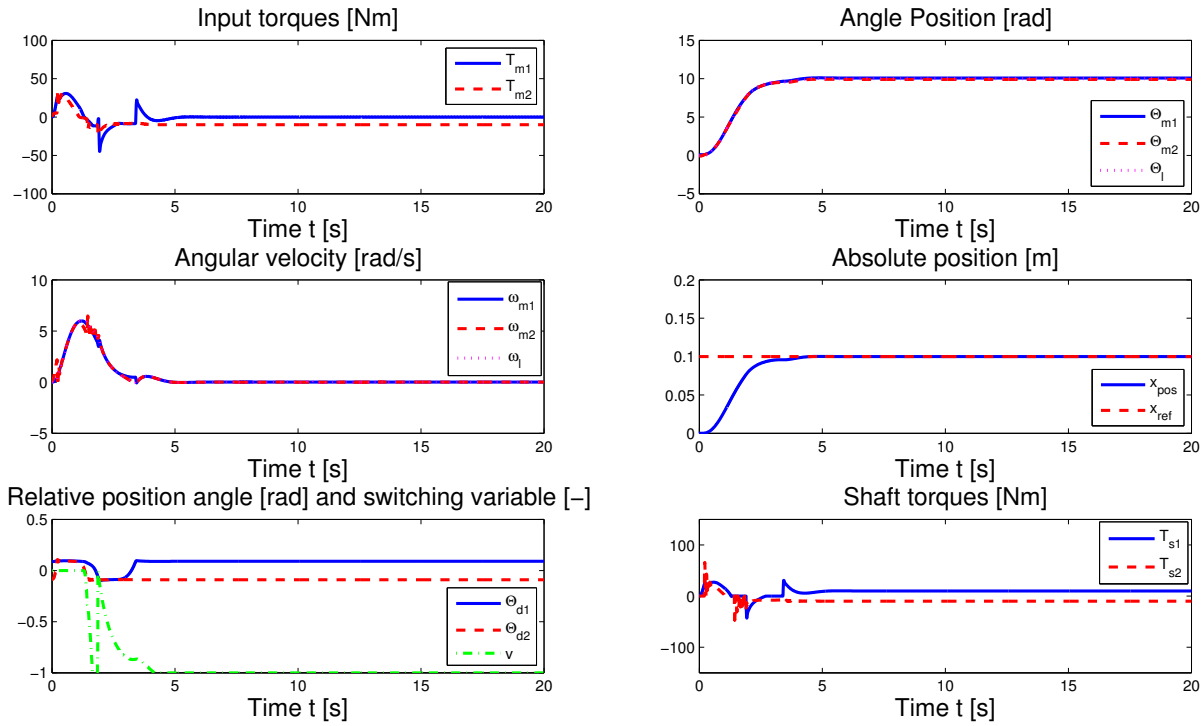

Figure 4.21: Dual motor control with $v = f(\Theta_{d1}, e_{abs})$. This alternative shows a satisfactory behavior, similar to the case when $v = f(e_{abs})$. But it could eventually lead to an inverse response behavior.

4.6.6 Comparison of the different switching-strategies for a sequence of input-positions

Now, all three different switching-strategies are tested and compared for the following sequence of input-positions $x_{pos,ref} = [0.1, 1, -2.5, 0]$, with $x_{pos,start} = 0$. No disturbances are considered, that is $T_d = 0$. The results are presented in Figs. 4.22, 4.23 and 4.24.

Here, defining $v = f(e_{abs})$ seems to achieve the best performance in terms of a smooth and efficient motion. Even in the undisturbed case the variant using $v = f(\Theta_{d1})$ shows up to have an undesired behavior, as can e.g., be observed by the oscillations in v around $t = 12$ [s].

Operating with a switching-function based on both variables, also leads to a less advantageous performance as determining v only depending on the relative error e_{abs}. The

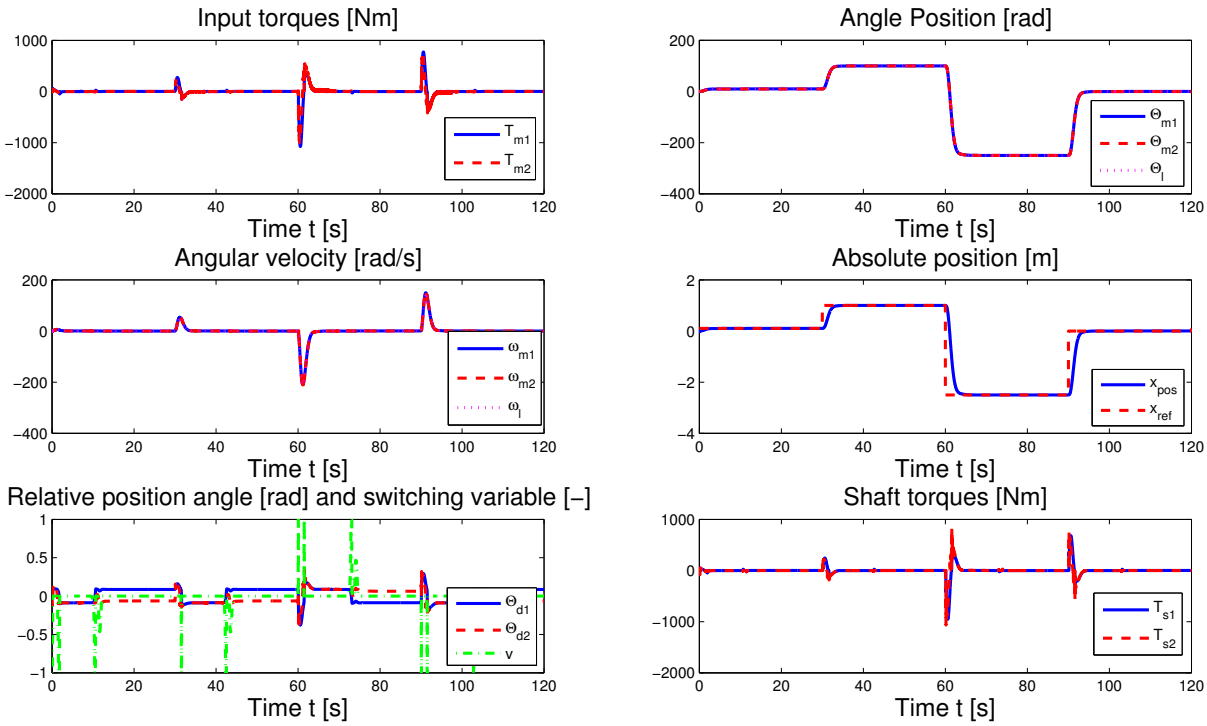

Figure 4.22: Input-sequence with $v = f(\Theta_{d1})$. This variant has an undesired behavior, as can e.g., be observed by the oscillations in v around $t = 12$ [s].

main disadvantages of the combination are higher input and shaft torques of Motor_1, which might be provoked by the intention of closing the backlash gap in the beginning of a position change. In that situation, the motors are forced to act against each other and only Motor_1 is used as driving motor.

In conclusion, the most promising strategy seems to be the one based on $v = f(e_{abs})$ and will therefore be used for further analysis. Another advantage of this variant is that measuring the position angles Θ_{m1} of Motor_1 and Θ_l of the load becomes unnecessary.

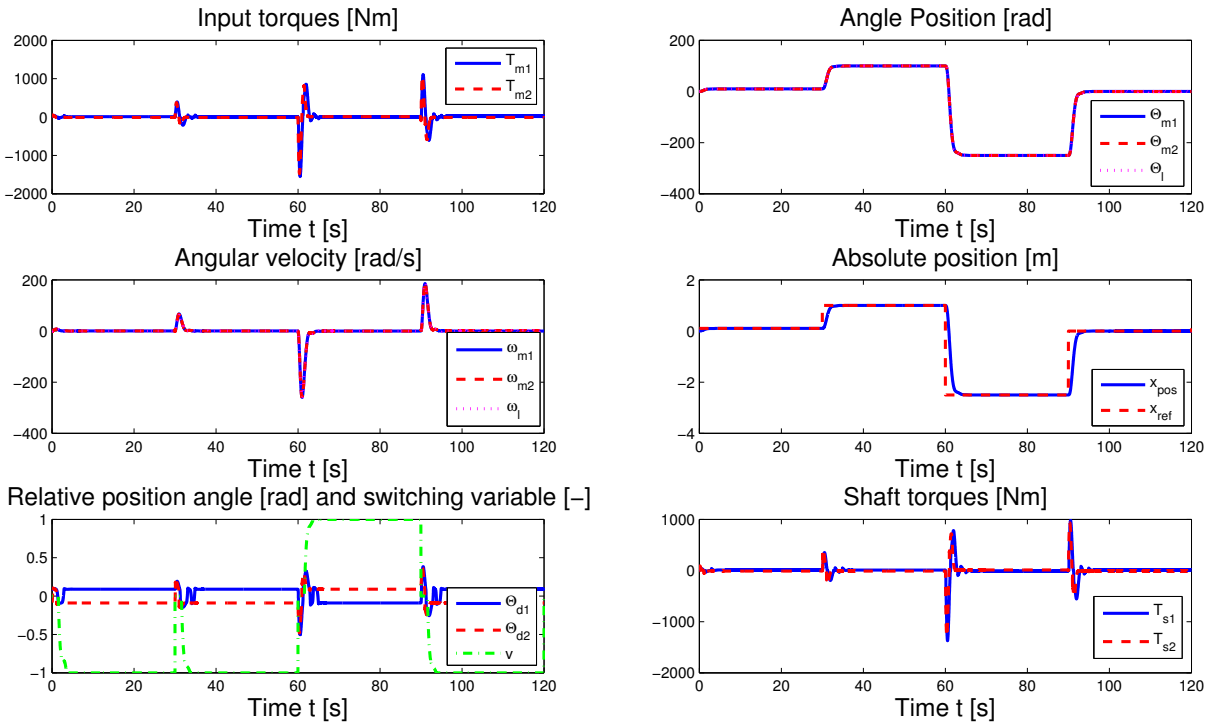

Figure 4.23: Input-sequence with with $v = f(e_{abs})$. This strategy seems to achieve the best performance in terms of a smooth and efficient motion.

4.7 Validation of the results of Matlab/Simulink in Dymola

Now, the simulation software Dymola [10] is used to verify the validity of the Matlab/Simulink model and the simulation results obtained with it. Therefore, all the different operating strategies presented in the previous sections are implemented and tested in Dymola. The model shown in Fig 4.25 is used as starting basis.

Dymola is a tool for modeling and simulation of integrated and complex systems for use within automotive, aerospace, robotics, process and other applications. It is based on the open Modelica modeling language, which allows the user to create new libraries or modify the existing ones.

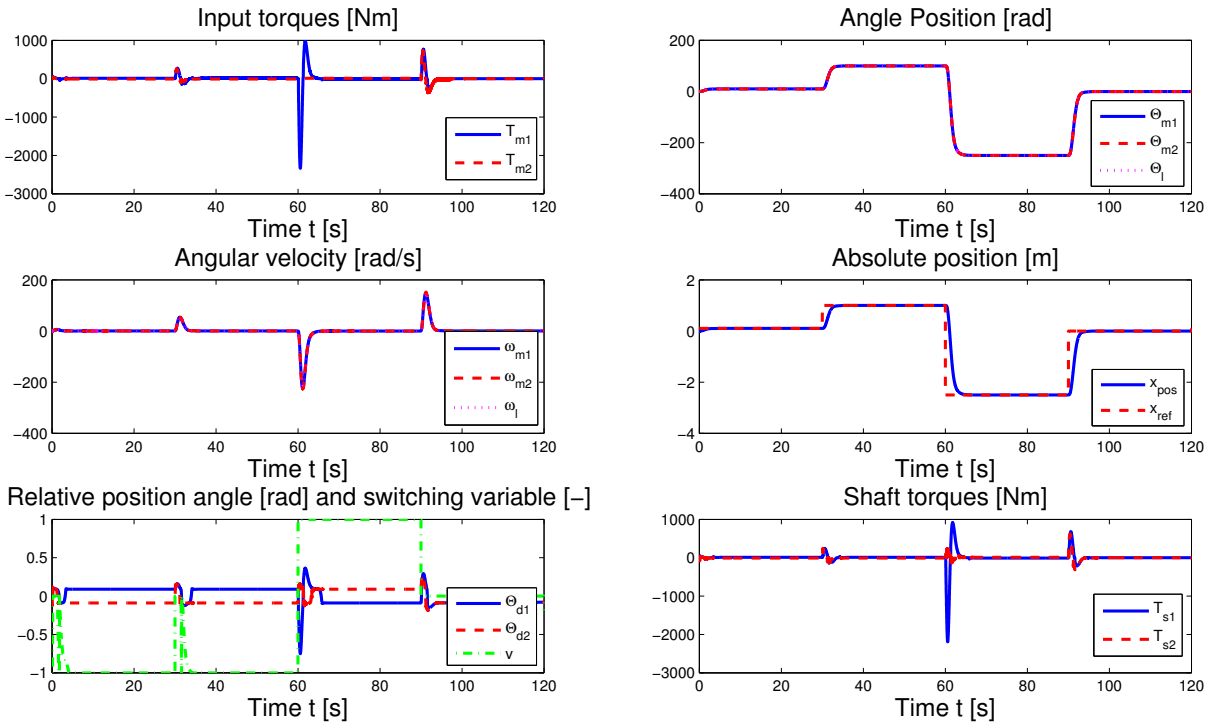

Figure 4.24: Input-sequence with $v = f(\Theta_{d1}, e_{abs})$. The main disadvantages of the combination are higher input and shaft torques of Motor_1, which might be provoked by the intention of closing the backlash gap in the beginning of a position change. In that situation, the motors are forced to act against each other and only Motor_1 is used as driving motor.

In comparison to the Matlab/Simulink environment, the modeling approach of Modelica is not signal-based, but object-oriented and based on the real physical structure of the system. This allows the equations to have no specified 'direction', as it occurs in Matlab/Simulink and gives a high importance to the physical connectors of the different blocks. The aim of Modelica is to relocate the whole mathematics into each block. The more descriptive manner of modeling in Dymola, makes it also interesting for simulation of complicated systems.

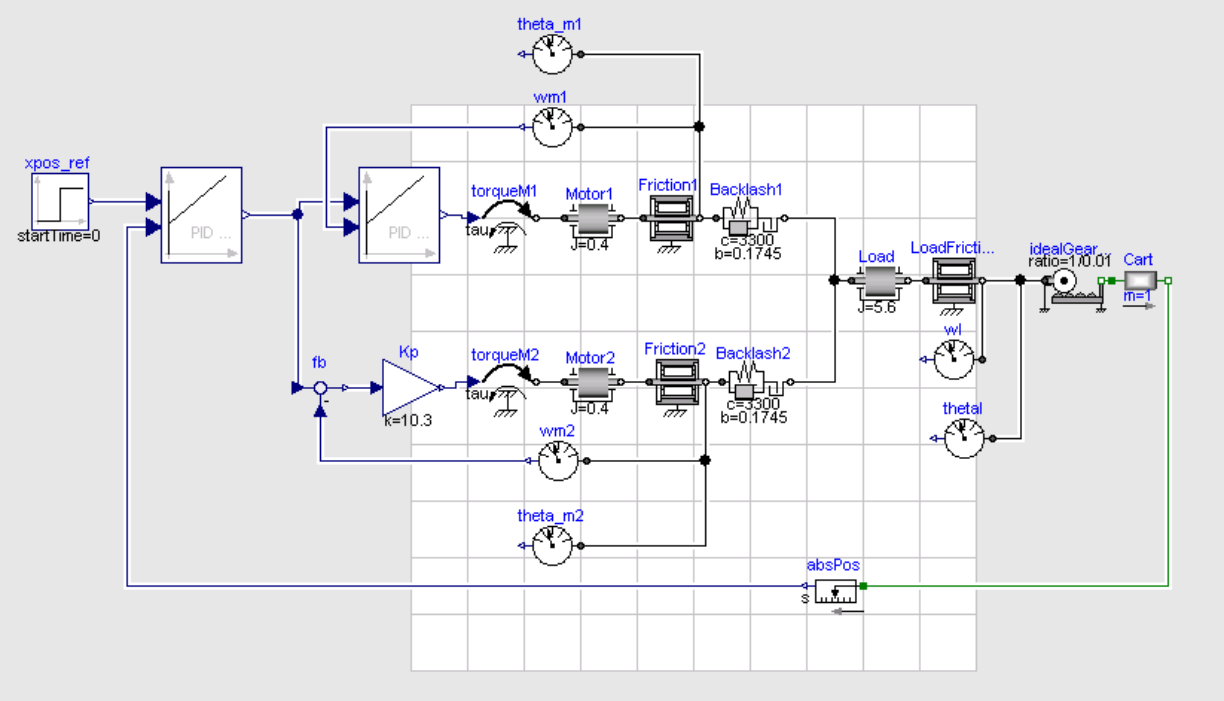

Figure 4.25: Three-mass system consisting of two motors and one load in Dymola. The backlash is represented using the mechanical backlash block, which is already implemented in Dymola.

This work is mainly done for two reasons:

- To check the correct implementation of the Matlab/Simulink model (see Fig. 4.2).
- To take advantage of the different modeling/coding approach of Dymola, in order to verify the simulation results obtained with Matlab/Simulink.

4.7.1 Dymola model

The model implemented in Dymola is also based on the three-mass model derived in Section 4.1. Consequently, it consists of two driving motors and one load, which are connected by a backlash exhibiting shaft. The implementation is illustrated in Fig. 4.25.

The backlash is represented using the mechanical backlash block, which is implemented in the Dymola Mechanical Rotational Library. Note that this backlash implementation differs from the description of Nordin´s *exact* backlash model, which was used in the

Simulink model. Several different implementations for Nordin´s model in Dymola lead to errors due to an algebraic loop when compiling the model. Hence, the backlash model already included in the Dymola library is used.

In Dymola the mechanical backlash block is implemented as a modified version of a dead-zone model, [7]. The shaft torque is determined according to

$$T_{si} = \begin{cases} k_s(\Theta_{di} - \alpha) + \min(k_s(\Theta_{di} - \alpha), c_s\omega_{di}), \\ \text{if } \Theta_{di} > \alpha \text{ and } k_s(\Theta_{di} - \alpha) + c_s\omega_{di} > 0 \\ 0, \\ \text{if } \Theta_{di} > \alpha \text{ and } k_s(\Theta_{di} - \alpha) + c_s\omega_{di} \leq 0 \\ 0, \\ \text{if } |\Theta_{di}| \leq \alpha \\ 0, \\ \text{if } \Theta_{di} < -\alpha \text{ and } k_s(\Theta_{di} + \alpha) + c_s\omega_{di} \geq 0 \\ k_s(\Theta_{di} + \alpha) + \max(k_s(\Theta_{di} + \alpha), c_s\omega_{di}), \\ \text{if} \Theta_{di} < -\alpha \text{ and } k_s(\Theta_{di} + \alpha) + c_s\omega_{di} < 0. \end{cases} \tag{4.85}$$

In order to avoid confusions, it is remarked that in comparison to the implementation in Matlab/Simulink the backlash block of Dymola needs the total backlash gap as input value for the backlash size ($b = 2\alpha$). Inside the block, the calculation of the shaft torque is then effectuated using $b_2 = \frac{b}{2}$.

The available measurements are the same as in the Matlab/Simulink model, these are the absolute position of the load (x_{pos}), the motor and load angle positions (Θ_{m1}, Θ_{m2}, Θ_l) and the motor velocities (ω_{m1}, ω_{m2}).

4.7.2 Comparison

For the simulation, the Dormand Prince integration method 'Dopri45' of order 5 and a tolerance of 0.001 is chosen, as this configuration is equivalent to the one used before in Matlab/Simulink, namely the there implemented 'ode45'-solver.

It can be stated, that the simulation results obtained in Dymola for the different strategies are quite similar to those obtained with Matlab/Simulink and underline the validity of latter. For demonstration purposes, the results for two cases are presented in Fig. 4.26 and Fig. 4.27. The reference value is again set to $x_{pos,ref} = 0.1$ $[m]$ and the system is initially in contact, that is $\Theta_{d1}(t = 0) = \alpha$ and $\Theta_{d2}(t = 0) = -\alpha$.

The first case represents the operation strategy based on a constant torque $T_{m2} = -10$ $[Nm]$, which starts acting after $t = 50$ [s]. As expected, without the stabilizing torque the system undergoes limit cycles after reaching its final reference position $x_{pos,ref} = 0.1$ $[m]$. This occurs around $t = 20$ [s]. The constant torque starts acting after $t = 50$ [s] and leads to an oppression of the limit cycles. The developing of the different values for the absolute position, the position angles of the motors and the load, as well as their angular velocities equal their respective developments obtained with the Matlab/Simulink simulation environment (see Fig. 4.16). The same holds for the input and shaft torques.

The second case demonstrates the behavior of the system, when operating with a switching-strategy based on $v = f(e_{abs})$. This has turned out to be the most promising strategy according to the analysis in Section 4.6. The same observations as in the previous case can be made. That is, the results are quite equal to those obtained in Matlab/Simulink.

Therefore, it can be stated that the previous analysis and the simulation results are confirmed by the results obtained in Dymola and underline their validity. Especially it is remarked, that the limit cycles can be avoided using any of the two backlash models, which is an indicator for the reliability of the proposed control structure.

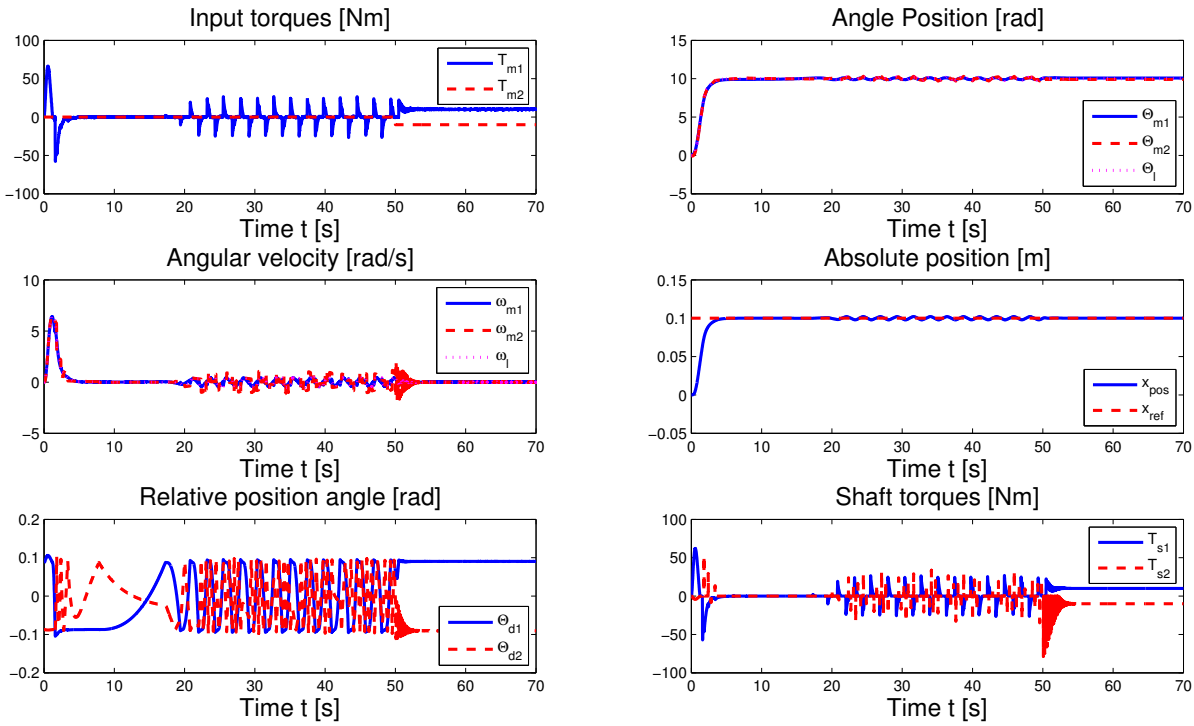

Figure 4.26: Dual motor control with constant torque $T_{m2} = -10$ [Nm] at $t = 50$ [s] simulated with Dymola. The limit cycles appear approximately after 20 [s] as in the Matlab/Simulink simulation and can be oppressed by a constant torque, which starts acting after 50 [s].

4.8 Parameter optimization for $v = f(e_{abs})$

This section aims to improve the system performance by optimizing the controller parameters and the switching of the slave motor. For the optimization the best-rated strategy based on the absolute error e_{abs} is chosen. Thus, the switching parameters e_{max} and e_{min} are used as tuning parameters.

For this purpose, the Optimization Function of the Dymola Design Library is used. This design tool provides several optimization algorithms and allows to optimize parameters of a Dymola model with respect to certain criteria. An introduction to the function is given in [21].

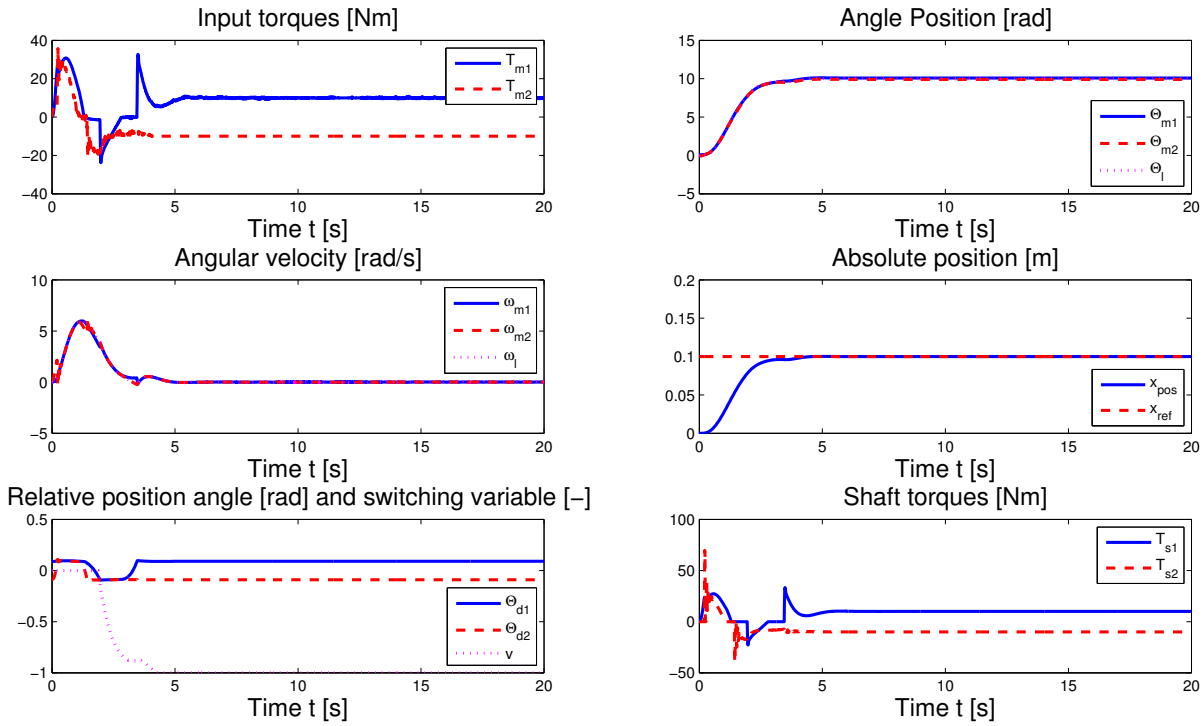

Figure 4.27: Dual motor control with $v = f(e_{abs})$ simulated with Dymola. The limit cycles are oppressed and the required controller energy is distributed on both motors in the beginning of the motion. Furthermore a smooth response is obtained and the strategy is robust against disturbances. The results equal those obtained in Matlab/Simulink.

4.8.1 Controller-parameter optimization

In a first step, we aim to optimize the outer-loop PID-controller. Therefore the following cost function is defined

$$f = \min(\max(\frac{1}{W_1}\text{riseTime}(x_{pos}) + \frac{1}{W_2}\text{overshoot}(x_{pos}) + \frac{1}{W_3}\text{settlingTime}(x_{pos})) \tag{4.86}$$

with $W_1 = 1.7473$, $W_2 = 10^{-4}$ and $W_3 = 3.957$.

For the optimization the model operating with a constant torque on the second motor is chosen. The values of the weighting parameters correspond to the obtained results of

Table 4.1: Optimization of controller parameters. The Genetic algorithm gives the best result. The start value of the cost function is 3.00354.

Optimal values $[K_p,T_i,T_d]$	**Optimization method**	**Optimal value f**
$[292.01, 1.24, 0.01]$	Pattern Search	1.67645
$[229.32, 1.38, 0.05]$	SQP	1.82310
$[223.38, 1.4, 0.073]$	Simplex	1.88427
$[281.92, 1.25, 0.087]$	Genetic Algorithm	1.67730

the characteristics when simulating with the previously designed controller of Section 4.2. Thus, we aim to improve the system performance regarding its step response with respect to the settling time, the overshoot and the rise time.

The available tuning parameters are K_p, T_i and T_d of the PID-controller. For the optimization we set the following bounds on the parameters

$$Kp \in [100, 300]$$
$$Ti \in [0.5, 2],$$
$$Td \in [0.01, 0.1].$$

The optimization is carried out using the different algorithms implemented in the Optimization-function. An overview of the results is provided in Table 4.1. As starting values the nominal values of the designed PID-controller in Section 2.2 are used. The start value of the cost function is then 3.00354.

The best results are obtained by Pattern Search and Genetic Algorithm. When checking the parameter sets in Matlab/Simulink, the set of the Genetic Algorithm seems to be the most appropriate solution and will be used in the further analysis.

4.8.2 Switching-parameter optimization

In the present case, the following cost function is defined

$$f_1 = \min(\max(\frac{1}{W_1}\int_0^T (u_1^2 + u_2^2)d\tau + \frac{1}{W_2}\text{overshoot}(x_{pos}))), \tag{4.87}$$

with $W_1 = \psi \cdot 2165$ and $W_2 = 3 \cdot 10^{-4}$. The weighting parameters correspond to the values obtained for the characteristic parameters of the optimization function, when operating with the previously chosen values $e_{max} = 0.25$ and $e_{min} = 0.01$, as well as an input step reference of $x_{pos,ref} = 0.1$[m] and a simulation time of $t = 10$[s]. As optimization goal consists of minimizing the energy input by avoiding any overshoot in the system´s step response, the energy input is additionally weighted with factor $\psi = 10$.

For the optimization different start values and optimization methods are chosen. As initial values for the switching parameters two sets are chosen, $[e_{max} = 0.5, e_{min} = 0.25]$ and $[e_{max} = 0.25, e_{min} = 0.01]$ The cost function has then a start value of $f_1(start) = 9.54322$ and $f_1(start) = 10.9464$ respectively. An overview of the different setups and the corresponding results is given in Table 4.2. The tuning parameters are limited to $e_{max} \in [0.1, 1]$ and $e_{min} \in [0.01, 1]$ in order to avoid switchings in the area where limit cycles occur.

All algorithms give similar results for the optimal switching parameters. These lay in a range of $e_{max} \in [0.62, 0.69]$ and $e_{min} \in [0.40, 0.45]$. Only the SQP and the Simplex-method lead to different results when starting with $e_{max} = 0.25$ and $e_{min} = 0.01$. However, the Genetic Algorithm and the Pattern Search seem to give more reliable results, as the value of the cost function and the optimal switching parameters are almost identical for both initial sets.

To recheck the optimization results, the cost function f_1 is reformulated to f_2

$$f_2 = \min(\max(\frac{1}{W_1}\int_0^T (u_1^2 + u_2^2)d\tau, \frac{1}{W_2}\text{overshoot}(x_{pos}))), \tag{4.88}$$

Then the start values are $f_2(start) = [8.85308, 0.690137]$ and $f_2(start) = [10.02246, 0.924029]$. The results of this optimization are shown in Table 4.3.

Table 4.2: Optimization of switching parameters with cost function f_1 of Eq.(4.87). The Genetic algorithm gives the best results. The start value of the cost function is 10.9464.

Start values	**Optimization method**	**Optimal value f_1**	**Optimal values**
$[0.5, 0.25]$	Pattern Search	9.08898	$[0.69, 0.41]$
$[0.5, 0.25]$	SQP	9.06205	$[0.62, 0.44]$
$[0.5, 0.25]$	Simplex	9.08140	$[0.63, 0.45]$
$[0.5, 0.25]$	Genetic Algorithm	9.06148	$[0.62, 0.45]$
$[0.25, 0.01]$	Pattern Search	9.08444	$[0.68, 0.4]$
$[0.25, 0.01]$	SQP	9.47738	$[1, 0.01]$
$[0.25, 0.01]$	Simplex	9.19005	$[1, 0.24]$
$[0.25, 0.01]$	Genetic Algorithm	9.06148	$[0.62, 0.45]$

For the cases with initial values $[e_{max} = 0.5, e_{min} = 0.25]$ the results are similar to the ones obtained with the previous cost function. However, for the initial set $[e_{max} = 0.25, e_{min} = 0.01]$ it seems to exist at least two different minima, one in the neighbourhood of $[e_{max} = 1.0, e_{min} = 0.1]$ and one around $[e_{max} = 0.6, e_{min} = 0.4]$. Again the Genetic Algorithm gives the best results. The optimal values for the switching parameters obtained with this method are identical to the ones obtained with the previous cost function.

The latter corresponds to the already obtained minima using the first cost function f_1 and f_2, with the first set of initial values $[e_{max} = 0.5, e_{min} = 0.25]$. As its value is inferior to the minimum around $[e_{max} = 1.0, e_{min} = 0.1]$, one can conclude that a pair of parameters $[e_{max} \approx= 0.6, e_{min} \approx 0.4]$ may satisfy the optimization goal best.

As a consequence, the switching parameters are set to $[e_{max} = 0.6, e_{min} = 0.4]$. Then the integrated square sum of the required input signals for a reference step of $x_{pos,ref} = 0.1$[m] and a simulation time of $t = 10$[s] is reduced from 2165 to 1845, which means an energy saving of 15[%].

Table 4.3: Optimization of switching parameters with cost function f_1 of Eq.(4.88). The Genetic algorithm gives again the best results. The start values of the cost function are [10.02246, 0.924029].

Start values	**Optimization method**	**Optimal value f_1**	**Optimal values**
$[0.5, 0.25]$	Pattern Search	$8.50622, 0.51865$	$[0.67, 0.40]$
$[0.5, 0.25]$	SQP	$8.60525, 0.51835$	$[0.55, 0.33]$
$[0.5, 0.25]$	Simplex	$8.49155, 0.57118$	$[0.60, 0.44]$
$[0.5, 0.25]$	Genetic Algorithm	$8.49167, 0.57253$	$[0.61, 0.45]$
$[0.25, 0.01]$	Pattern Search	$8.80359, 0.65697$	$[1, 0.033]$
$[0.25, 0.01]$	SQP	$8.81529, 0.66332$	$[1, 0.01]$
$[0.25, 0.01]$	Simplex	$8.55782, 0.58015$	$[0.98, 0.28]$
$[0.25, 0.01]$	Genetic Algorithm	$8.49013, 0.57150$	$[0.62, 0.44]$

4.9 Nonlinear MIMO controller

In this section a nonlinear MIMO control law for the position of the cart is depicted. It is obtained by combining the nonlinear, smooth switching control law based on $v = f(e_{abs})$ of Subsection 4.6.4 with an additional switching between the master/slave-assignment of the motors.

The master/slave-assignment of Motor_1 and Motor_2, which so far has been considered to be constant, is designated depending on the driving direction of the system. This is possible as both motors are equal. The aim of this additional implementation is to close the backlash gap always on the same side of the gears connecting the motors and the load. This could be e.g. on the outer side. The master-motor is regarded as main driving motor, whereas the slave-motor is used whether as supporting driving motor or for closing the backlash gap.

By using a constant master/slave-assignment, the backlash gap is closed whether on the inner or the outer side of the gear connecting the second motor and the load depending on the direction of the motion. The switching-strategy defined in Subsection 4.6.4 closes

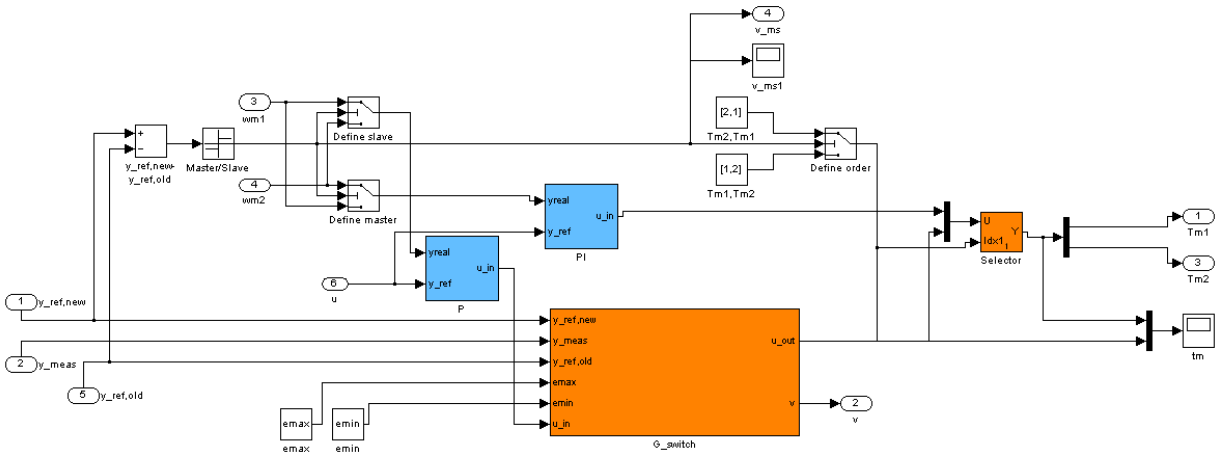

Figure 4.28: MIMO control law structure in Simulink.

the backlash gap on the outer side when the motion occurs in negative direction and on the inner side when the motion occurs in positive direction. This can be omitted by varying the assignment of the master- and slave-motor.

Therefore, the switching variable $v_{Master/Slave}$ for the master/slave-assignment is defined as follows

$$v_{Master/Slave} = \text{sign}(x_{ref,old} - x_{ref,new}) \tag{4.89}$$

and the assignment is stated as

$$MasterMotor = \begin{cases} \text{Motor}_1, & v_{Master/Slave} = -1, \\ \text{Motor}_2, & v_{Master/Slave} = 1. \end{cases} \tag{4.90}$$

The marking of Motor_1 and Motor_2 is according to Fig. 4.1. Practically, this means that Motor_1 is assigned to be the master-motor for motions in negative direction, whereas Motor_2 acts as master for motions in positive direction according to the definition in Fig. 4.1. An overview of the implemented structure is given in Fig. 4.28.

The resulting structure is then combined with the switching-strategy for the slave-motor based on $v = f(e_{abs})$, as described in Subsection 4.6.4 and the optimized controller of Section 4.8. In total, one obtains a nonlinear MIMO control law.

A comparison between the performance with and without an additional switching between the master/slave-assignment of the motors is shown in Fig. 4.29 and Fig. 4.30.

One can observe, how in the first case with a constant master/slave-assignment the relative position angles Θ_{d1} and Θ_{d2} change their signs depending on the direction of the motion. In contrary, using a variable master/slave-assignment leads to the desired behavior of closing the backlash gap always on the outer side of the contact-gears. This is stated by the constant allocation of the signs of Θ_{d1} and Θ_{d2}. However, they undergo the same transition when it comes to a position change of the cart as in the non-switching case. There the backlash gap is once traversed completely in both directions, which is due to the acceleration and breaking processes. But besides the different acting of the motors, there are no significant differences visible in the performance of the whole system.

The same observations can be made by designing the master/slave-switching in a way, that the backlash gap is always closed on the inner side of the gears.

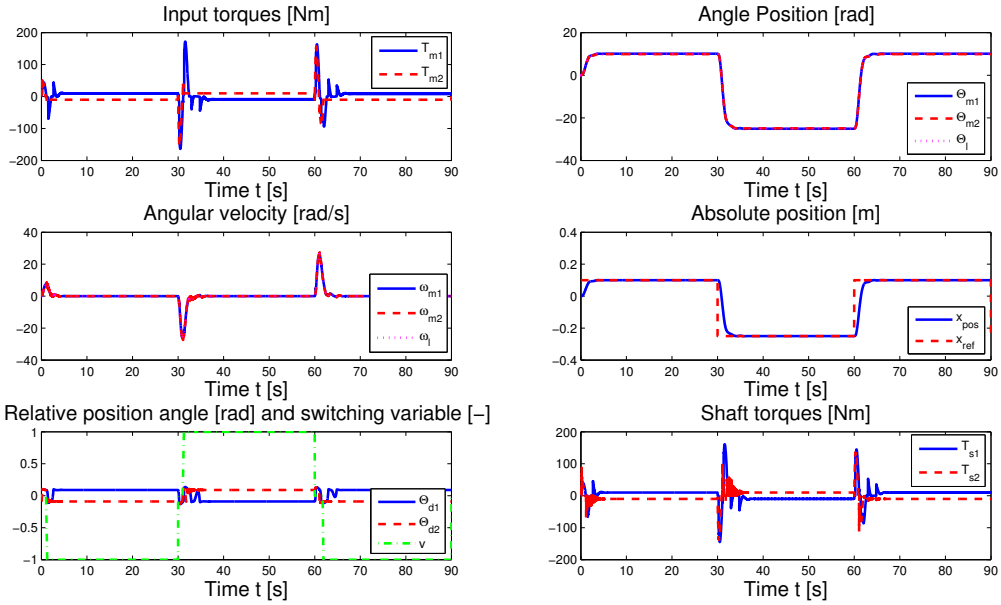

Figure 4.29: Dual motor control of a three-mass system based on $v = f(e_{abs})$ with no additional switching of the master/slave-assignment of the motors. One can observe, how the relative position angles change their signs depending on the direction of the motion of the system.

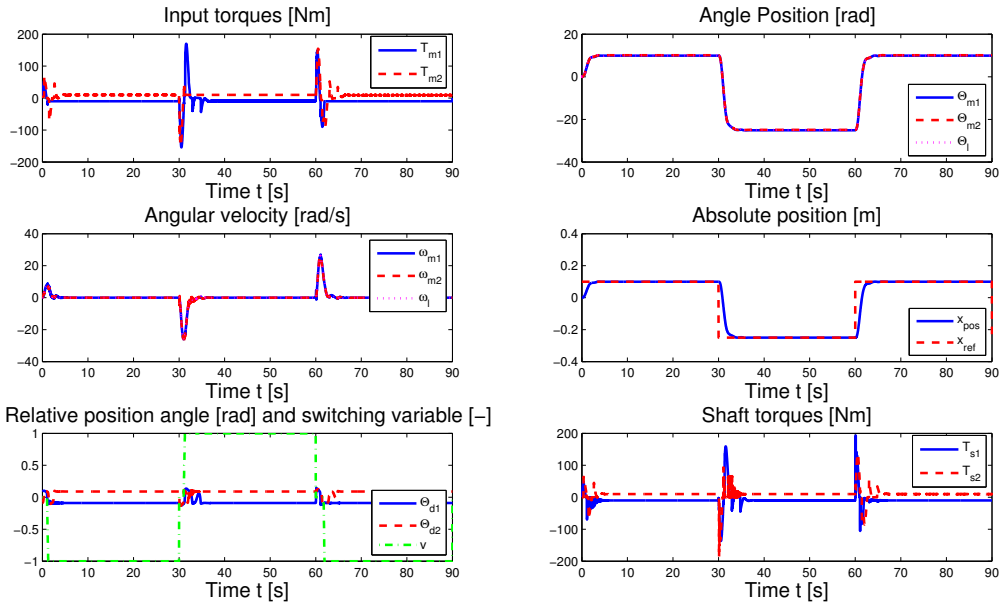

Figure 4.30: MIMO control law for the dual motor control. Dual motor control of a three-mass system based on $v = f(e_{abs})$ with additional switching of the master/slave-assignment of the motors. One can observe, how the relative position angles maintain their signs independently on the direction of the motion of the system. Besides, no other improvement in the performance is achieved.

4.10 Summary

In this chapter, a dual motor control for a nonlinear three-mass system is proposed. The considered masses represent two motors and a cart of a parallel kinematic robot. First, the model equations are introduced in Section 4.1. Then, a linear cascaded controller for the absolute cart position is designed and tested in simulations in Section 4.2. Further, in Section 4.3 the system behavior is analyzed under the assumption of a constant torque acting on the second motor. The system´s equilibrium points and their stability characteristics are derived. Furthermore, conditions for the global stability of the system are given in dependency of the constant input. The results are by simulations in Matlab/Simulink in Section 4.5. Subsequently, several switching strategies for the operation of the second motor are provided in Section 4.6 aiming to improve the system performance mainly in meanings of the required energy input. These approaches lead to a nonlinear, smooth

switching control law. In Section 4.7 the simulation results are checked in Dymola and in Section 4.8 the controller and switching parameters for the best approach are optimized. Finally, in Section 4.9 a nonlinear MIMO control law for the dual motor control problem is proposed based on the previous introduced implementations and an additional switching between the master-/slave-assignment of the two motors.

Chapter 5

Conclusions and outlook

5.1 Conclusions

In this work, different nonlinear approaches for reducing the backlash effect in a parallel-kinematic robot are presented. All approaches are based on the incorporation of a second motor to the driving system. In Chapter 4, the process is modeled as a nonlinear three-mass system in which two masses represent the motors and the remaining mass represents the load or cart of the robot. Backlash exists between each motor and the load.

It is shown, that the system can be locally and globally stabilized by the additional motor which acts in opposite direction of the main driving motion when backlash may occur. Different control strategies for the operation of the dual-motor drive based on a nonlinear, smooth switching-function are introduced and tested in simulations in Matlab/Simulink and Dymola. The switching function allows to improve the system performance and reduce the required energy input.

The most promising strategy is based on the determination of the switching variable using the relative position error e_{abs}. For this implementation an optimization of the controller and switching parameters is carried out using the Design-Optimization tool in Dymola. Subsequently, a nonlinear MIMO controller for the dual-motor drive is proposed and tested in simulations. The MIMO control allows to define the side where the backlash gap should be closed and may therefore improve the stiffness of the system.

All methods are first derived in Chapter 2 on a simplified nonlinear two-mass model of the process. In Chapter 3, they are tested on an experimental setup representing a nonlinear two-mass system exhibiting backlash and the simulation results are verified. Thereby, the analytical and simulation results of Chapter 4 are confirmed and a similar performance on the real system can be expected.

5.2 Outlook

Future work might cover mainly two aspects:

- The implementation and testing of the proposed dual motor control on a real three-mass system exhibiting backlash and a parallel-kinematic robot respectively. This has already been started by another master student at the department.
- To deepen the analytical stability analysis of the nonlinear three-mass system by extending the analysis from the constant input case to the nonlinear, smooth switching controller. Hereby, hybrid methods such as piece wise quadratic Lyapunov functions may be of interest, see [24] or [25].

Bibliography

[1] http://www.smerobot.org, 20.04.2009.

[2] M. Nordin and P.-O. Gutman (2002). Controlling mechanical systems with backlash - a survey. In *Automatica* 38 (pp. 1633-1649).

[3] A. Lagerberg (2001). A literature survey on control of automotive powertrains with backlash. Report, Control and Automation Laboratory, Department of Signals and Systems, Chalmers University of Technology, Göteborg, Sweden.

[4] M. Nordin (2002). Nonlinear backlash compensation for speed controlled elastic systems. Ph.D. thesis, Division Optimization and Systems Theory, Department of Mathematics, The Royal Institute of Technology, Stockholm, Sweden.

[5] B. Brochier (2006).Control of a Gantry-Tau Structure. Master thesis, Department of Automatic Control, Lund University.

[6] G. Brandenburg and U. Schäfer (1989). Influence and adaptive compensation of simultaneously acting backlash and Coulomb friction in elastic two-mass systems of robots and machine tools. In *Proc. ICCON'89* (pp WA-4-5), Jerusalem, IEEE.

[7] M. Nordin, J. Galic and P.-O. Gutman (1997). New models for backlash and gearplay. In *International Journal of Adaptive Control and Signal Processing*, Vol. 11 (pp 49-63).

[8] W. Gawronski, J.J. Beech-Brandf, H.G. Ahlstrom, Jr., and E. Maneri (2000). Torque-Bias Profile for Improved Tracking of the Deep Space Network Antennas. In *IEEE Antennas and Propagation Magazine*, Vol.42, No.6.

[9] Z. Haider, F. Habib, M.H. Mukhtar and K. Munawar (2007). Design, Control and Implementation of 2-DOF Motion Tracking Platform using Drive-Anti-Drive Mechanism for Compensation of Backlash. In *IEEE International Workshop on Robotic and Sensors Environments*, Otawa, Canada, 12-13 October 2007.

[10] http://www.dymola.se, 20.04.2009.

[11] G.H. Choi, H. Nakamura and H. Kobayashi (1996). Calibration of servo systems with redundant actuators. In *Proceedings of IFAC world congress*, San Francisco (pp. 169-174).

[12] K.J. Åström and T. Hägglund (2006). Advanced PID Control. ISA, 1st edition.

[13] P. Rostalski, T. Besselmann, M. Baric, F. Van Belzen and M. Morari (2007). A hybrid approach to modelling, control and state estimation of mechanical systems with backlash. In *International Journal of Control* Vol.80, No. 11 (pp. 1729-1740).

[14] D. Xue, Y. Chen, and D. P. Atherton (2007). Linear Feedback Control Analysis and Design with MATLAB. Society for Industrial and Applied Mathematics.

[15] http://www.mathworks.nl/matlabcentral/fileexchange/21663, 20.04.2009.

[16] D.G. Luenberger (1967). Canonical Forms For Linear Multivariable Systems. In *IEEE Transactions On Automatic Control*, Volume AC-12, No. 3 (pp. 290-293).

[17] R. Boneh and O. Yaniv (1999). Reduction of Limit Cycle Amplitude in the Presence of Backlash. In *Transactions of the ASME* Vol. 121 (pp. 278-284).

[18] J. Oh and D.S. Bernstein (2005). Step Convergence Analysis of Nonlinear Feedback Hysteresis Models. *American Control Conference*, June 8-10, 2005, Portland, USA.

[19] J. Oh, B. Drincic and D.S. Bernstein (2009). Nonlinear Feedback Models of Hysteresis. *IEEE Control Systems Magazine*, Volume 29, No. 1 (pp. 100-119).

[20] Cohen, J., Cohen P., West, S.G. and Aiken, L.S. (2003). Applied multiple regression/correlation analysis for the behavioral sciences. (3rd ed.) Hillsdale, NJ: Lawrence Erlbaum Associates.

[21] H. Elmqvist, H. Olsson, S.E. Mattsson, D. Brück, C. Schweiger, D. Joos, M. Otter (2005). Optimization Design and Parameter Estimation. The Modelica Association.

[22] H. Khalil (1996). Nonlinear Systems. Prentice Hall Macmillan, 2cond edition.

[23] M.Morari, W. Schaufelberger, P. Parrio, A. Glattfelder (2003). Analysis and closed loop angular speed control of a flexible shaft. http://control.ee.ethz.ch/∼ ifa-fp/wiki/uploads/Main/ExperimentsSummer/21_flexshaft_I-EN.pdf, 20.04.2009.

[24] S. Hedlund (2003). Computational Methods for optimal Control of Hybrid Systems. Dissertation, Departmemt of Automatic Control, Lund Institute of Technology.

[25] http://control.ee.ethz.ch/∼ mpt/, 20.04.2009.